1-1-2011

Development of a Shore Profile Algorithm for Tidal Estuaries Dominated by Fine Sediments

Kimberly Collins Pevey

DEVELOPMENT OF A SHORE PROFILE ALGORITHM FOR TIDAL ESTUARIES

DOMINATED BY FINE SEDIMENTS

By

Kimberly Collins Pevey

A Dissertation
Submitted to the Faculty of
Mississippi State University
in Partial Fulfillment of the Requirements
for the Degree of Doctor of Philosophy
in Civil and Environmental Engineering
in the Department of Civil and Environmental Engineering

Mississippi State, Mississippi

April 2011

DEVELOPMENT OF A SHORE PROFILE ALGORITHM FOR TIDAL ESTUARIES

DOMINATED BY FINE SEDIMENTS

By

Kimberly Collins Pevey

Approved:

_____
William H. McAnally
Research Professor of
Civil and Environmental Engineering
(Major Professor)

_____
James L. Martin
Professor of
Civil and Environmental Engineering
(Co-Major Professor, Graduate
Coordinator)

_____
Rutherford C. Berger
Adjunct Professor of
Civil and Environmental Engineering
(Committee Member)

_____
Scott Douglass
Professor of
Civil Engineering
University of Southern Alabama
(Committee Member)

_____
Sarah A. Rajala
Dean of Bagley College of Engineering

Name: Kimberly Collins Pevey

Date of Degree: April 30, 2011

Institution: Mississippi State University

Major Field: Civil and Environmental Engineering

Major Professor: Dr. William H. McAnally

Title of Study: DEVELOPMENT OF A SHORE PROFILE ALGORITHM FOR
                  TIDAL ESTUARIES DOMINATED BY FINE SEDIMENTS

Pages in Study: 143

Candidate for Degree of Doctor of Philosophy

The purpose of this work is to generate a shore profile algorithm to be used in estuaries dominated by fine sediments. Numerical models are continually evolving to enhance the overall accuracy of results. However, the typical shore profile is defined as a vertical wall. This work defines the shore as a nonlinear profile which will provide more realistic models.

A variety of shore profile equations were examined and tested against a field site, Weeks Bay, Alabama. The most applicable, an equation by S. C. Lee, was modified in order to calculate the entire shore profile length. The distance from the land-water interface to the depth at which sedimentation is negligible can now be modeled with a single equation. Recommendations for the practical aspect of implementation into a numerical model are also considered.

DEDICATION

To my little man, Parker.

ACKNOWLEDGEMENTS

I owe my deepest gratitude to my graduate advisor and mentor, Dr. William McAnally. Without his guidance and expert advice, this work would not have been possible. He provided support and motivation throughout my graduate studies, and I attribute much of my knowledge to his teachings. I also want to acknowledge the support of my committee, Drs. James Martin, Charlie Berger, and Scott Douglass.

I am also especially grateful to my graduate student colleagues and staff who participated in my field data collection efforts. It was hard work, and I appreciate the time and effort they put forth on the hot, swampy shores of Weeks Bay.

Finally, I would like to thank my family. I am vastly grateful to my parents for teaching me that I can do anything I put my mind to and for emphasizing the importance of an education. I am also especially thankful to my sister who has always been supportive of my long educational journey and encouraged me along the way. Lastly, I would like to thank my husband, Carter, for bolstering my confidence in the way only a best friend could. I am eternally grateful for his love and support.

TABLE OF CONTENTS

Page

LIST OF TABLES

LIST OF FIGURES

ix

CHAPTER I

INTRODUCTION

Numerical modeling of shoreline change is an area of considerable interest due to its impacts on diverse ecosystems as well as local economies. For example, land loss in coastal Louisiana is destroying valuable habitat for a billion dollar fishery industry (USGS 1995), and shoreline erosion in Chesapeake Bay is considered to be a primary source of excessive nitrogen enrichment (Hardaway 1999).

In parallel with growing interest in shoreline erosion, advances in numerical modeling and computing power are allowing for more accurate and detailed predictions. In the past, shorelines have been represented in numerical models as vertical walls, or at best, a constant slope. In reality, the shoreline is a region of complex contouring across the land-water interface. Therefore, modeling the shoreline as a detailed nonlinear profile offers the opportunity to develop more realistic numerical models.

1.1   Objective

The purpose of this work is to generate an algorithm for fine sediment shoreline erosion and deposition which can then be implemented in a hydrodynamic and sediment transport model. The algorithm is also intended to calculate the evolution of the shoreline contour over time.

1

1.2   Acknowledgements

1.3   Background

Estuaries are among the most difficult geophysical environments to model. A multitude of physical forcings – tides, river flows, waves, and density currents – and

2

nonlinear sediment responses make numerical modeling exceedingly complex. Many studies have attempted to characterize and predict estuarine event response and evolution by generating empirical relationships which can only be applied to the estuary for which they were designed. Few have used physics-based principles to define the environment, and these are highly complex and require numerical analysis.

Erosion and deposition equations have been used to calculate transport rates of bottom sediments in estuaries. However, very few production-level equations have been developed which characterize erosion and deposition of the shoreline as a contour, and none of them are being utilized in estuarine models. Using an algorithm to define realistic shoreline profiles as well as predict erosion and deposition in this region will significantly increase the accuracy of numerical models in the nearshore zone.

1.4   Approach

The approach to achieve the objective was two-fold. The first portion consisted of data collection to define estuarine shorelines while the second focused on analysis to provide a descriptive algorithm. The primary field data collection was conducted in Weeks Bay, Alabama, an estuary dominated by fine sediments. Vertical profiles of several sites along the shoreline were monitored monthly. Salinity profiles were taken at three locations on each profile. Sediment samples were collected periodically to determine changes in particle size over time. In addition, tidal and meteorological data were collected at the site over the course of the project.

The field data collection associated with this project was used as a testing ground for various new techniques in data acquisition. From high-tech to low-tech, several methods were attempted and used with varying success.

A new approach was used to analyze changes in profile (over time and from location to location). Wavelet transforms have a multitude of applications, and unlike Empirical Orthogonal Function (EOF) analysis, the results have intrinsic real-world meaning. Wavelets were used in this project to determine relationships between physical forcings and changes in shoreline contour.

The analysis was developed on a tiered basis. The Tier 1, or simplest, approach was used to gain a rough understanding of the profile geometry through the use of Microsoft Excel. A Slope Analysis was completed which plotted and fit simple curves to the raw data. In Tier 2, Wavelet theory was applied as a unique effort to gain a more in-depth understanding of the data. Lastly, in the Tier 3 approach, the most complex analysis implementing shoreline erosion equations were examined. The most applicable of these was improved upon and implementation into a numerical model was then considered. The tiered analysis ensures that the final results are reasonable based upon the results previous tiers, thereby minimizing mistakes.

1.5 Scope

The overarching goal of this work is to develop an equation or series of equations which will mathematically describe estuary shoreline evolution. Specifically, this work is intended to accurately define shore profile shape continuously from the land-water interface to the depth at which sediment transport becomes negligible.

The focus of this research is a shallow estuary which is primarily wind-driven with small tidal range and shorelines inhabited by various marsh grasses. The generated equation is also only applicable to shorelines which are dominated by fine sediments. However, significant importance was placed on maintaining a physics-based algorithm

4

with limited empirical parameters, thus generating an algorithm which can be used in a variety of energy environments.

CHAPTER II

ESTUARINE SHORELINE EVOLUTION

2.1   Background physics

Coastal environments are among the most complex and least predictable environments in the world. The independent relationships between the variety of physical forcings are difficult to define and the inter-connectivity of these relationships is more difficult still.

Estuaries are affected by tides, winds, precipitation, fresh and saltwater inflows, recreational and commercial boat traffic, and storm events. Each of these forcings is dynamic both spatially and temporally. Horizontal spatial scales for the forcings may vary on the order of 100 feet. Variations in the temporal scale are on the order of minutes for changes in waves, months for seasonal variation, and years for fresh water inflow changes caused by draughts, urban withdrawals, and land cover changes (Roberts 2001).

Table 2.1   Time and space scales (adapted from Roberts 2001).

Time scales	
turbulence	< 1 second
waves	1 - 10 seconds
depth/settling velocity	minutes - hours
tidal cycle	12 hours
consolidation of sediment	days
time between wave events	days - months
spring - neap cycle	2 weeks
seasonal wave climate	annual seasonal cycle
time between major storms	> 1 year
relative mean sea level change	> 100 years
major climate change	> 10,000 years
Space scales	
primary grain size	microns
particle aggregate	0.1 - 1 mm
microtopography of mudflat	1 - 10 mm
drainage channels	0.1 - 10 m
ridge/runnel dimensions	0.1 - 10 m
tidal range	1 - 10 mm
mudflat width	50 m - 5 km
estuary dimensions	10 - 100 km

2.1.1   Fine Sediments

Sediments whose effective diameters are smaller than 64 µm are considered fine sediments. Grain size greatly affects the physics of sediment transport. The behavior of fine sediment is dictated by an entirely different set of properties and physics than coarse sediment; however, a sediment whose grain size distribution contains only 10 to 20% fines will behave like a fine sediment.

Typically, individual fine sediment grains are shaped as either plates or rods. Plates are extremely thin, flat particles which have a high surface area to volume ratio. Rods are plates which have 'curled' to form a cylindrically shaped rod. Individual

7

particles have such small mass, that they are unable to deposit due to Brownian motion keeping them in suspension.

Each individual particle has surface and body forces which can cause them to be attracted to one another. When particles collide, the forces cause them to attach in a snowball fashion through a process known as flocculation. The group of particles is known as a *floc*. In order for deposition to occur, fine sediment particles must form flocs to increase their effective mass.

Environmental parameters can greatly influence flocculation including turbulence, salinity, and particle concentration. Too much turbulence, however, will cause flocs to break apart. An increase in salinity will slightly increase the rate of flocculation and deposition.

2.1.2   Sedimentation

Sedimentation occurs when particles from within the water column deposit to become a portion of the bed. The process of sedimentation of fine sediments is affected significantly by flocculation, as discussed above.

Increased velocity and wave action will increase the energy of the system and can reverse sedimentation by the resuspension of sediments back into the water column. Re-entrainment of previously deposited material occurs when the shear stress applied by the water column exceeds the critical shear stress of the bed and particles re-enter the water column.

Sediment beds can generally be separated into two categories: consolidated bed and newly deposited bed. Consolidated beds are older sediments which have had time to settle and form a relatively firm bed. The weight of the upper sediments forces fluid out

8

of the bed matrix and increases consolidation. A newly deposited bed will generally be very soft and will have a very low critical shear stress. Fluid mud falls between these categories.

2.1.3   Fluid Mud

Fluid mud is characterized by a high concentration mixture of fine sediments and water which is dominated by hindered settling (Mehta and McAnally 2008). It exhibits the unique property of being able to flow similar to a fluid yet also has a high sediment concentration. Fluid mud has been found to have bulk densities near water in the range of 1,080 and 1,200 kg m^{-3} (McAnally et al. 2007).

Studies have shown fluid mud to exist in locations across the world. It can exist in thin layers or several feet thick and can be formed in several ways. Fluidization of bed sediments during wind wave or storm events can cause the short-term formation of fluid mud. Positive and negative pore pressures caused by passing waves can induce velocities within the pores. The drag created by the pore fluid velocity can then balance the force of gravity of the particle, significantly reducing settling velocity.

Fluid mud can also be formed by aggregation of particles through flocculation to generate a more permanent bed feature. There are several factors which contribute to the generation of fluid mud, including grain size distribution, water velocity, and wave energy.

2.2   Shoreline Evolution

The term *shoreline* can include anywhere from the high-water mark to the point at which the orbital velocity of waves no longer affect the bed. In this report, shoreline is meant to include this entire nearshore region, particularly highlighting the vertical face

9

created by wave impact. This area, shown in Figure 2.1, may or may not be inhabited by marsh grass near the water line.
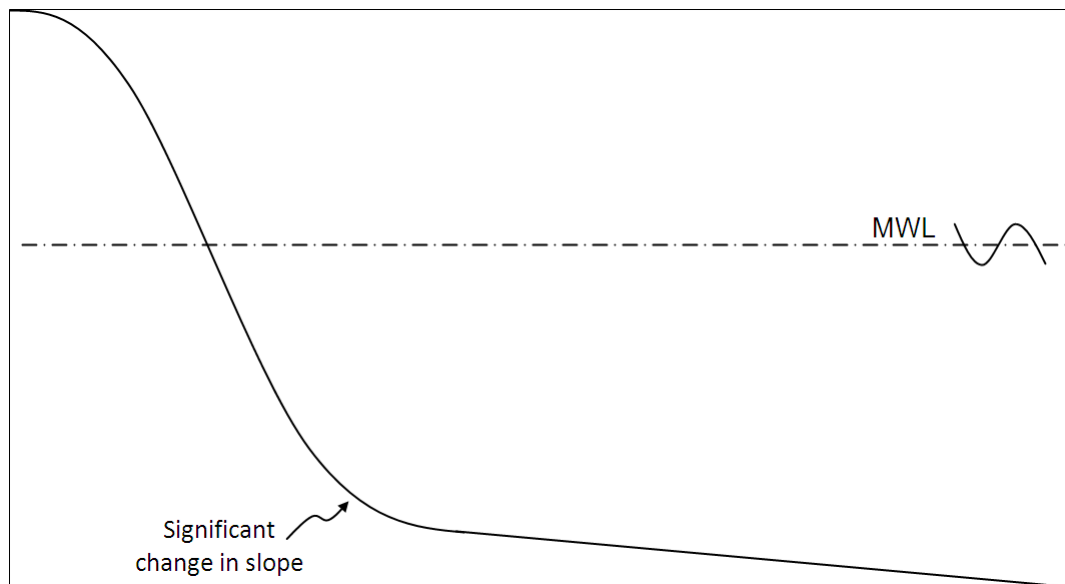
Figure 2.1   Schematic of typical profile

Erosion and deposition of fine sediments are dictated by the shear stresses acting on the sediment bed. When the shear stress exceeds what is known as critical shear stress, erosion will occur. The same concept can be applied to the shoreline, although several more physical factors come into effect. Wind waves are often the most important factor in shoreline change. In addition, flow velocities, including tidal effects, can also play a significant role in shoreline erosion. Deposition can occur during quiescent conditions, but is dependent on available sediment loading from source waters. Grain size distribution also affects the erosion rates given that finer sediments require less energy to erode.

Advancements in the field of fine sediments have lead to estimates of shear stresses at the water-sediment interface. Following this, a multitude of research and

10

subsequent publications linking shear stress to erosion have emerged. However, the scope of shear stress is too minute to efficiently apply in a hydrodynamic model. Models require a broader estimation of erosion based on physical forcings. The goal of this work is to achieve this with minimal loss of accuracy.

Longshore transport, the movement of sediments laterally along a shoreline, can be caused by water velocities, tides, and primarily suspended sediment concentration (Rodriguez 2000). Sediment loading is an important aspect of longshore transport and the calculation of shoreline change. Areas of deposition caused by longshore transport, often in the form of a bar or spit, can frequently be found adjacent to areas of erosion.

Marsh grass can also play a significant role in the reduction of erosion. Grasses act as energy absorbers causing incoming waves to be dissipated more quickly. The peat substrate in which marsh grass is typically growing can flex to absorb wave energy and the root systems also help to physically hold the sediments in place.

2.3 System Energy

The amount of energy in a system greatly affects the hydrodynamics as well as the stability of the shoreline and bed sediments. Energy is input into the system primarily by fresh water velocity, tides, and wind waves. The velocity of water laterally along the estuarine shore, known as the longshore current, is dependent on these three driving factors. Breaking waves approaching the shore at an angle also generate longshore currents; the wave itself pushes the water laterally as the remainder of the wave impacts the shore in turn. Rising and falling tides in an estuary have the potential to reverse the general velocity, causing a flux in energy.

11

Waves are often the leading cause of erosion on shorelines due to the combination of their destructive forces. When waves impact the shoreline, their energy is transferred as a force upon the sloped surface of the shore. The speed and turbulence of breaking waves, along with the resulting positive and negative pore pressures caused by advancing and retreating waves can also play a role in erosion. The pressure variation under waves can also cause fluidization of unconsolidated bed sediments, leaving them more susceptible to erosion.

The energy associated with wave height and velocity is discussed below. Wave energy as a function of wave height is described as

$$E_w = \tfrac{1}{8}\rho g H^2 \hspace{4cm} \text{Equation 2.1}$$

where ρ is water density, g is acceleration due to gravity, and H is wave height. The rate at which waves carry energy to the shore is known as energy flux. Energy flux per unit width is

$$\varepsilon_w = \tfrac{\partial}{\partial x}(E_w C_g) \hspace{4cm} \text{Equation 2.2}$$

where ε_w is the energy flux, E_w is wave energy and C_g is the group velocity. The relationship between wave celerity and water depth is defined as

$$C = \sqrt{gh} \hspace{4cm} \text{Equation 2.3}$$

where g is acceleration due to gravity, and h is water depth.

The relationships between individual wave velocity, C, and group velocity, C_g, are taken as

$$C_g = nC \hspace{4cm} \text{Equation 2.4}$$

and

12

$$n = \tfrac{1}{2}\left(1 + \frac{2kh}{\sinh 2kh}\right)$$ Equation 2.5

where k is wave number and h is water depth.

In the nearshore area, n approaches 1; therefore, this document will consider group velocity to be equal to individual velocity.

2.4 Shore Profile Equations

Many profile equations which have been developed for shoreline erosion were generated for medium to high energy environments with most being applicable on sandy coasts. The typical tidal ranges and wave energy are higher than in the study site used for this work. When algorithms are developed, the unknown coefficients are calculated based on applied profiles. Because each environment is different, these coefficients can widely vary from location to location. Trends and relationships are developed based on physical factors of each location. However, low energy environments are often left out of the calculations leading to skewed results and making the determination of applicable coefficients difficult for the user.

The most accurate shoreline erosion equations are derived from changes in profile. A profile equation for coarse sediments has long been established from the work of P. Bruun (Dean 2002). However, the complexity of fine sediments requires a multifaceted approach. R. Kirby (2002) originally documented the correlation between concavity of profiles and erosion or deposition. Kirby proposed that erosion-dominated shores are typically concave whereas accretion-dominated shores are typically convex (Figure 2.2). Additionally, accretion-dominated shores are those in which the physical forcings do not overcome the stability of sediment bed. Limited sea level rise and abundant sediment supply can also lead to accreting shores; the converse is true of

13

erosion-dominated shores. Following Kirby's initial publication, researchers tested his theory with a variety of methods, and the theory is now widely accepted.
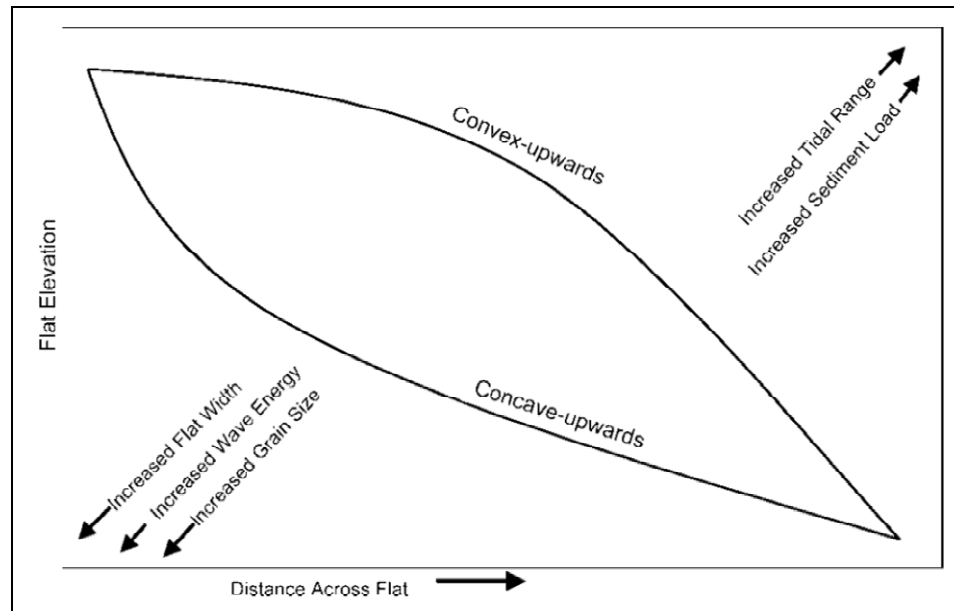
Figure 2.2   Schematic of profile geometry with physical forcings (used with permission, Bearman 2010).

Bearman analyzed 2958 profiles at 766 locations using eigenfunction analysis in an attempt to confirm the theory presented by Kirby. The concavity was used as the mode of variability tested by the eigenfunction analysis. For this method the profiles were converted into a unitless scale using 30 total points. Using this method, 86.1% of the variability was explained, showing good agreement with the theory presented by Kirby (Bearman 2010).

Another approach is to relate wave dissipation to profile shape. Two common wave dissipation equations are described as

$$H(x) = H_0 e^{-k_i x} \hspace{3cm} \text{Equation 2.6}$$

and

14

$$H(x) = H_0 \left(\tfrac{1}{1+\alpha x} \right) \hspace{4cm} \text{Equation 2.7}$$

where $H(x)$ is wave height at distance x, H_0 is the incident wave height, and k_i and α are wave attenuation parameters (Dean 2002).

Perhaps the most accurate and certainly the most widely published fine sediment shoreline equation is that developed by S.C. Lee (1995). Initially, Lee combined and mathematically manipulated Equations 2.1, 2.2, 2.3 and 2.6 to develop a new profile equation:

$$h = h_o e^{4\bar{k}_i (x - x_o)} \left(\frac{x}{x_o} \right)^2 \hspace{3cm} \text{Equation 2.8}$$

where k_i *bar* is an average wave attenuation coefficient and (h_o, x_o) is the terminal water depth and distance offshore.

Lee defines the terminal depth as the point offshore in which sediments are no longer impacted by wave activity. At the land-water interface, an erosional scarp can develop due to erosion caused by wave action. The above equation works well in fine sediment environments; however, it does not allow for inclusion of an erosional scarp. To account for this, Lee developed an additional slope term which adds an empirical coefficient and a profile-specific coefficient. Lee's final equation is described as

$$h = Fye^{-\beta y} + (h_0 - Fye^{\beta y})e^{4\bar{k}_i (y_0 - y)} \left[\frac{y}{y_0} \right]^2 \hspace{2cm} \text{Equation 2.9}$$

where F=slope at land-water interface, β=empirical coefficient, k_i=wave attenuation coefficient, y=distance along profile, y_0=location at which waves influence the bed (Lee 1995).

The datasets utilized by Lee appeared to have good correlation with Equation 2.9. However, in small, shallow bays such as Weeks Bay, the nearshore corrector produces

15

minimal changes to the profile. Examination of the corrector term and further discussion of these equations can be found in Chapter 8.

CHAPTER III

STUDY SITE

3.1   Project Area

The project area focused on Weeks Bay, where a site-specific experiment design was created and implemented over several months. Weeks Bay is a small (3 mi^2) bay which empties into eastern Mobile Bay near the town of Fairhope in southern Alabama. The watershed includes the Fish River catchment and the Magnolia River catchment (Figure 3.1 and Figure 3.2).

Much of the bay is bordered by marsh grass with scattered residential housing located along the shoreline. Vessel traffic within the bay is very low; the bay is traversed only by local recreational fishermen and Weeks Bay NERR researchers. The bay is shallow, with depths only reaching 3 meters in the deepest portions (NOAA, 28 Dec 2010). There is a shallow channel which runs north to south across the bay. It was dredged for the construction of a bridge on the north side of the bay and has not been maintained since construction.
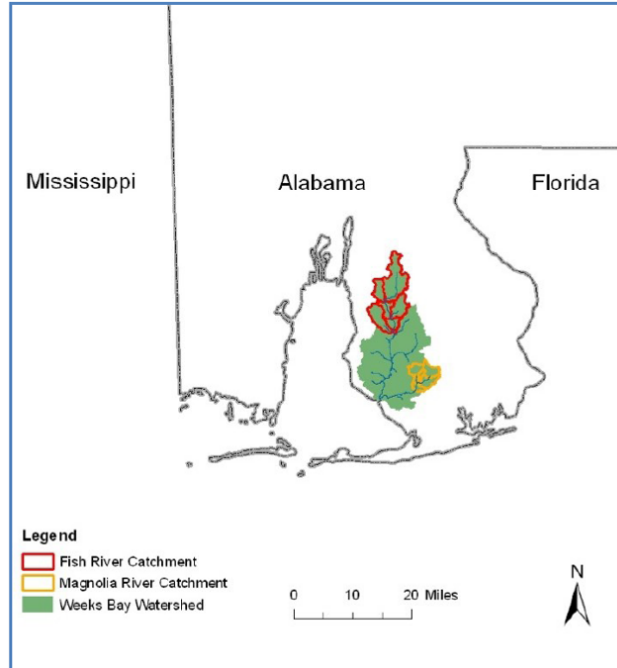
Figure 3.1   Weeks Bay watershed with USGS catchment areas (used with permission, Diaz-Ramirez 2010).

Figure 3.2   Profile locations in Weeks Bay (Google 2010).

18

As discussed in Chapter 1, the bay and much of the surrounding lands are part of the Weeks Bay National Estuarine Research Reserve. The research reserve was created to protect the watershed for long-term research, water quality monitoring, and to educate the public about sustaining the rich ecosystem (Weeks Bay, 1 Sept 2010).

3.2   Weeks Bay NERR Data Stations

The Weeks Bay NERR maintains several data stations which monitor water quality parameters at 15 minute intervals year-round. These have been used to collect baseline measurements such as salinity and temperature (See Figure 3.3 and Table 3.1. The NERR system also maintains a meteorological station just north of the bay. These datasets are available to the public at the NERR Centralized Data Management Office (NERRS, 1 Sept 2010).

Figure 3.3   Weeks Bay station locations (Google 2010).

Table 3.1   Station reference guide

WKBSHMET	Safe Harbor Met Station	Meteorological
WKBFRWQ	Fish River	Water Quality
WKBMBWQ	Middle Bay	Water Quality
WKBMRWQ	Magnolia River	Water Quality
WKBWBWQ	Weeks Bay	Water Quality
8732828	NOAA Tide Gauge	Tides

3.3   Hydrodynamics

Weeks Bay has two primary fresh water inflows, the Fish River and the Magnolia River (Figure 3.2). Located at the north end of the bay, the Fish River flows at an average annual daily mean of more than 110 cfs (USGS, 1 Sept 2010). The Magnolia River flows

20

into the bay on the eastern shore with an average annual daily mean of over 30 cfs (USGS, 1 Sept 2010). Both of these river gages are located not at the mouth of the rivers, but further upstream in the watershed. Because only about 36% of the watershed is gaged, the actual flow is significantly higher than the above flow rates (Diaz-Ramirez 2010). Further discussion on the prediction of the ungaged flows can be found in Section 3.5.

Because Weeks Bay is a shallow bay (less than 3m), it is often driven primarily by wind forcings. The dominant wind direction changes with season. Over the course of this project, all directions were accounted for, but winds are dominantly out of the north, ranging from northwest to northeast (NERRS, 1 Sept 2010).

Fresh water inflows can also dominate the hydrodynamics during periods of low wind and high river flow. Under these conditions, a weak clockwise circulation cell sets up on the west side of the bay, and the bay may become stratified. This was noted by the Weeks Bay NERR researchers and can be seen in the ADH model of the bay (See ADH model description in Section 3.4).

The salinity in the bay is brackish due to the relatively small mouth of the bay (about 500 ft). The reduced flow area lowers salinity and causes increased mixing at alternating tides. Typical salinities range from 1 psu[1] to over 20 psu with an average of around 8 psu (NERRS, 1 Sept 2010). As expected, a salinity gradient can be found from north to south across the bay with lower salinities found near the mouths of the rivers.

Weeks Bay has a mean tide range of 1.30 ft and a diurnal tide range of 1.54 ft (NOAA, 31 May 2010). Although tidal fluctuations are relatively small, they can affect hydrodynamics. During certain conditions, the waters near the mouth of the bay become

---

[1] Practical salinity units which is approximately equivalent to the traditional "ppt" notation.

stratified with a strong pycnocline separating the heavier saline water from the fresh river water. In addition, under rare conditions near the mouth of the bay, opposing flows can occur with the incoming tide flowing inward beneath the lighter outgoing fresh water.

3.4   Profile locations

Profiles, or cross-sections perpendicular to the shoreline, were set up along the shore of the bay to monitor short-term erosion and deposition. The locations of these profiles were chosen primarily by the location of fine sediment banks and secondarily by the boundary of the Reserve property. As discussed in the previous section, the primary wind direction has a significant affect on the composition of the shorelines. The northeast portion of the bay contains only sands to at least two feet in bed depth. The southern bay is bordered by private lands and housing. For these reasons, the northeast and southern shores of the bay were avoided. The section of the bay analyzed in the project, the northwest portion, contains fine sediments down to at least two feet and is within the NERR boundary.

Six profiles were established in Weeks Bay; the locations of which can be found in Figure 3.2. Each profile was roughly 130 feet in total length, beginning about 30 feet within the marsh and extending perpendicular to the shoreline into the bay about 100 feet. A schematic of the typical profile can be found in Figure 3.4. A detailed description of the setup of profiles can be found in Chapter 4.
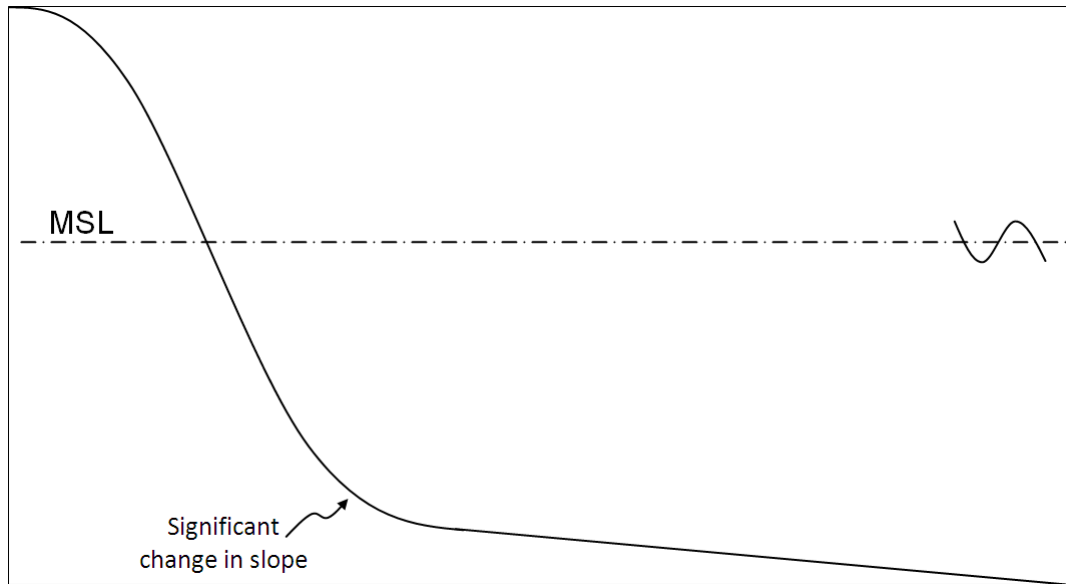
Figure 3.4   Schematic of typical shore profile.

3.5   ADaptive Hydraulic Model (ADH)

The ADaptive Hydraulic Model is a hydrodynamic model which can include salinity, tides, and sediment. The strength of the model lies in the fact that it is open-source and subroutines can be added to the model to enhance the users' purpose. Also, unique to this model is its adaptive grid. During model computation, if the error between subsequent time steps exceeds the set tolerance, the grid will 'adapt' or redefine into a finer mesh. The work in this document was generated to be implemented into a hydrodynamic model such as ADH.

An ADH model of Weeks Bay has been generated by J. Sharp which includes tides and salinity (Sharp 2009). Comparison of measured versus model tides and salinity show good correlation. A screen grab of the model can be seen below in Figure 3.5. It is intended that this model be used as a testing ground for the conclusions generated from this research.

23
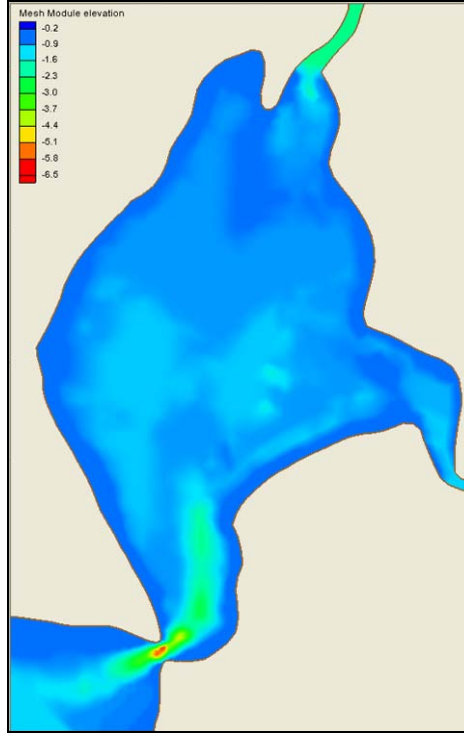
Figure 3.5   Screen grab of velocity magnitude in ADH model of Weeks Bay.

3.6   HSPF Model of Weeks Bay

An HSPF Model of Weeks Bay has been generated by Diaz-Ramirez (2010). Since only a portion of the Fish and Magnolia River catchments (36% of the watershed) is gaged by the USGS, an HSPF model was implemented to estimate the remaining portion of the watershed (Figure 3.1). The simulated annual fresh water inflow ranged from 81,000 cf to 235,000 cf, with an average of 190,000 cf. The average daily mean flow of 441 cfs, about 3 times that of the gaged flow (Diaz-Ramirez 2010).

24

CHAPTER IV

DATA COLLECTION

The data collection process was an important portion of this work. The nearshore region is one of the most difficult in which to measure elevations. Fine sediments have very little weight-bearing capacity which makes traditional elevation monitoring difficult. Also, near the land-water interface, it is not possible to utilize traditional depth sensing equipment. For these reasons, there are very few datasets available in this region; therefore, data were collected specifically for this project. Data collection continued over a period of three months.

4.1   Field Experiment Design

Changes in the contour of the shoreline were measured by establishing cross-sections, or profiles, in Weeks Bay. Each profile was approximately perpendicular to the shoreline and extended from about 30 feet landward, within the marsh grasses, to roughly 100 feet into the bay. A total of six profiles were set up in the northwestern portion of the bay. The locations of these profiles can be found in Figure 3.2 in Chapter 3.

The initial experiment design utilized an Acoustic Doppler Current Profiler coupled with a handheld GPS. The devices were programmed to export data in real-time to a file where the data were compiled into XYZ after the application of correctors. The technique was used to obtain bathymetry from the deepest portion of the profile to the shallow limits of the ADCP, which was roughly two feet. A land level was then used to obtain elevations from dry land to the limits of the ADCP.

25

After the first trip, the measurement method was redesigned. The specific model of ADCP proved to be a hindrance as it was designed for rivers with no wave action. It was determined that the accuracy of the handheld GPS greatly diminished as the system was moving. In addition, tying the two datasets together (land level and ADCP) induced unacceptable errors. Therefore, the ADCP was removed from the experiment entirely. Subsequent trips brought further changes and improvements until the experiment was accurate and efficient in its measurements.

The final experiment design was created with accuracy as the primary goal, and ease of measurement being a close second. A land level was used to measure depth across the entire profile. A digital level was chosen to make measurements accurate as well as quick and easy. To maintain an accurate line of the cross-section, a dolphin constructed of two 2" PVC pipes was used at the bay end of the cross-section to mark the end of the profile. A steel rod or tree was used as the landward end of the section. A rope was then attached to each end and pulled as tight as possible to provide a visual reference (Figure 4.1). A schematic of the profile can be found in Chapter 3 in Figure 3.4.

Figure 4.1   Weeks Bay profile ready for measurement.

Horizontal and vertical benchmarks, local to each profile, were established. The initial plan of establishing wooden stakes as vertical benchmarks had to be abandoned due to a lack of weight-bearing subsurface. Since the entire experiment revolved around the benchmark being stationary, a new method was devised. Nails were placed in two nearby trees and were used as vertical benchmarks. A horizontal benchmark was established with a wooden stake placed along the profile. This method was acceptable since it was only used for a horizontal distance, not a vertical benchmark. In this manner, each profile had its own independent reference system.

The design initially used only a standard bar code rod; however, it was quickly noted that the rode sank into sediments. The combination of the weight of the rod and the small foot made it difficult to feel the surface of the mud and hold it in place while measurements were taken. An estimated error range of 3 to 6 inches was not acceptable

27

and another solution was required. Since the weight of the rod could not be altered, a larger foot was needed to distribute the weight across a greater surface area. The land portion of the level required the small footprint in order to accurately measure the sediment surface between the dense marsh grasses. Beyond the marsh grasses, the foot was attached and utilized for the remainder length of the profile. For this reason, it was also necessary that the foot be easy to remove. The new foot was constructed out of thin sheet metal and attached by two compression bolts.

4.2   Physical data collection

4.2.1   Sediment samples

During the initial field evaluation, core samples were taken to determine the locations of the profiles. The cores were visually inspected to ensure that fine sediments penetrated a minimum of 18 inches before the location was deemed acceptable for the project. The results led to the locations of the profiles in the northwest portion of the bay.

During most data collection trips, grab samples were taken of the surface sediments with a Mini-Ponar dredge in three locations along each profile. Grab samples were analyzed to determine grain size distributions and organic content. A typical grain size distribution can be found in Figure 4.2.

Organic matter ranged from less than 1 percent to 55 percent with an average of around 10 percent. Complete results can be found in the Appendix. A listing of D_{80}, D_{50}, and D_{20} can be found in Table 4.1.
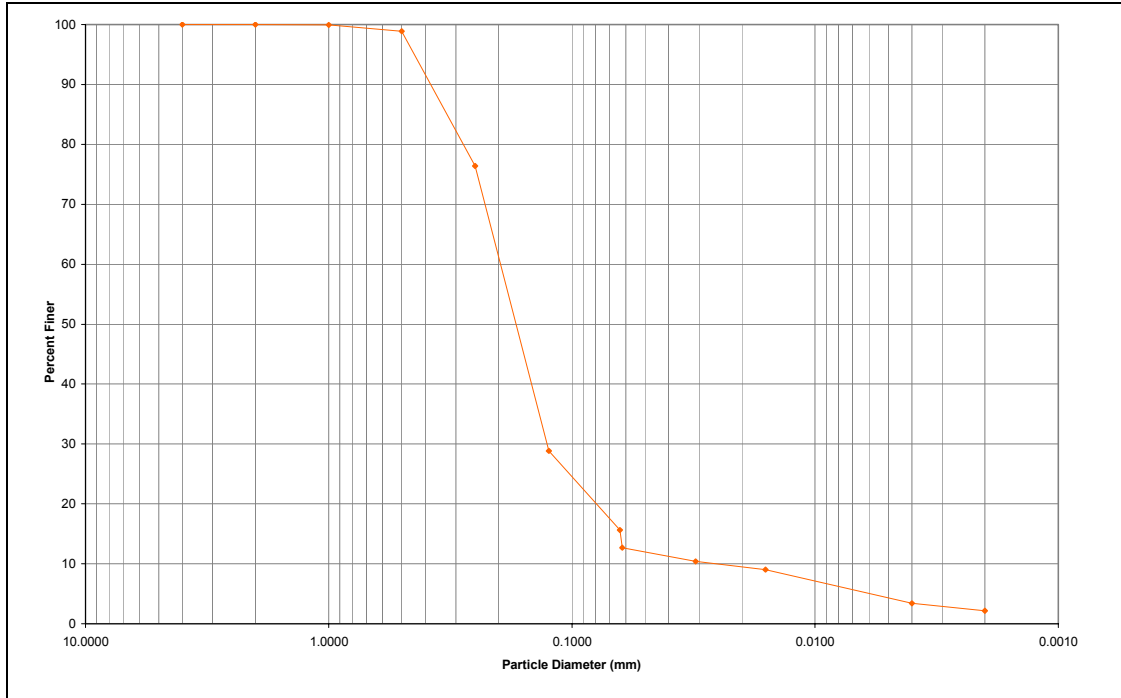
Figure 4.2   Typical grain size distribution curve.

Table 4.1   Summary of grain size distributions.

| Date | Profile | Slope | | ki | Location A | | | D80/D20 | D50/D20 | D80/D50 | Fetch mi |
		Upper	Lower		D20	D50	D80				
3/26/10	CS1	-0.0636	-0.0089	0.119	0.083	0.16	0.24	2.9	1.9	1.5	1.26
	CS2	-0.1835	-0.0094	0.7114	0.021	0.06	0.18	8.6	2.9	3.0	1.06
3/5/10	CS3	-0.1074	-0.0178	0.4873	0.008	0.09	0.18	23.4	11.0	2.1	1.13
	CS4	-0.1024	-0.0155	0.2584	0.008	0.09	0.19	24.1	10.8	2.2	1.38
	CS5	-0.0679	-0.0098	0.0483	0.069	0.15	0.24	3.5	2.2	1.6	1.37
	CS6	-0.112	-0.0147	0.0889							1.42
4/15/10	CS1	-0.0674	-0.0092	0.1296							1.26
	CS2	-0.1611	-0.0088	0.4996							1.06
	CS3	-0.1167	-0.0206	0.341	NO SEDIMENT DATA AVAILABLE						1.13
	CS4	-0.1065	-0.0201	0.2016							1.38
	CS5	-0.063	-0.0099	0.3767							1.37
	CS6	-0.1049	-0.0164	0.0585							1.42
5/6/10	CS1	-0.0673	-0.0091	0.2137	0.085	0.17	0.29	3.4	2.0	1.7	1.26
	CS2	-0.1491	-0.0076	0.596	0.007	0.049	0.16	21.6	6.6	3.3	1.06
	CS3	-0.1262	-0.0155	0.3445	0.007	0.069	0.18	24.3	9.3	2.6	1.13
	CS4	-0.1063	-0.0193	0.0848	0.007	0.09	0.19	29.2	13.8	2.1	1.38
	CS5	-0.066	-0.0101	0.4873	0.110	0.17	0.25	2.3	1.5	1.5	1.37
	CS6	-0.1201	-0.0162	0.0553	0.054	0.13	0.21	3.9	2.4	1.6	1.42
5/21/10	CS1	-0.0704	-0.009	0.176	0.081	0.17	0.25	3.1	2.1	1.5	1.26
	CS2	-0.1531	-0.0077	0.615	0.041	0.013	0.09	2.2	0.3	6.9	1.06
	CS3	-0.1057	-0.0166	0.0566	0.007	0.08	0.17	24.3	11.4	2.1	1.13
	CS4	-0.109	-0.0207	0.0469	0.008	0.076	0.17	22.7	10.1	2.2	1.38
	CS5	-0.0672	-0.0095	0.4293	0.090	0.18	0.25	2.8	2.0	1.4	1.37
	CS6	-0.107	-0.0152	0.0581	0.063	0.15	0.22	3.5	2.4	1.5	1.42

29

4.2.2   Water Samples

Water samples were taken at the beginning of the project at locations spread across Weeks Bay. Total suspended sediments analysis was run on these samples.

A simultaneous collection of water and velocity measurements was initially scheduled. ISCO automated water samplers were to be used to collect water samples at two hour intervals over two tidal cycles at the mouths of the Fish and Magnolia River and the mouth of the Bay. During the same period, an ADCP was to be used to obtain velocity profiles at these three locations. This would allow for validation and improvement of the sediment budget established by Sharp. However, this data collection effort was canceled due to the oil spill response discussed later in this chapter.

4.2.3   Wave height

Wave height data were collected with a Wave Logger II at a central profile over a three week time period. The wave height was recorded at the highest possible frequency, 2Hz, which allowed the data to capture wave frequencies as high as 1 cycle per second. The initial plan was deploy the wave gauge at each profile, but was only deployed at one location due to the oil spill response.

4.3   Other data gathering

In addition to the data collected during the leveling of profiles, other physical and water quality data were also collected.

4.3.1   Salinity

As discussed in Chapter 3, Weeks Bay NERR has four data sondes deployed in the bay. Each sonde is mounted to a piling, thus fixing the measurement vertically. The locations and reference information for these sondes can be found in Figure 3.3 and Table

30

3.1. The sondes collect mostly water quality data, but other data such as salinity and temperature were collected for the duration of the project.
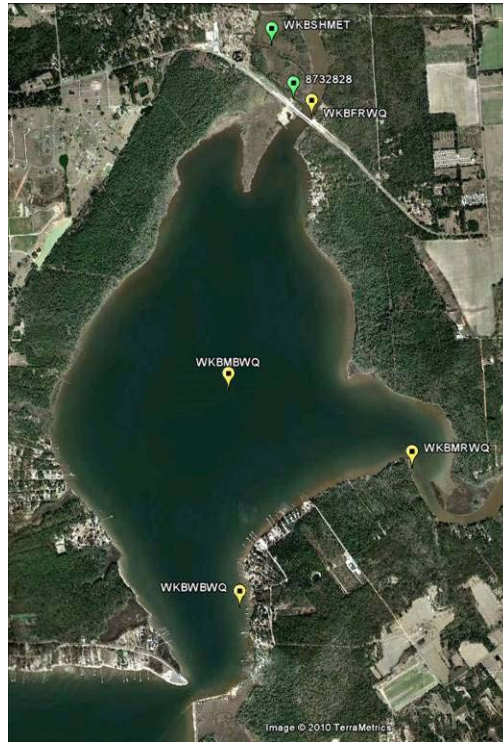
Figure 4.3   Weeks Bay station locations (Google 2010).

Table 4.2   Station reference guide

WKBSHMET	Safe Harbor Met Station	Meteorological
WKBFRWQ	Fish River	Water Quality
WKBMBWQ	Middle Bay	Water Quality
WKBMRWQ	Magnolia River	Water Quality
WKBWBWQ	Weeks Bay	Water Quality
8732828	NOAA Tide Gauge	Tides

31

4.3.2 Tides

Tidal data were collected from NOAA tide gage station number 8732828 (NOAA, 31 May 2010). Six-minute data were recorded for the duration of the project. The location of this station can be found in Figure 3.3.

During the Deepwater Horizon oil spill response, several efforts were made to protect the NERR shores. In addition to booms deployed along the shoreline and across the mouths of the rivers, a new concept was implemented. Barges were placed across most of the mouth of Weeks Bay then sunk to create a solid barrier. It was initially thought that this would allow river flow to exit, but may not allow tidal inflow.

The nearest tide gage, located three miles away near the entrance to the Fish River, was used to test this theory. Analysis of the tide gage data, however, showed tidal influence regardless of the barge placement. While the range was slightly decreased, the tides were not completely diminished.

4.3.3 Meteorological Data

Meteorological data were collected from the NERRS Centralized Data Management Office (CDMO) data export system. Fifteen minute meteorological data including wind speed and direction were recorded. These two datasets were used to correlate with wave heights as discussed in Chapter 6.

4.4 Bathymetry data

The bathymetry data used for the ADH grid was gathered from the NOAA website and is a compilation of all available data (NOAA GEODAS, 28 Dec 2010). The Weeks Bay grid is a 1 arc second grid and the rivers are a 3 arc-second grid (Sharp 2009).

The bathymetry data were then converted into a triangular finite element grid shown in Figure 4.4.
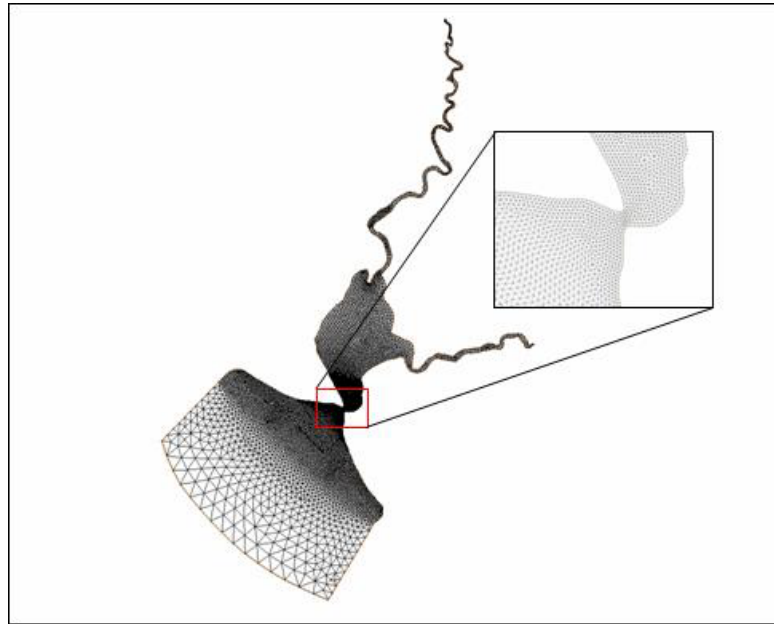
Figure 4.4   Finite element grid for Weeks Bay (used with permission, Sharp 2009)

4.5   Sediment Budget

A sediment budget was created for Weeks Bay by J. Sharp for NGI. The budget was generated based on USGS monitoring and approximations of the ungaged catchment areas. A collection of water samples over two tidal cycles was planned in order to validate and improve the sediment budget.

4.6   Salinity comparison to cross-sections

Salinity was measured at three different locations along each profile on each field trip. These were compared to the continuous data collection by the stationary sondes deployed by the Weeks Bay NERR. The two were in high correlation, with the only difference being the profile salinities contained salinity over depth. Because the profiles

33

are relatively shallow and wave action is almost always present, stratification of salinity was at most 1 psu; therefore, it was deemed that the NERR salinity measurements could be used without adjustments.

4.7   Environmental Hazard

Data collection was disrupted by the Macondo 252 (TransOcean *DeepWater Horizon*) oil spill response. The well released 4.93 million barrels (±10%) or 205.8 million gallons of crude oil between April 20 and July 15, 2010. On September 19, 2010 a relief well was completed and the well was officially deemed dead (OSAT 2010). During this time and the following months while the coast was threatened by the environmental dangers of oil, the coast guard and local communities took a variety of measures to protect the bays and shorelines.

Shorelines were mostly protected by floating booms which have a skirt that extends several inches or feet into the water. The shorelines of Weeks Bay were protected by deepwater booms which had a skirt of over one foot. These booms prohibited passage of a vessel and subsequent research.

In addition, the mouth of the bay was blocked by several large barges which were filled with water and purposefully sunk to reduce flow. While this technique may have protected the bay from intruding oil, it radically changed the hydrodynamics of the bay. Measurements for this project were halted due to these protective measures.

4.8   Aerial Photography

Initially, aerial photography was anticipated being used to analyze long-term evolution of Weeks Bay shorelines. However, all photographs collected were aerials of Mobile Bay with Weeks Bay only roughed in. With the large scale of Mobile Bay, there

34

was a lack of good resolution in Weeks Bay. The aerials of Weeks Bay were not of high enough quality to be properly evaluated.

CHAPTER V

DATA ANALYSIS APPROACH

Data analysis provided the critical link between field data collection and the final algorithm developed. A multi-faceted approach was taken in order to examine all possible solutions. Previously developed equations were examined as well as the derivation of two new equations. The work presented here attempted to maintain accuracy by emphasizing known physics over empirical parameters in order to develop an equation which can be easily implemented into a hydrodynamic model.

5.1   Data Analysis Approach

A tiered approach was used for the data analysis portion of the project. For this approach, three separate tiers are used. The first tier is a rough, quick analysis used to get a general idea of the solution. The second tier is a more in-depth analysis in which a fairly good approximation to the solution is obtained. Lastly, the third tier approach is used to gain full understanding of the solution.

The Tier 1 Approach used in this analysis was a slope analysis. The Tier 2 Approach was an application of Wavelets theory using Matlab. The Tier 3 Approach was an analysis of previously developed equations and improvement upon the most applicable profile equation using Matlab.

36

5.2 Software

The work completed in this document was analyzed primarily using two software packages. Microsoft Excel was used to complete data compilation and the more simplistic analyses while Matlab was used for the more detailed analyses. The slope analysis and statistical analyses were also conducted using Excel.

The vast majority of the work utilized only Matlab and its additional 'toolboxes' (Mathworks 2011). Specifically, the Wavelets toolbox was utilized for a portion of the project and is discussed in Chapter 7. M-files, programmed scripts for Matlab, were generated specifically for the processing of the data used in this project. These scripts were created to allow the file to be generically used for any dataset after simple preprocessing.

5.3 Challenges

The main challenge of this project was data collection. Shoreline data for fine sediments is not readily available since it is so difficult to collect. Locating datasets appropriate for this project was a challenge that led to the development of the data collection project in Weeks Bay. Even with the use of the most up-to-date technology, gathering data for this region can be problematic, and thus, a simplistic data collection process was developed.

Lidar appears particularly useful since personnel do not need to traverse a region of sediments which have no weight-bearing capability, and Lidar can cover large regions at a time. However, regions with fine sediments have higher turbidities, and Lidar cannot resolve less than two feet of depth. Therefore, if Lidar is to be used, it must be flown under extremely low tides in a region where the tide range is great enough to capture the full shoreline. These restrictions limit its capabilities.

37

Other useful technologies such as side-scan sonar, multi- or single-beam echosounders, or ADCPs, all have accuracy and resolution issues when it comes to fine sediments. These technologies rely on changes in density to determine the location of the bottom. However, as the density of sediment approaches that of water (as in many fine sediment beds), the accuracy of the depth reading is compromised. For this reason, these devices have limited use in such an environment.

One of the greatest challenges with this project is the choosing of an appropriate vertical zero for each profile. In most previous applications, a standard zero has been chosen such as MSL or MLLW. However, this is not always an appropriate solution and can vary greatly from location to location. In the case of San Francisco Bay and other areas where the tidal range is high, the MSL can be significantly below the shoreline. In these cases, the developed equations cannot be used. A portion of this work analyzed potential alternatives for locating the origin.

CHAPTER VI

SLOPE ANALYSIS

6.1 Slope Analysis

As discussed in previous chapters, concavity of a shoreline profile can be used as an indicator for depositional or erosional environments (Kirby 2002). On a very simplistic level, concavity and inflection points can be estimated by analyzing the changes in slope across profiles.

It can be easily noted that each shore profile has a distinct 'upper' and 'lower' region (Figure 6.1). Changes over time as well as the relationship between the upper and lower slopes were analyzed for the Weeks Bay dataset. In much the same way as a change in concavity or the severity of concavity may be an indicator for profile evolution, it was considered that changes in slope would act as a similar indicator and would also be mathematically measurable.
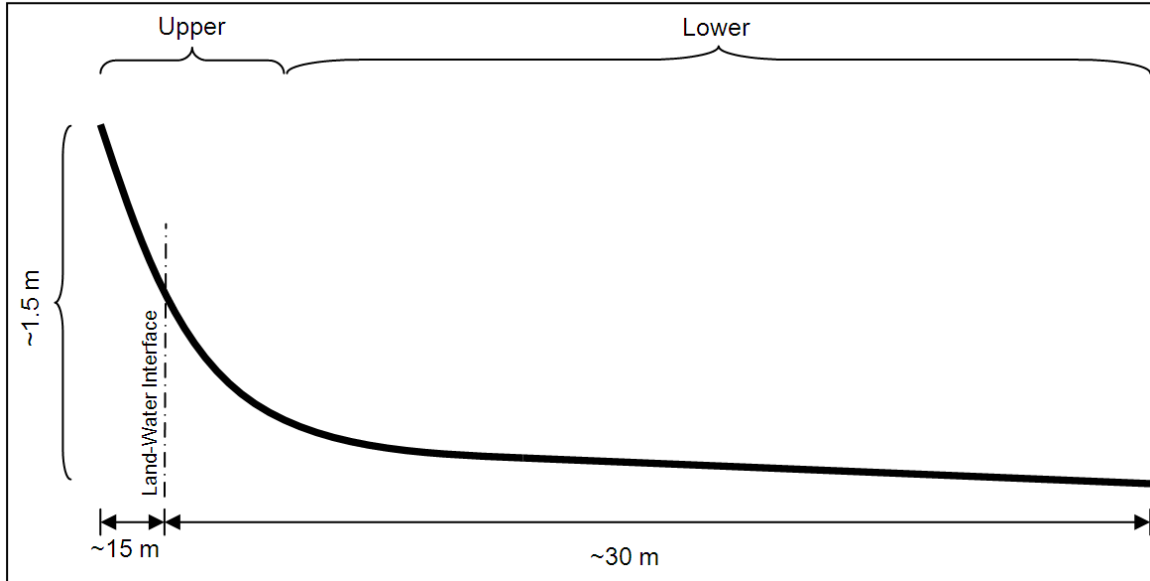
Figure 6.1   Schematic of profile used for slope analysis.

6.2   Approach

For this Tier 1 Analysis, Microsoft Excel was chosen as the software package for analysis. Excel was most appropriate for use in the simplistic manner of the Tier 1 analysis. As previously mentioned, the coordinate system origin was an important topic in this work.

As a first step, the dry portion of the land was removed to ensure that a second inflection point found at the upper portion of the shore was not included. It should also be noted that the bay-ward endpoint for each profile in Weeks Bay was chosen arbitrarily at a depth of around 5 feet after meeting the initial criteria of at least 100 ft in profile length. For the slope analysis setup, the inflection point was chosen as the origin for the new coordinate system. This easily divides the profile into two distinct regions: upper and lower.

Initially, the inflection point was taken as the most visually acceptable location along the profile. The data were then separated into the upper region and the lower

40

region. In an attempt to make the approach as objective as possible, a best fit linear trend was separately fit to both and the upper and lower section. The intersection of these two lines was deemed the 'new' origin.

The two sections were then analyzed somewhat independently. Linear, first-, second-, and third-order polynomials were fit to each section of data. The R^2 value was analyzed to determine the best fit line for each profile section. The slope data were then compiled and compared to identify relationships between the variables (including fetch, date, relationship between upper and lower slope, grain-size distributions and, discussed in Chapter 8, k_i).

6.3   Slope Comparison Analysis

A numerical summary of the slope analysis results can be found in Table 6.1 below. Graphical comparison of the upper and lower slope changes over time appears to be very stable across the data collection period, as can be seen in Figure 6.2 and Figure 6.3. The largest change that can be seen in Figure 6.2 is the decrease in slope at Profile CS2. This change is the largest of the samples, yet is still only 0.04 ft/ft, easily within error tolerances. Figure 6.3 demonstrates even less variance and reinforces the conclusion that no significant change is occurring. Since there were negligible changes in slope over time, a single date for each profile was used for the remaining slope analyses.

Table 6.1   Result of slope analysis and fetch

| Date | Profile | Slope | | Fetch mi |
		Upper	Lower	
3/26/10	CS1	-0.0636	-0.0089	1.6
	CS2	-0.1835	-0.0094	0.8
3/5/10	CS3	-0.1074	-0.0178	1.0
	CS4	-0.1024	-0.0155	1.1
	CS5	-0.0679	-0.0098	1.3
	CS6	-0.1120	-0.0147	1.3
4/15/10	CS1	-0.0674	-0.0092	1.6
	CS2	-0.1611	-0.0088	0.8
	CS3	-0.1167	-0.0206	1.0
	CS4	-0.1065	-0.0201	1.1
	CS5	-0.0630	-0.0099	1.3
	CS6	-0.1049	-0.0164	1.3
5/6/10	CS1	-0.0673	-0.0091	1.6
	CS2	-0.1491	-0.0076	0.8
	CS3	-0.1262	-0.0155	1.0
	CS4	-0.1063	-0.0193	1.1
	CS5	-0.0660	-0.0101	1.3
	CS6	-0.1201	-0.0162	1.3
5/21/10	CS1	-0.0704	-0.0090	1.6
	CS2	-0.1531	-0.0077	0.8
	CS3	-0.1057	-0.0166	1.0
	CS4	-0.1090	-0.0207	1.1
	CS5	-0.0672	-0.0095	1.3
	CS6	-0.1070	-0.0152	1.3
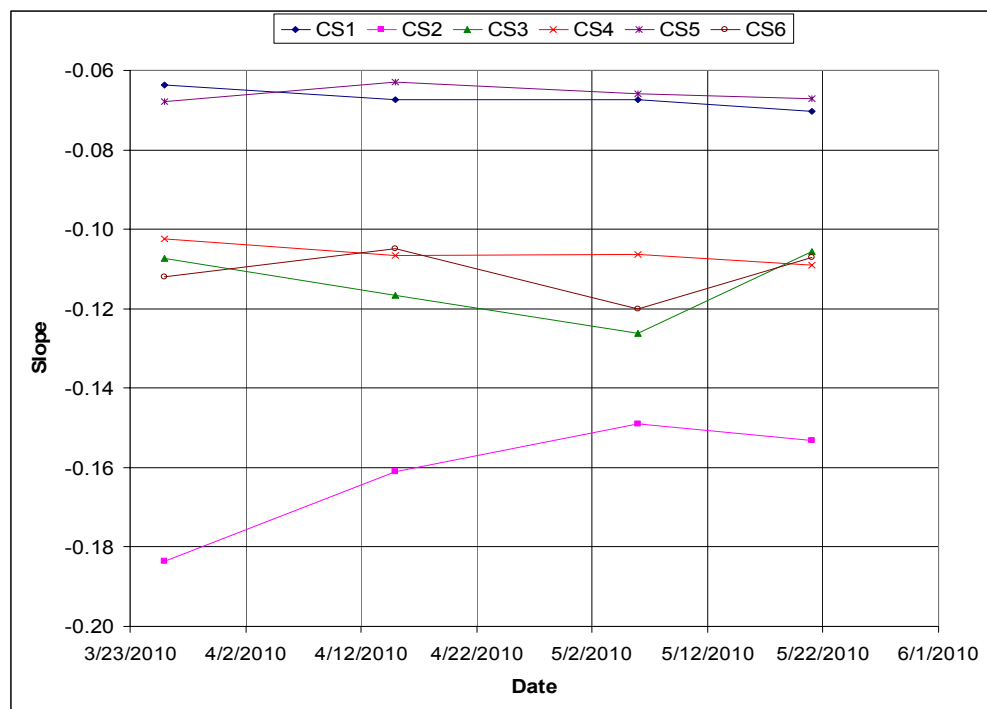
Figure 6.2   Changes in Upper Slope over Time

42
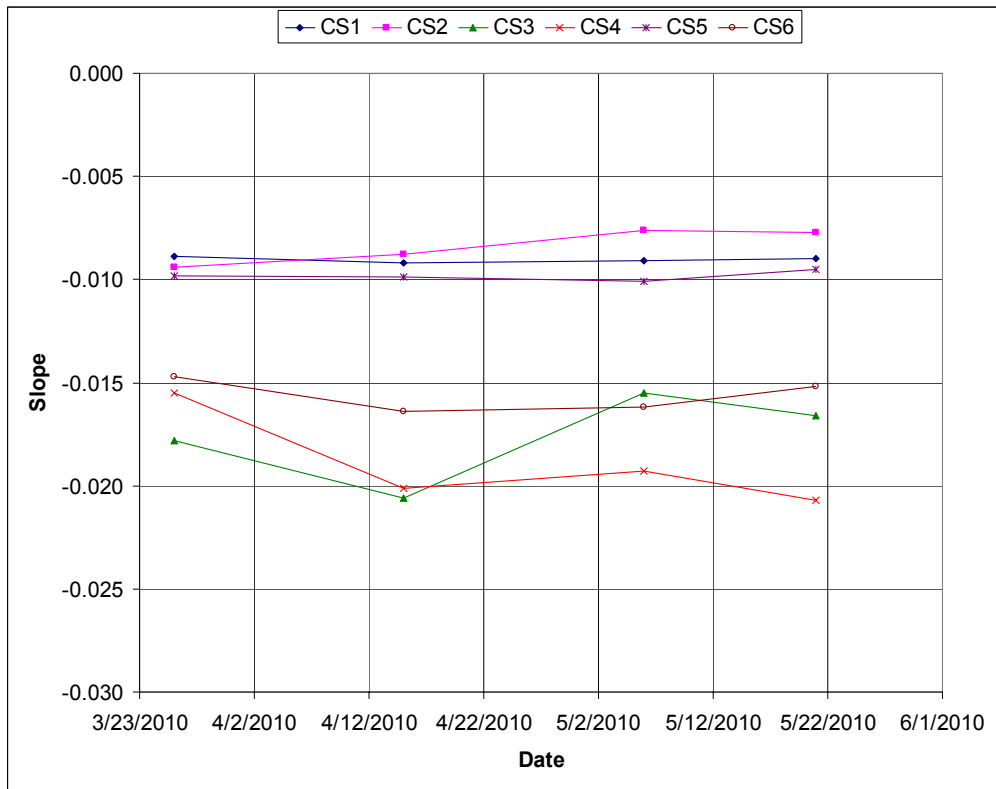
Figure 6.3   Changes in Lower Slope over Time

Additionally, there does not appear to be any direct relationship between upper and lower slope at each profile. Figure 6.4 clearly shows the independence of upper and lower slope. The clusters of data points indicate individual profile relationships which do not change significantly across data collection times.

43
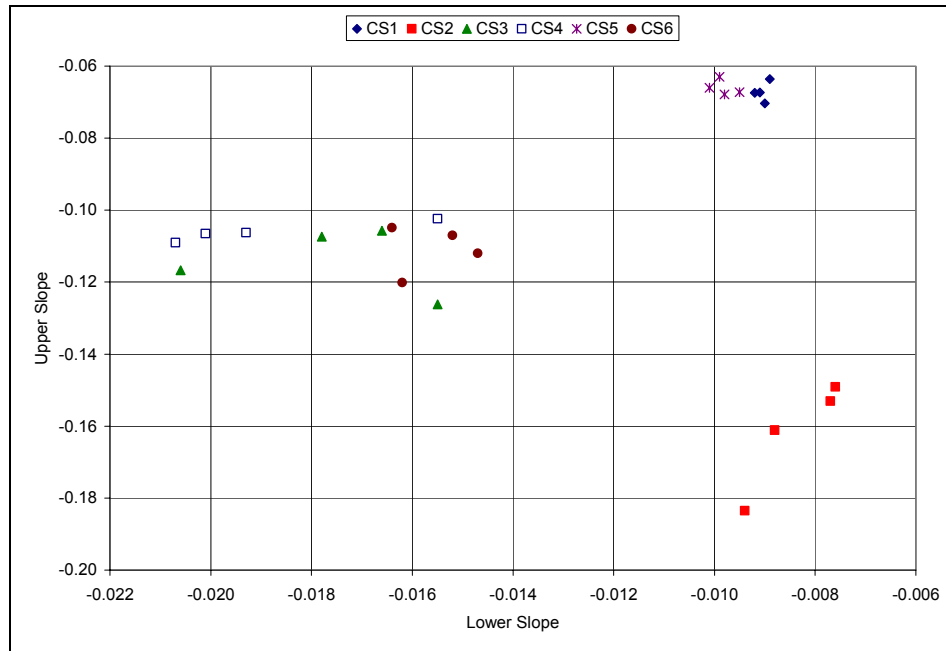
Figure 6.4   Upper slope versus lower slope.

6.4   Fetch Analysis

An abundance of physical factors affect the shape of the shoreline. One of the

biggest factors is wave action, which is closely tied to fetch length in bays and estuaries.

Fetch is a major factor that contributes to the wave height associated with a given wind

speed. As wind travels over a stretch of water, the energy from the wind is imparted to

the water, thus building greater wave height over longer fetches. In Weeks Bay, the fetch

changes from the southernmost profile to the northernmost profile. These differences

cause slight changes in the energy environment of each profile, thus causing variations in

grain-size distributions and profile shape.

Fetch was calculated based on the assumption that wind approaching the shore in

a 90° swath will have a much larger effect than the remaining directions. A fetch length

was measured at 45°, 22.5°, 0°, -22.5°, and -45°, with 0° being roughly perpendicular to

the shoreline. The averages of these values were then calculated. Figure 6.5 shows the

44

fetch calculation guide and the five angles recorded for calculation. As an additional step, the dominant wind was considered and the associated dominant fetch was also measured and recorded. The results for both average fetch and dominant fetch can be found in Table 6.2.
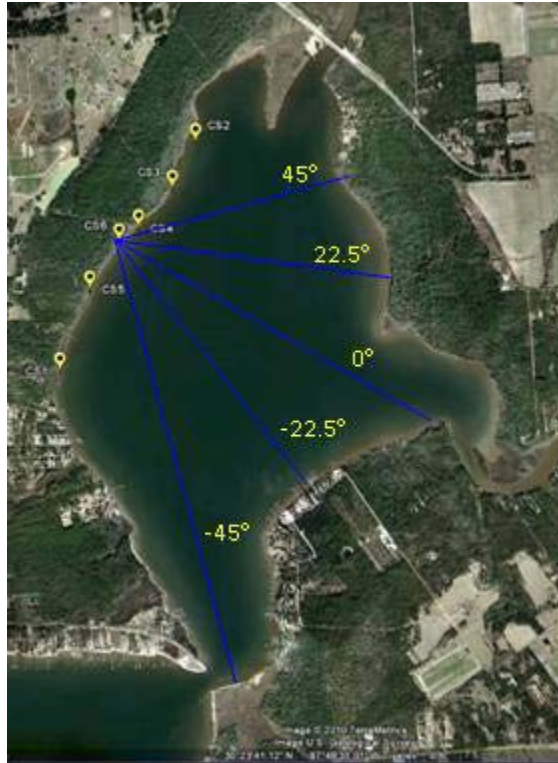
Figure 6.5   Fetch calculation guide.

Table 6.2   Fetch measurements by profile.

Profile Number	Average Fetch (mi)	Dominant Fetch (mi)
CS1	1.26	1.52
CS2	1.06	0.36
CS3	1.13	0.80
CS4	1.38	0.98
CS5	1.37	1.28
CS6	1.42	1.08

Overall, the differences between average fetch and dominant fetch are relatively small. Profile CS2 had a large difference because it was located in the extreme northern portion of the bay and with a dominant wind out of the north, the profile was blocked by the northern shores. It also important to note that Profile CS2 had the largest change in upper slope. Additionally, it is located very near the outlet of the Fish River and may be affected by the fresh water flows and sediment loading of the river more than the other profiles.

The upper and lower slopes were compared to the measured values for fetch (Figure 6.6 and Figure 6.7). The lower slopes do not appear to be affected by fetch, which supports the hypothesis that the slope changes are due to wave energy. The waves are too small to significantly affect the lower slopes (see discussion on waves in Chapter 7).

It can be seen in Figure 6.6 that there is a slight negative correlation between the upper slope and fetch. Additionally, the relationship between upper slope and dominant fetch shows a significant negative correlation (Figure 6.7).

46
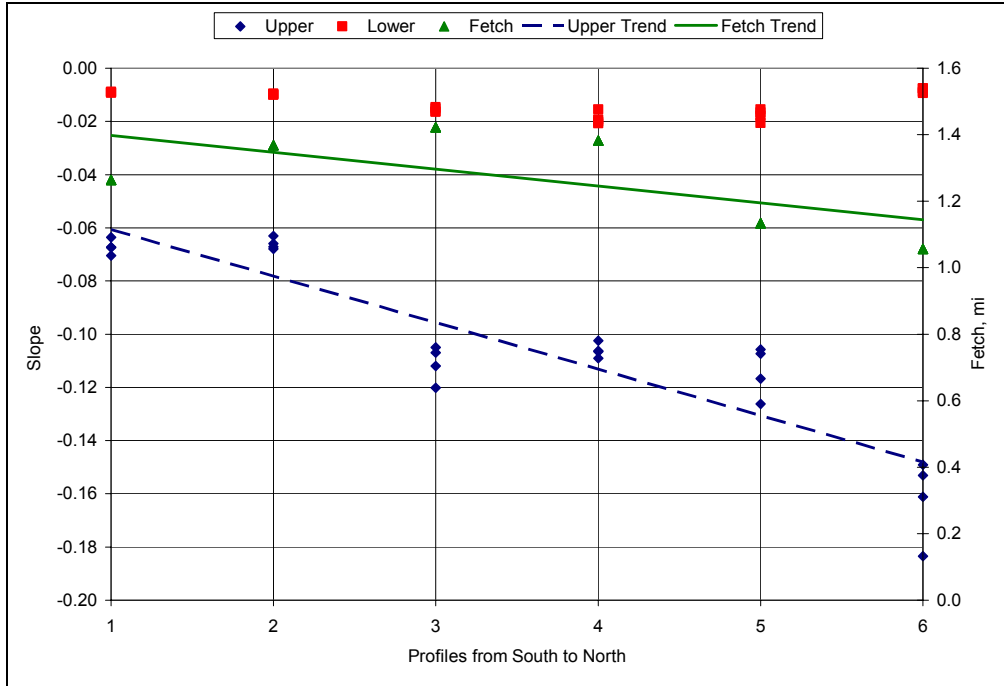
Figure 6.6   Upper and lower slope trends with location and fetch.
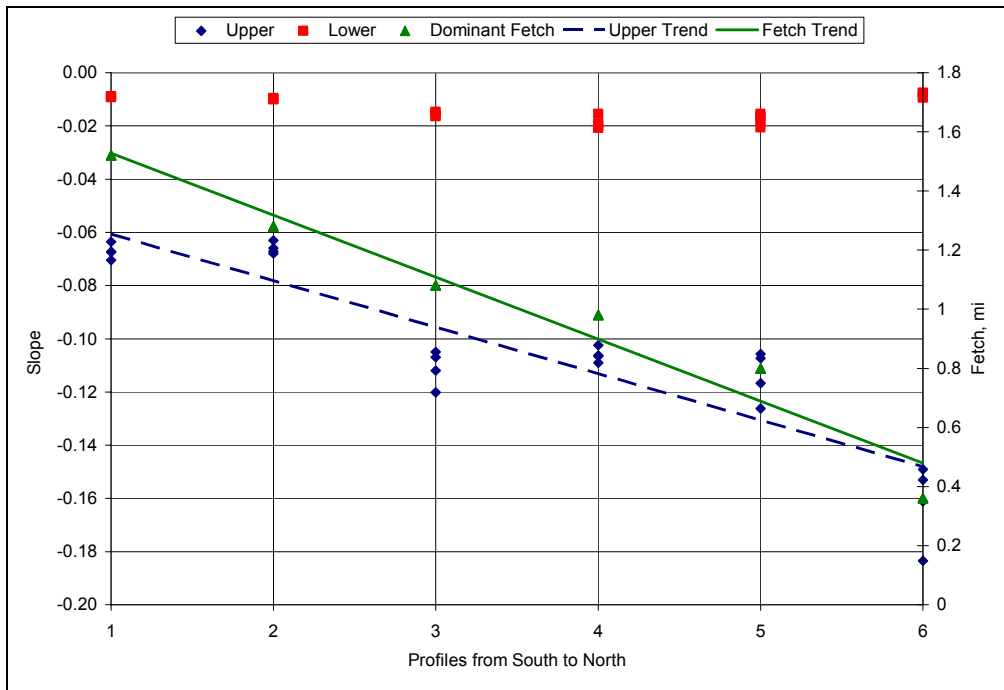
Figure 6.7   Upper and lower slope trends with location and dominant fetch.

47

The upper slope changes from -0.06 on the southernmost profile to about -0.16 on the northernmost profile. As the fetch decreases, the steepness of the slope increases. As a slope becomes more negative, the steepness increases. This result is counterintuitive and goes against the hypothesis that the system is wind-driven. However, it is also important to note that the differences in fetch, as well as the differences in slope, do not vary widely across profiles. The lack of dramatic change, coupled with the small data collection window, could be affecting these results.

6.5   Mathematical Analysis

After shifting the coordinate system origin, a combination of best-fit curves were applied to each dataset on the upper and lower slopes. The second order trendline had the highest R^2 values, but as can be seen in Figure 6.8, there are some problems associated with the fit. The fit to the lower slope is, in general, a poor fit. Additionally, the intersection of the two lines causes a significant break point due to the difference in slope.
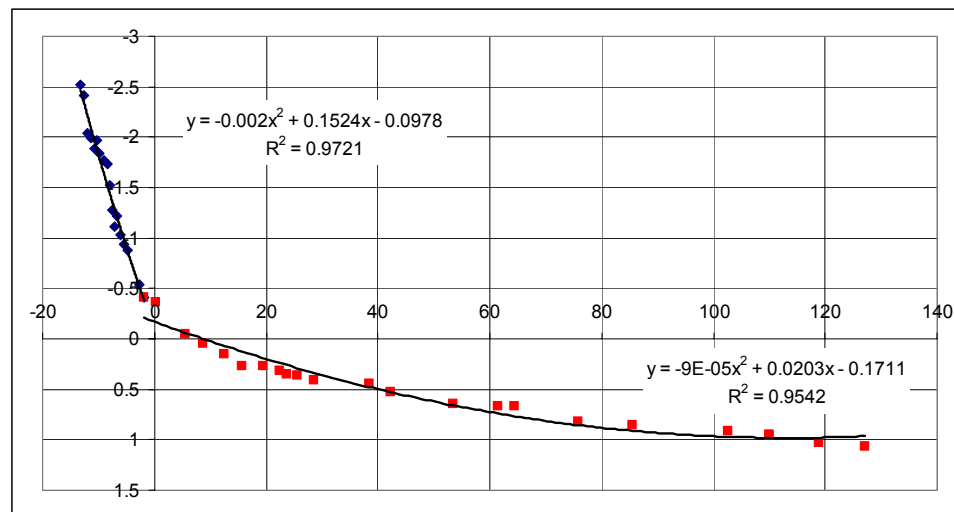
Figure 6.8   Initial curve-fitting upper and lower slopes.

48

In an attempt to reconcile this problem, the upper and lower datasets were combined and re-evaluated. Again, the second order polynomial gave a relatively good fit to the data (Figure 6.9). Comparing Figure 6.8 and Figure 6.9, it can be seen that the fit to the lower slope is slightly less desirable, but the break point has been resolved. For input into a numerical model, the smoother line would be the more desirable result.

The chart displays the equation $y = -0.0036x^2 + 0.1038x - 0.3925$ and $R^2 = 0.9783$.
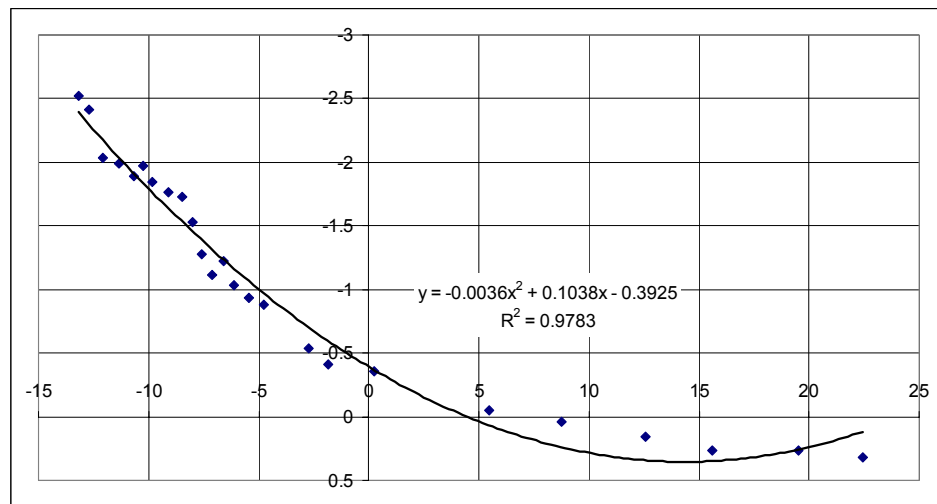
Figure 6.9   Second-order polynomial curve-fitting profile

Recall the total length of each profile was chosen somewhat arbitrarily (roughly 130 ft total length). For this reason, it is possible to remove as much of the interior, or bay-ward, data points as necessary. In order to resolve the poor fit at the lower slope, data were removed until an optimal fit was found. Comparing Figure 6.9 and Figure 6.10, the R^2 values are close, but Figure 6.10 is a significantly better fit. Figure 6.11 has the same fit as Figure 6.10 but shows the entire dataset. Additionally, the remaining data points proceed in a direction similar to the endpoint of the trendline instead of the dramatic break point seen in Figure 6.8.

49
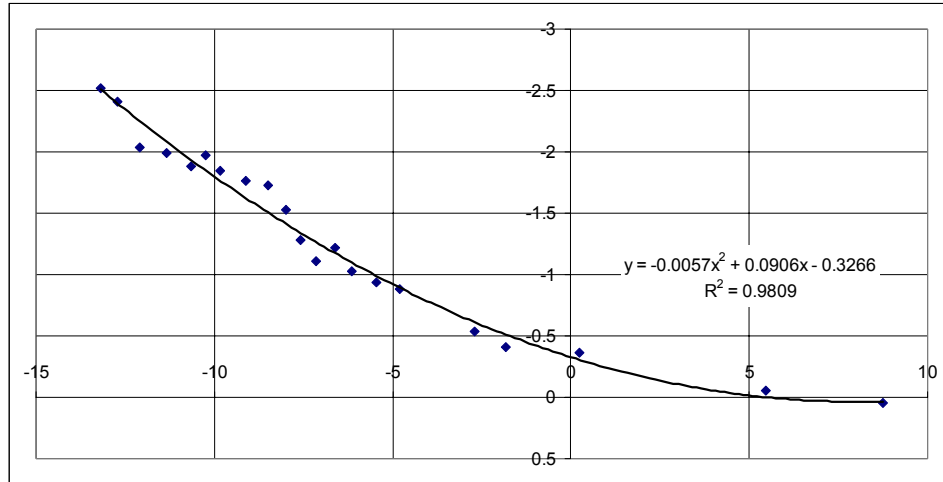
Figure 6.10   Final second order polynomial curve-fit.
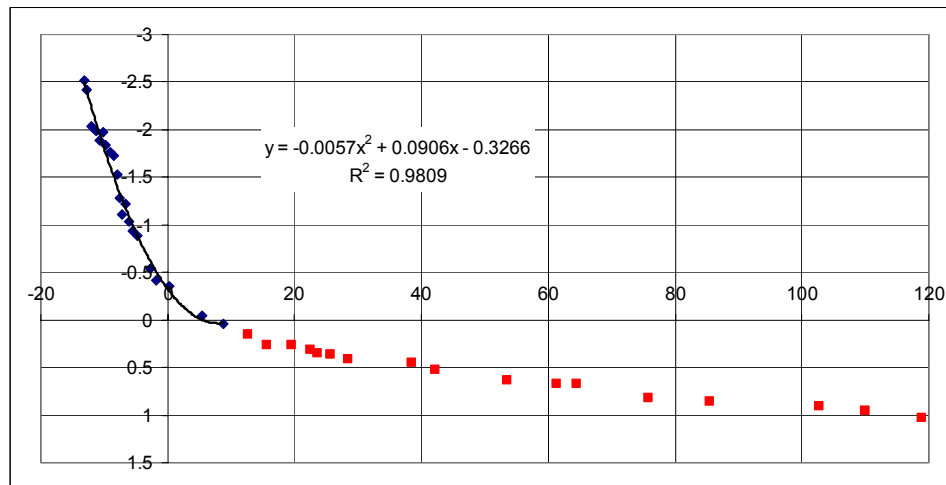
Figure 6.11   Final curve-fit showing entire profile.

6.6   Conclusion

According to the curves of changes in slope over time, there is a negligible amount of change occurring during the time frame of the experiment. This could have been due to the length of the sampling period being too short, the method of measurement being too imprecise, or because the season was relatively quiet and most sediment movement only occurs during storm events.

50

The initial visual analysis chose a break point between upper and lower slopes which was at the center of the inflection point and too far land-ward. However, there is a slight trend to the location of the break points using the upper versus lower profile linear-fit method. If the break point is chosen as the point at which the slope no longer changes significantly (just beyond the inflection point), the fit can be easily made. Of course, while this is qualitative, it was the best approach found for this method. Additionally, the initial location of the origin has been deemed inappropriate and will be analyzed further in later chapters.

CHAPTER VII

WAVELETS ANALYSIS

Wavelet theory has a multitude of applications from de-noising sound waves to image compression. Because each waveform is unique, each has a different set of applications depending on the dataset and the desired result. A new, unique approach was taken to analyze the data by applying wavelets to the shoreline profiles. With a quick glance at a profile of the vertical face of the shoreline, it can be seen that it has curvature that exhibits certain wave-like qualities. This concept led to the thinking that the shoreline could be analyzed as a wave using wavelets to better understand and track changes over time.

7.1   Wavelets Background

A wavelet is any number of waveforms which produce wave-like oscillations. These can be used to transform datasets into a wavelet function which can be manipulated and analyzed. Wavelets are most often used in signal processing and data compression. However, the ability to apply numerous wavelet functions to analyze a signal allows the method a variety of uses.

Wavelets are generally used for signal processing in which the signal, *S(t),* typically a time series, is transformed from the time domain to some arbitrary domain specified by the wavelet function. However, time can be replaced by any continuous parameter such as the profile distance used in this work. The general form of the continuous wavelet is described as

52

$$W(\omega,\tau) = \int_{-\infty}^{\infty} S(t)\Psi_*(\omega,\tau)\, dt \qquad\qquad \text{Equation 7.1}$$

where

$$\Psi_* = \frac{1}{\sqrt{\omega}}\Psi\left(\frac{t-\tau}{\omega}\right) \qquad\qquad \text{Equation 7.2}$$

and ω is the scale factor, τ is the dummy variable, and Ψ is the wavelet function. The wavelet function is satisfied by:

$$\int_{-\infty}^{\infty} \Psi(\omega,\tau)\, dt = 0 \qquad\qquad \text{Equation 7.3}$$

The original signal can be reconstructed back into the original domain by:

$$S(t) = \iint W(\omega,\tau)\Psi(\omega,\tau)\, d\omega\, d\tau \qquad\qquad \text{Equation 7.4}$$

The Wavelets Toolbox in Matlab contains coding for 15 different wavelets. For this work, two wavelets were chosen which the best results for the dataset: the Daubechies (order 2) (Figure 7.1) and the Meyer wavelets (Figure 7.2).
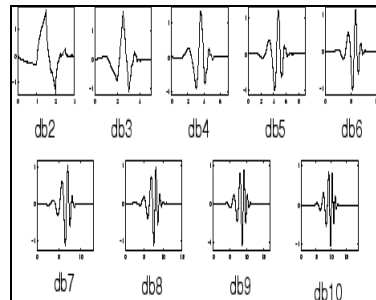
Figure 7.1   Daubechies waveform (© 2011 The MathWorks, Inc., image used by express permission).

53
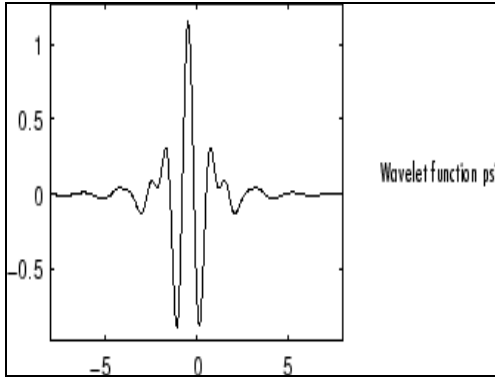
Figure 7.2   Meyer waveform in the frequency domain (© 2011 The MathWorks, Inc., image used by express permission).

The Daubechies wavelet was chosen for the accuracy of the results obtained. The Meyer wavelet was thought to produce better results due to the structure of the wavelet itself. Both of these wavelets exhibited the best overall fit given the options provided by Matlab.

Wavelet analysis is essentially a multi-step filtering process. With each application, or level, a low pass filter and a high pass filter are applied. The low pass filter produces what is known as the Approximation (*A*) (corresponding to ω in Equation 7.2) and the high pass filter produces the Detail (*D*) (corresponding to τ in equation 7.2) (Figure 7.3).
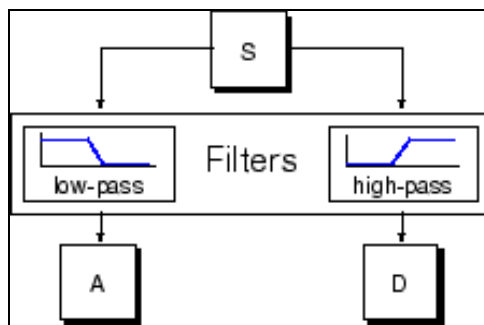
Figure 7.3   Application of wavelet to signal, *S* (© 2011 The MathWorks, Inc., image used by express permission).

54

After the first application of the filter, the results are then down-sampled to reduce the number of data points by one-half. Data compression is one result of the down-sampling. This process can be repeated several times, applying the filters again to the Approximation from the previous level. Figure 7.4 shows a schematic of a level 2 wavelet application to a 1000 sample signal. The wavelet coefficients can be retained for signal reconstruction in the case of data compression or, as in this work, analyzed for trends between datasets.
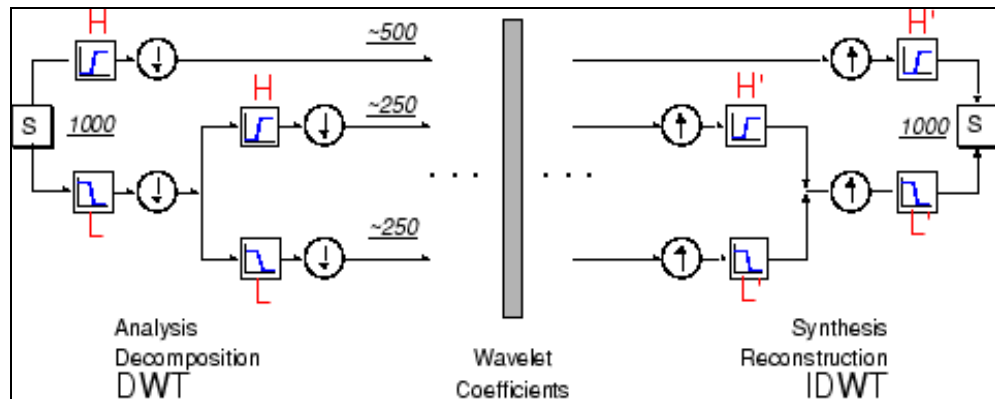
Figure 7.4   Overview of signal decomposition and reconstruction (© 2011 The MathWorks, Inc., image used by express permission).

With each subsequent level, the wavelet is again applied to the previous Approximation array and a new Approximation and Detail are generated (Figure 7.5). The original signal can be reconstructed by adding the final Approximation coefficients and the sum of the Detail coefficients. Figure 7.5 demonstrates the relationship between the original signal and the Approximation and Details.
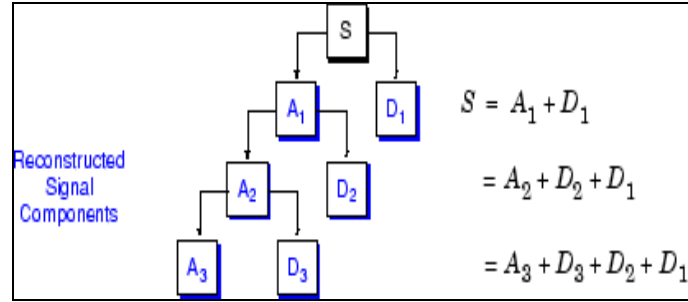
Figure 7.5   Tree diagram of decomposition and reconstruction of wavelet (© 2011 The MathWorks, Inc., image used by express permission).

Matlab utilizes the relationship

$$S = A_n + \sum_{i=1:n} D_i$$
Equation 7.5

to reconstruct the signal from the coefficient arrays, where A is the Approximation array, D is the Detail array, S is the reconstructed signal, and n is the level number. The equivalent continuous form of Equation 7.4 is found in Equation 7.4.

Because each level of decomposition reduces the number of data points by one-half, the number of levels applicable to each dataset is dependent on the number of data points in the analysis.

7.2   Data Preprocessing

The profile data for Weeks Bay were used in this analysis. The data first had to be put into a format in which the profiles could be compared easily. Each profile was scaled to the range [0 1] in both the vertical and horizontal dimensions. In order to prevent skewing of the results due to the variety of density of data points along the profile, cubic spline interpolation was used to create uniformly spaced datasets. Each profile was required to have different spacing in order to obtain the best-fit cubic spline for each profile. Too little resolution in the cubic spline resulted in lost features while too much resolution resulted in the generation of false artifacts. Figure 7.6 shows the optimal

56

correlation between the Raw Data and the cubic spline data for four different data collection days at a single profile.
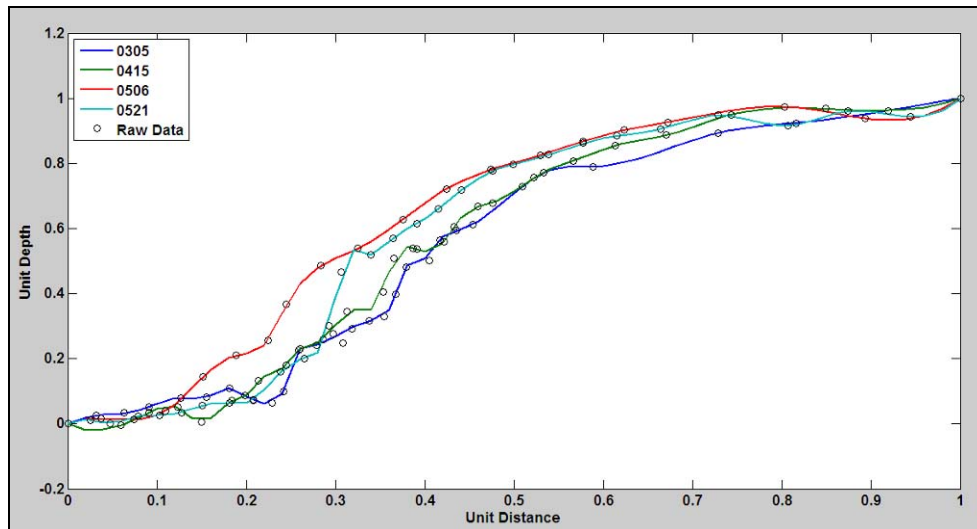
Figure 7.6   Comparison of original data to cubic spline

It can be seen that the optimal spacing was not always consistent across data collection days; therefore, the best overall spacing was chosen for each profile. The spacing used for each profile can be found in Table 7.1.

Table 7.1   Cubic spline spacing for each profile

Profile No.	Unit Spacing
CS 1	0.02
CS 2	0.02
CS 3	0.04
CS 4	0.01
CS 5	0.01
CS 6	0.01

Wavelets were then applied to the resulting cubic spline datasets. Based on the least number of data points obtained from the cubic spline, the highest level of Wavelet decomposition which could be applied to all profiles was level 5.

57

7.3 Wavelets Results

When wavelets were applied to the data, Level 1 appeared to have the best fit, but in order to obtain a variety of results, Level 5 was also run for each profile and day. For the level 1 application, the method produces only one of each Approximation and Detail, as in Figure 7.3. For the Level 5 application, one Approximation and five Detail arrays are generated for each level.

The wavelet results, Approximation, A, and Detail, D, were analyzed to discern relationships between the two, as well as relationships between the data collection days and the profile number. The mathematical relationship between A, D, and S can be seen in Equation 7.5; it was anticipated that the results also had a significant relationship to the physical forcings of the environment. These would be discernable in comparison of the results of one profile to another or in the comparison of day to day results.

The comparison of A and D proved to be insignificant. Figure 7.7 shows a typical plot of A versus D, representative of both the Daubechies and the Meyer wavelets.
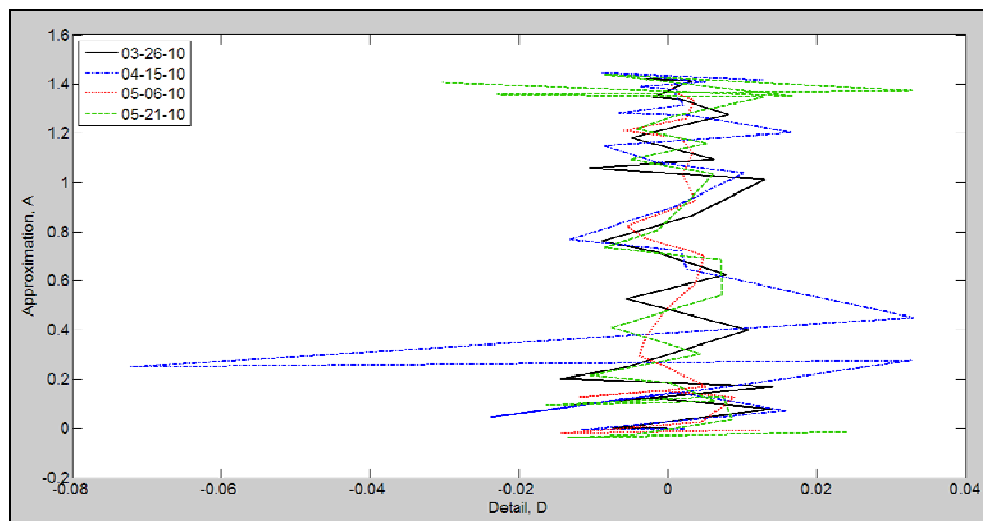
Figure 7.7   Representative plot of Approximation, A, versus Detail, D

58

The main use for the wavelet coefficients, A and D, is to provide a method of reconstructing the signal from the compressed dataset. In this work, relationships between A and D and physical forcings were analyzed, but it is also important to note the accuracy of the reconstruction using these coefficients. Figure 7.8 and Figure 7.9 show the raw data and Level 1 reconstructed dataset for the Daubechies wavelet for Profile CS1 on two different days. It can be seen in these figures that the reconstruction is flawed. The reconstruction begins in equality with the original signal, but then slowly increases beyond the original dataset. The discrepancy between the two increases as the profile length increases.

Additionally, Figure 7.8 shows the error induced by the cubic spline interpolation. The sharp peaks and troughs found in the reconstructed signal are artifacts of the interpolation and a numerical model may not be able to handle such sharp changes. The reason for this error is likely the fact that the cubic spline was forced to estimate the signal without high enough resolution. However, a higher resolution would have resulted in a similar array of errors from the other data collection days. It should also be noted that the same result does not occur in Figure 7.9 which has a smooth change in depth unlike the peaks and valleys found in Figure 7.8.
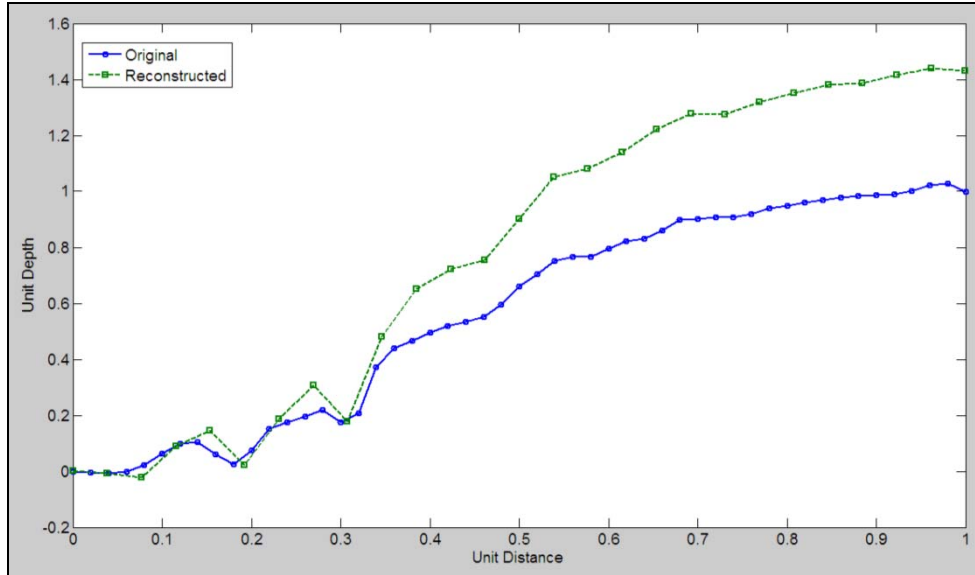
Figure 7.8   Original and reconstructed level 1 signals showing poor reconstruction.
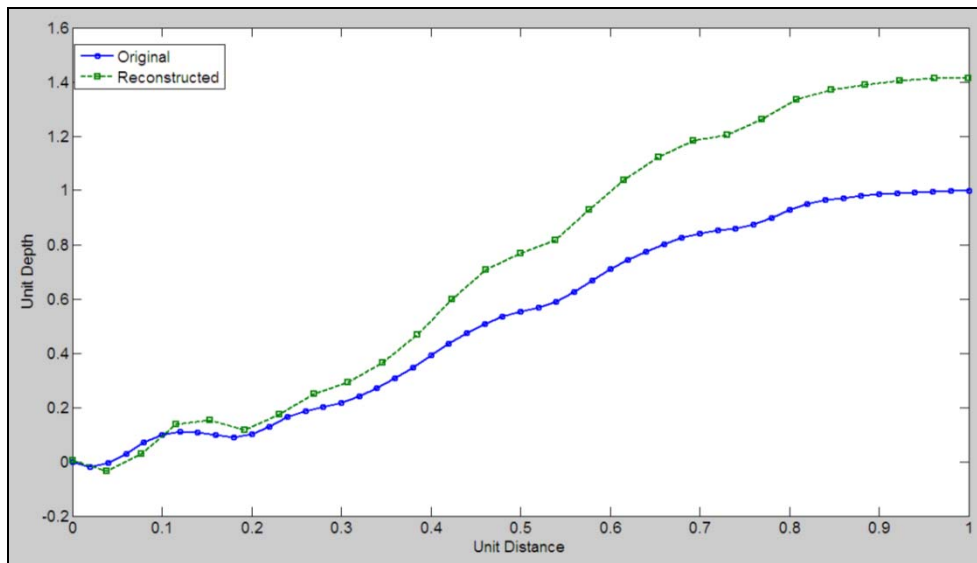
Figure 7.9   Original and reconstructed signal showing smooth reconstruction.

It can be noted that the reconstruction does retain a similar shape to the original signal. As an alternative, the reconstructed signal may be re-scaled [0 1], producing a relatively good match. While this method would produce highly correlated results, the additional manipulation would degrade the integrity of the results.

60

The Level 5 reconstruction was expected to be more accurate than the Level 1 reconstruction since there are more variables generated which should 'fine tune' the results. However, this was not the case. For both the Daubechies and Meyer wavelets, the level 5 results were extremely inaccurate. Similar to the Level 1 results, the level 5 results begin at zero, with no error. They slowly begin to deviate from the original signal. Figure 7.10 shows the individual Approximation and Detail results for a representative set of Daubechies wavelet coefficients. While the original cubic spline was ranged [0 1] in both the vertical and horizontal, the Approximation increases dramatically to approach 6 units in depth.
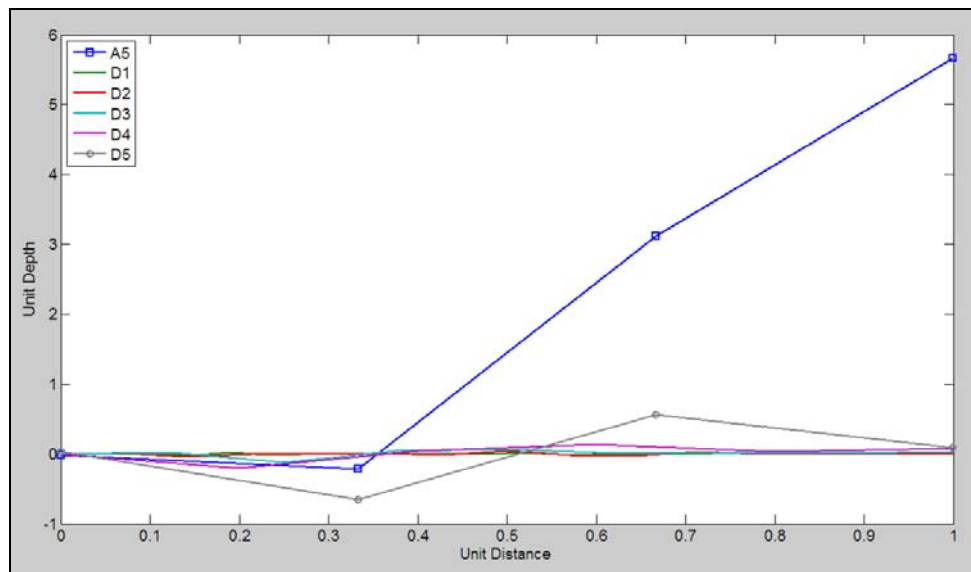
Figure 7.10   Daubechies Level 5 Wavelet Coefficients over profile length.

Due to the varying point densities, mathematical manipulation was required prior to applying Equation 7.5. The results are shown in Figure 7.11 and Figure 7.12. The Level 5 Approximation dominates the results, showing what should be the general profile shape, while the sum of the Detail coefficients shows more slight variations (Figure

61

7.11). The dramatic increase caused by the Approximation does not follow the general profile and the Detail array is unable to balance the change.
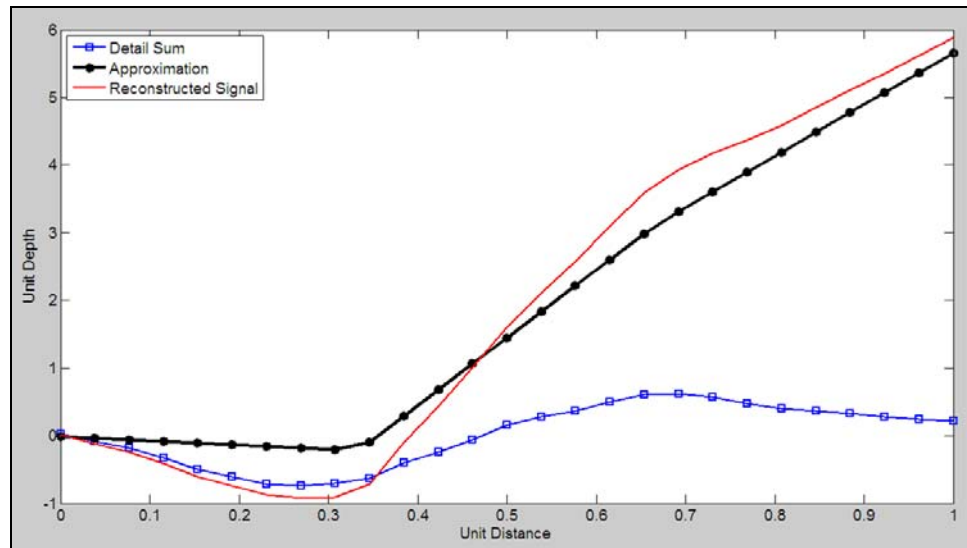
Figure 7.11   Reconstruction of Daubechies Level 5 Signal.

It is also important to note that the level 5 reconstructions of both the Daubechies (Figure 7.12) and the Meyer (Figure 7.13) wavelets, the approximation coefficients have distinct similarities to the original wavelet (Figure 7.1 and Figure 7.2).
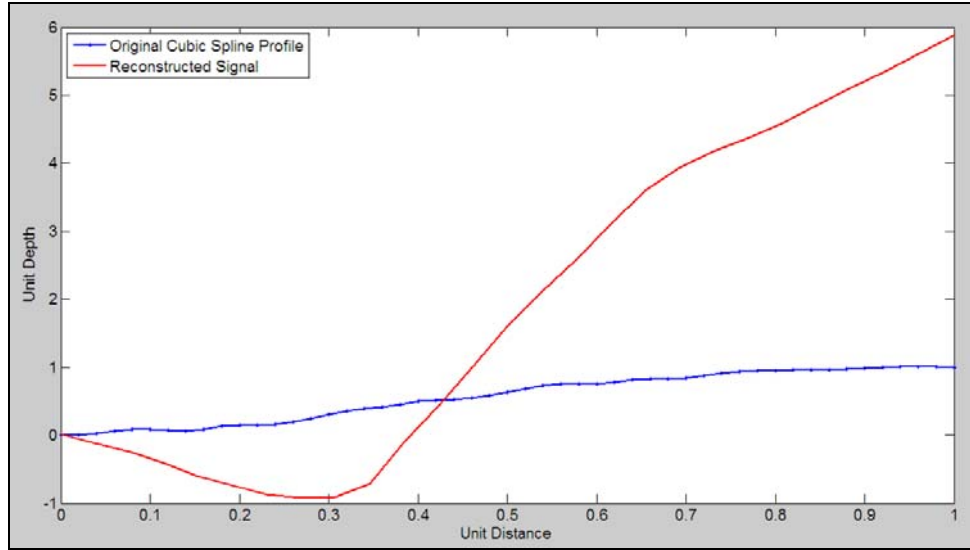
Figure 7.12   Comparison of Reconstructed Daubechies Signal and Original Signal.
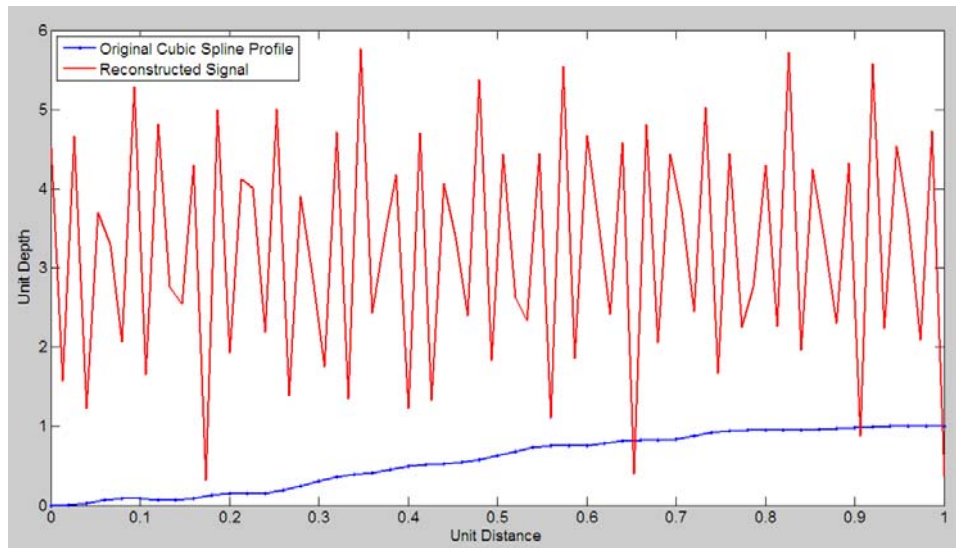
Figure 7.13   Comparison of Reconstructed Meyer Signal and Original Cubic Spline.

It is thought that the errors in the results are caused by the coefficients striving toward similarities with the original wavelet.

63

7.4   Conclusion

The wavelets theory is based on separating the main signal from the noise in the signal. It was thought that the 'main signal' or base shape of the profile would be somewhat constant while the 'noise' would be small differences in the profiles. The noise could be attributed to differences in characteristics such as grain size distribution and wave energy.

As the level is increased, the resulting Approximation begins to transform into the wavelet shape, often repeating itself over the signal length. The Detail array changes to accommodate this transformation and equalize Equation 7.5, effectively producing random results. The hypothesis was that either the Approximations or the Details could be analyzed for trends between profiles or physical properties of the profiles. However, if the results tend to approach the shape of the original wavelet, this hypothesis has already been proven incorrect.

Also, when the wavelet coefficients are used to reconstruct the original signal, the results continually overestimated the original signal. Inaccuracies can be attributed to the down-sampling that occurs during the wavelet application. As can be seen in Figure 7.8 and Figure 7.9, the reconstruction begins perfectly, and then gradually drifts higher than the original. The end results are incorrect by 40 to 60 percent.

Additionally, the relationship between *A* and *D*, as seen in Equation 7.5, can also be used to disprove the original hypothesis. The simplicity of this equation is its downfall. It is clear that relationships in nature are never this simple and thus, this relationship cannot be expected to reflect nature. While it was, however, expected that these could be the results of two separate sets of natural influences, it should not be expected that any natural relationship would have such a simplistic relationship.

64

It is concluded that traditional statistical analysis will be more useful to determine parameter relationships than this method.

7.5 Wave Data Analysis

Fast Fourier Transform (FFT) is a mathematical technique which is used to transform data from the space-time continuum to the frequency domain. This allows the data to be viewed from a different perspective and can provide a more in-depth understanding of the data.

Wave data were collected at a central profile in Weeks Bay over a three week period using a Wave Logger III by Ocean Systems. The data were collected at the highest possible frequency, 2 Hz, generating roughly 3.3 million data points. Running FFT on a dataset this size is not recommended since it requires an advanced computing power. The data were initially run in portions until a streamlined M-file could be generated to handle the entire dataset.

Because of the large sample size, all frequencies are well represented. Most of the wave energy lies in the frequency range of 0.5 to 1 Hz which corresponds to periods of 1 to 2 seconds (Figure 7.14). These small, high frequency waves were expected due to the relatively small size of the bay and the small inlet; no swells are able to enter or build up in the bay. Because the sampling rate was 2 Hz, all periods smaller than $2\Delta t$ will be aliased; therefore, the lowest period measured was 1 second.

65
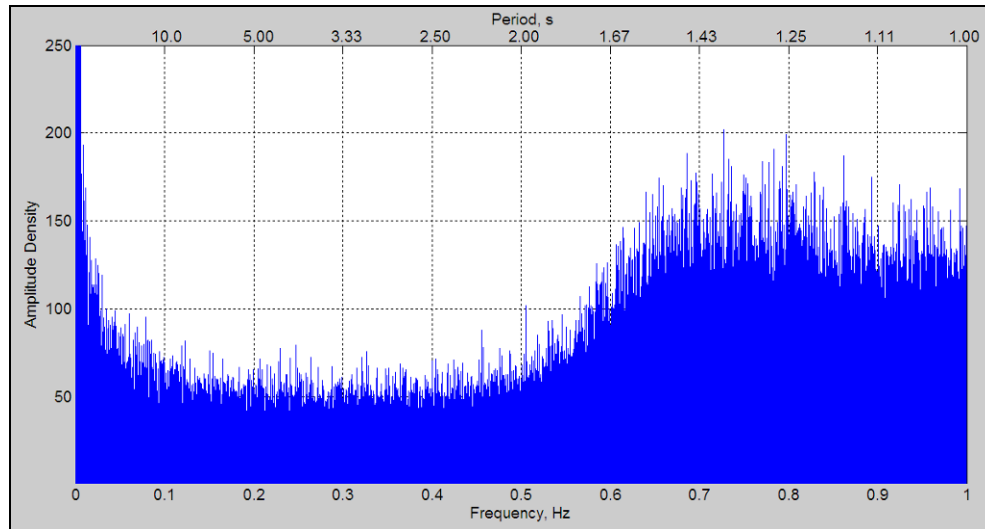
Figure 7.14   Fast Fourier Transform Results

A higher density of low frequency waves can also be seen in Figure 7.14, but this was expected. Tides were not removed prior to the FFT analysis, and thus were expected to appear as dominant frequencies in the results. Table 7.2 shows the dominant harmonic constituents for Weeks Bay and the associated frequencies. The effect of these can be seen in Figure 7.15 where only the lower frequencies were plotted against a large scale amplitude.

Table 7.2   Dominant Harmonic Constituents.

Const.	Amplitude	Frequency
	(ft)	(s^{-1})
K1	0.479	1.16E-05
O1	0.453	1.08E-05
P1	0.138	1.15E-05
Q1	0.095	1.02E-05
M2	0.066	2.24E-05
S2	0.033	2.31E-05

www.manaraa.com
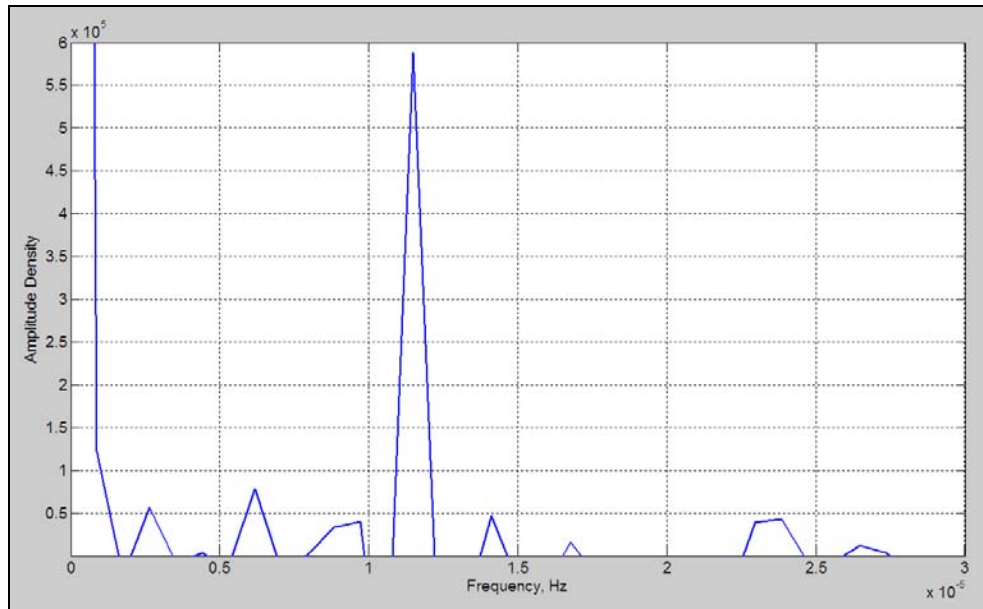
Figure 7.15   FFT results for low frequencies.

Some of the smaller frequencies found in Figure 7.15 can be attributed to tidal influences. Others may be occurrences of noise or random events. Given the number of data points in the analysis, noise is likely the cause of these anomalies. Comparing Table 7.2 and Figure 7.15 it can be seen that the harmonic constituents which most strongly affect tides, appear as dominant frequencies in the wave analysis.

CHAPTER VIII

QUANTIFYING SHORELINE EROSION

Shoreline evolution is a topic of great interest due to its implications in land loss, sediment as a pollutant, as well as loss of biological habitat. While many mathematical approaches have been taken to quantify shoreline evolution, none have specifically been designed to operate within a numerical model. The work presented here makes an attempt to bring the equations quantifying shoreline evolution to the scale of numerical models. In addition, application to a field site demonstrates the validity of select equations.

Of the mathematical equations previously generated, the equation developed by S.C. Lee, based on wave dissipation, appears to be the mostly widely accepted. While other equations were also evaluated, this is the primary equation used in this work. Attempts to improve the equation and alter it for implementation in a numerical model have been made.

8.1 Approach

The Tier 3 Approach to this work was to apply previously developed equations to the profiles collected in this project. The equations utilized have been widely accepted by the research community, and therefore it was hypothesized that at least moderately accurate results would be obtained. However, because the demonstration environment of Weeks bay is a low energy, shallow estuary, it was also expected that improvements could be made to the existing equations in order to improve accuracy.

Matlab was the main software used in the mathematical analysis portion of this approach, and Excel was used for a portion of the comparison work. The Matlab script and M-file format was invaluable for this analysis as it allowed for quick processing of large amounts of data. M-files can be written as a program to run within Matlab. As such, after initial inputs are established, the remainder of the program can run independently without further input from the user.

8.2   S.C. Lee Equation Overview

As discussed in Chapter 2, the equation developed by S.C. Lee (1995) was based on the change in wave height caused by bottom interaction as it approaches the shoreline. It was thought that the shore profile will match the change in wave height perpendicular to the shoreline. Lee has had acceptable success with this method in large applications, and the equation appears in a multitude of literature. Because it has been the most widely accepted equation for this purpose, it was chosen to be the focus of this work and was analyzed for accuracy and potential improvements.

Lee originally developed an equation which was derived from a wave height dissipation equation:

$$h = h_o e^{4\overline{k_i}(y-y_o)} \left(\frac{y}{y_o} \right)^2 \qquad \text{Equation 8.1}$$

where k_i *bar* is an average wave attenuation coefficient and (h_o, y_o) are the terminal water depth and distance offshore.   However, this equation did not account for the slight inflection caused by the on-shore berm.

69

To account for the inflection, Lee developed an additional slope term which added an empirical coefficient (β) and a profile-specific coefficient (F). Lee's final equation is described as

$$h = Fye^{-\beta y} + (h_0 - Fye^{\beta y})e^{4\bar{k}_i(y_0-y)}\left[\frac{y}{y_0}\right]^2 \qquad \text{Equation 8.2}$$

where F=slope at land-water interface, β=profile specific coefficient, k_i=wave attenuation coefficient, y=distance along profile, y_0=location at which waves influence the bed. (Lee 1995).

While this addition improved accuracy among the profiles Lee tested, it also introduced two new parameters to the equation. The addition of the slope term is practical, but also requires an addition calculation or field measurement. Additionally, the shoreline is often a sine-like curve with a constantly changing slope which makes defining F difficult. The second parameter, β, is a profile-specific empirical parameter, and Lee does not suggest any physical meaning behind this parameter.

The complete additional term in Equation 8.2, $Fye^{-\beta y}$, was generated to account for the inflection change at the upper end of the profile but was designed to be damped out for the majority of the profile.

8.3   Comparison of Lee's Equations

Lee's equation was applied to each Weeks Bay profile. Both forms of the equation (Equation 8.1 and Equation 8.2) were applied and the results were compared. Physical data collection was used to estimate known parameters, while an iterative approach was used to determine unknown parameters.

70

The values for the slope term, F, were obtained from the Tier 1 Slope Analysis while the values for β were obtained by E_{rms} minimized iteration. The results for beta and the associated E_{rms} values can be found in Table 8.1 and Table 8.2, respectively.

Table 8.1   Results for β

	Data Collection Trip			
	1	2	3	4
CS1	15.276	16.986	8.4494	23.278
CS2	0.0002	0.5028	0.0002	0.0002
CS3	0.0002	0.3656	0.1265	0.2498
CS4	2.5154	3.1051	0.1929	0.2594
CS5	1.2247	1.1016	0.0002	0.0895
CS6	1.9314	0.9685	1.2822	1.0220

Table 8.2   Results for E_{rms} for β

	Data Collection Trip			
	1	2	3	4
CS1	0.031	0.043	0.032	0.033
CS2	0.079	0.048	0.059	0.071
CS3	0.089	0.101	0.083	0.081
CS4	0.040	0.057	0.059	0.082
CS5	0.044	0.052	0.042	0.045
CS6	0.037	0.057	0.046	0.053

While Lee obtained improved results using Equation 8.2 with the corrector term, this was not true for the Weeks Bay dataset. The values obtained from the corrector in Equation 8.2 had little to no effect (on the order of 10^{-2}). Although the E_{rms} values are within reason, it can be seen from Table 8.1, that the range of beta values was 0.0002 to 23.278. A range of ten orders of magnitude is not acceptable. Figure 8.1 shows a typical profile comparing results from both Equation 8.1 and 8.2. Figure 8.2 demonstrates the magnitude of the corrector term on Equation 8.2.

71
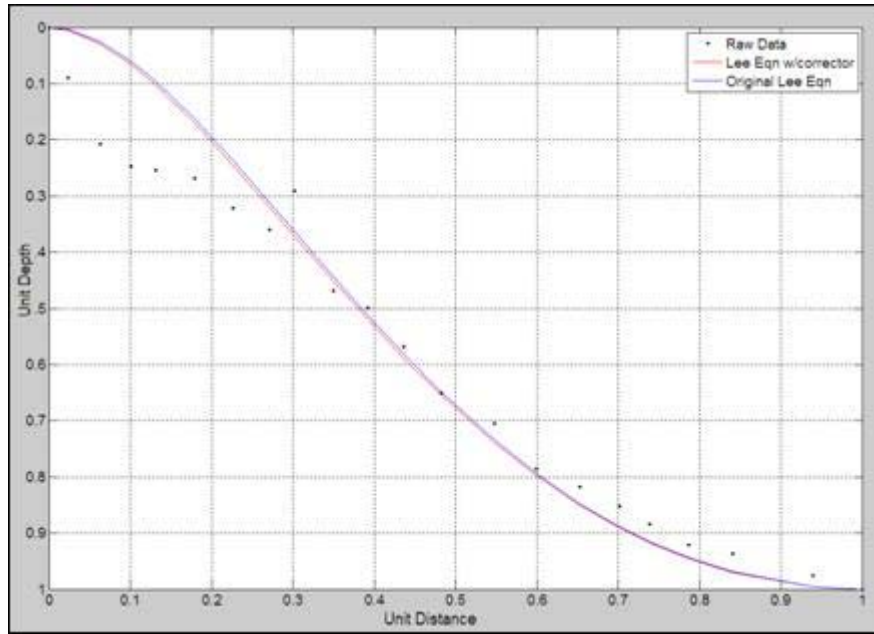
Figure 8.1   Comparison of original Lee equation to equation with corrector.
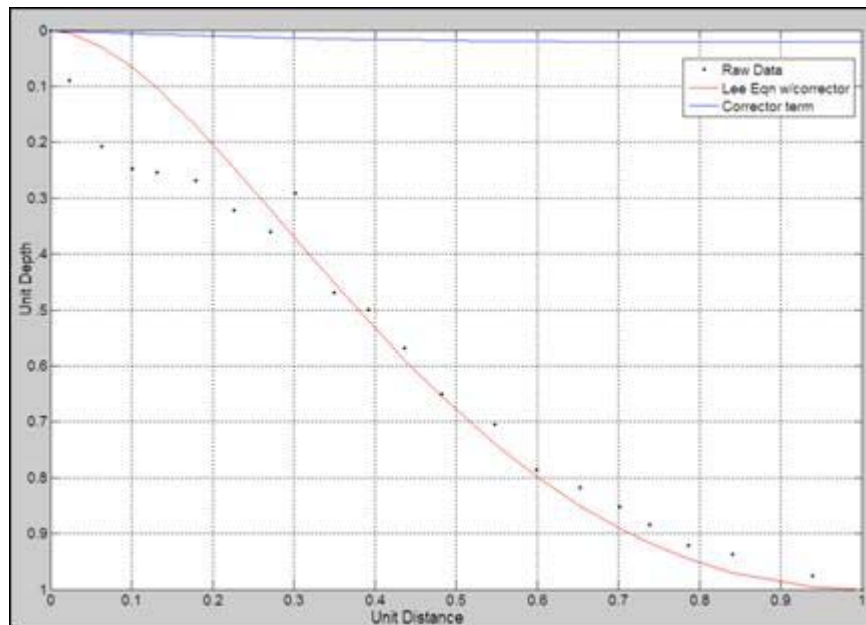
Figure 8.2   Lee equation showing effect of corrector term.

It is clear that the additional parameters added by Equation 8.2 do not significantly improve the results. For this reason, Lee's original equation, Equation 8.1, was utilized for the remainder of this work.

8.4   Location of Origin

As discussed in Chapter 6, the location of the origin in each profile is of significant importance. Equations typically utilize mean sea level (MSL), mean tidal level (MTL), or mean lower-low water (MLLW) as the horizontal axis with the vertical axis extending downward from the land-water interface (Figure 8.3). However, these are not always appropriate solutions. Additionally, the empirical parameters found in an equation will vary considerably depending on the location of the origin. For this reason, a significant effort has focused on attempting to find the most effective origin for the purpose of evaluating the shoreline.
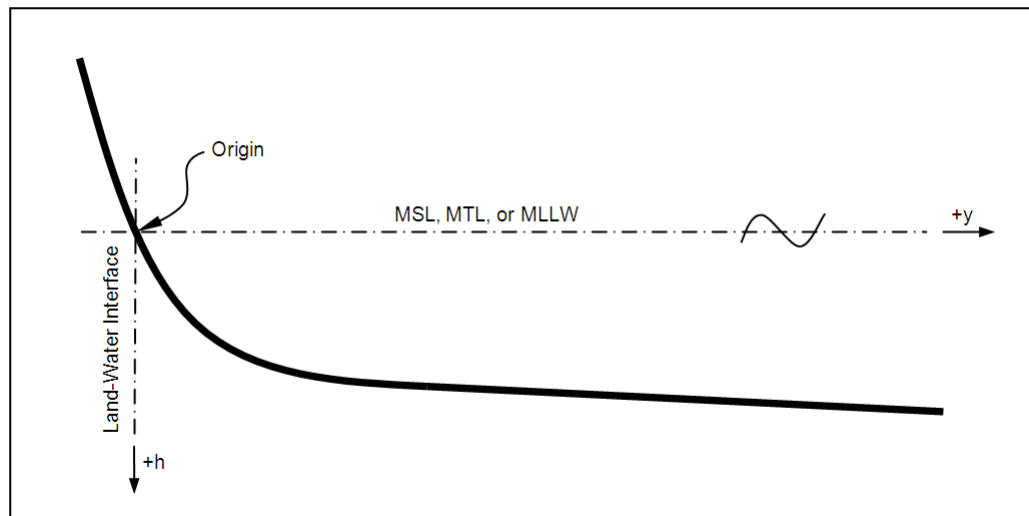
Figure 8.3   Profile schematic showing axes.

Taking the origin as the land-water interface of MTL generated the best results and also is the most logical choice. Another solution which arose is to take the peak of the on-shore berm as the origin. While using the on-shore berm as an origin produced effective results, the use of MTL was chosen since it can be universally applied without effects from tide range, geoid location, or other parameters affected by physical location.

Additionally, the location of the on-shore berm is not always available. In the case of Weeks Bay, there was not always a distinct on-shore berm in each profile. In other locations there may be a hard substrate or solid wall which prohibits the formation of a berm. This work focused on using the land-water interface of MTL as the origin since its location is only dependent on the water levels at the individual profile.

8.5   Terminal Depth

The definition of another critical location used in Lee's equation is the terminal depth. Lee defines the location of terminal depth, (y_o, h_o), of the profile as the 'active profile length' with regards to wave energy dissipation. In more specific terms, this is the point at which waves no longer interact with the sediment.

Weeks Bay is a small, shallow estuary with relatively small wave heights. As such, the active profile length is extremely small, making application of Lee's equation prohibitive. Taking the active profile length as a longer segment also generated poor results (Figure 8.4). Only when the terminal depth was taken as the location at which the slope changes significantly (the interior inflection point) was the equation found to have close correlation to measured data (Figure 8.5 and Figure 8.6).
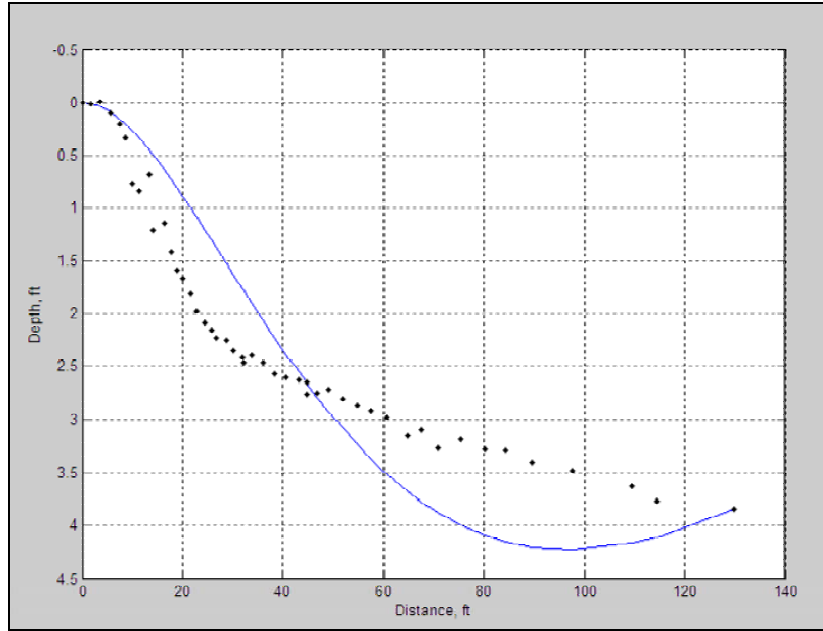
Figure 8.4   Application of Lee equation to entire profile.
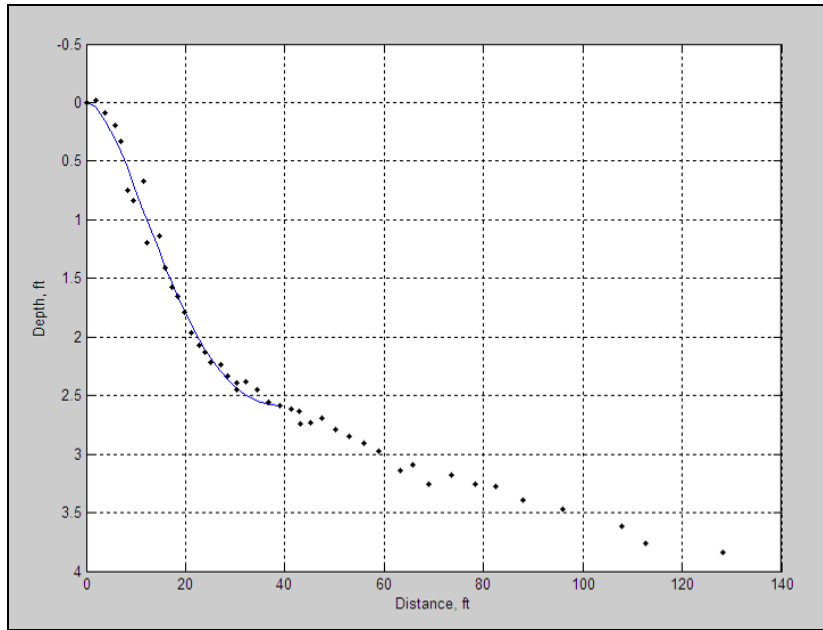
Figure 8.5   Application of Lee equation to upper portion of profile.

75
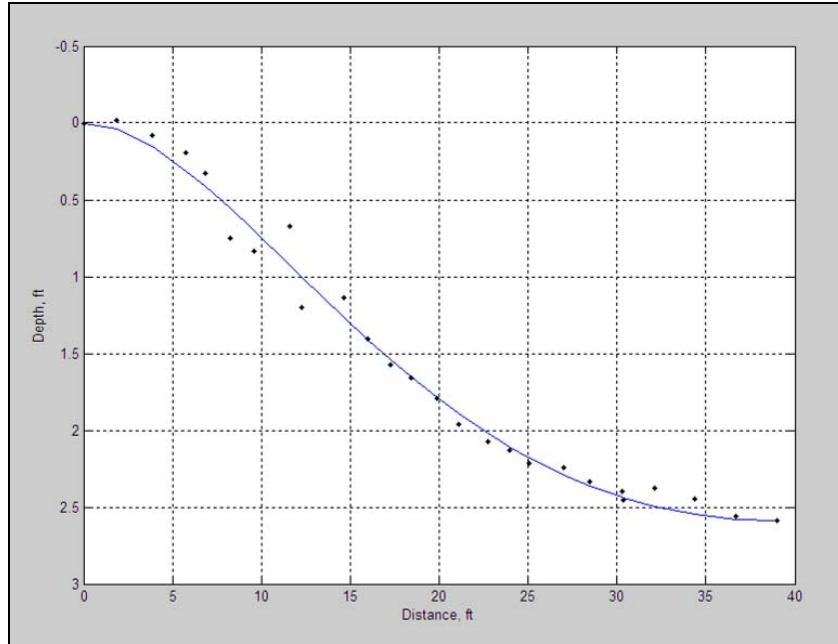
Figure 8.6   Application of Lee equation to upper profile, larger view.

A variety of scaling techniques were employed with varying success. The horizontal and vertical axes were scaled using the location of each profile's specific terminal depth, (y_o, h_o). Utilizing the interior inflection point of each profile as the terminal depth and scaling parameter was the most effective without introducing new parameters.

8.6   Determination of k_i

In order to apply Lee's equation, an iterative, multi-step process was developed using a Matlab M-file. Due to the limitations of the collected wave data, k_i was considered an unknown. It was hypothesized that although an iterative approach was used to determine k_i, the results would be accurate since the wave environment and bottom sediments vary only slightly from profile to profile. Figure 8.7 visually demonstrates the typical range of k_i values and the expected profile shape caused by this variation.

76
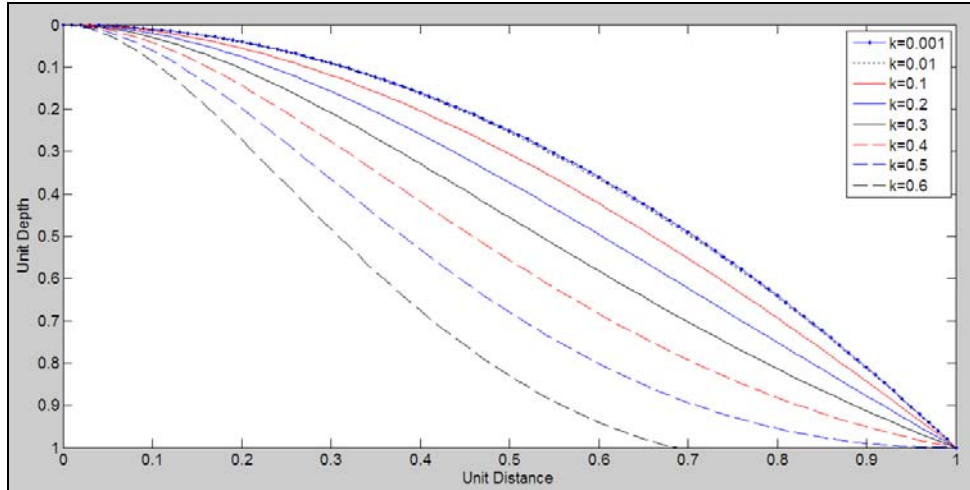
Figure 8.7   Variation of k_i on for a typical profile.

An M-file was set up to test 10,000 k_i values and record the error associated with
each one when compared to the original dataset. The same method was used to determine
β for Equation 8.2. A visual estimation was used to determine the location of (y_o,h_o),
taken as the interior inflection point. The M-file then recorded the k_i and error values
which were best-fit for the given profile. These k_i values were taken as the initial estimate
for k_i.

These k_i values change as the location of (y_o,h_o) is changed; as can be seen in
Figure 8.4 and Figure 8.5. The location of the inflection point was not a definitive
location and thus was attempted to be found mathematically. The raw data points were
analyzed around the visual location of the slope change. Each one was tested as the
terminal depth and the associated error for the profile was tabulated. The terminal depth
location producing minimal error was recorded. The k_i function was run once more
utilizing the error minimized (y_o,h_o) locations.

However, because the mathematically-determined locations were found by
minimizing error, the method tended to produce terminal depths which were significantly

77

different than the visual analysis. The erroneous results were caused by diminished errors associated with using fewer data points. For this reason, the terminal depths found by visual inspection were used for the remainder of the analysis.

Additionally, k_i is affected by the scaling of the profile. The k_i values were determined before and after scaling by terminal depth to examine possible correlation (Table 8.3 and Table 8.4). While the scaled results had no correlation to the previous unscaled values, both produce identical graphs. This is an important result as it demonstrates the variety of results that can be obtained from the same dataset.

Table 8.3   Unscaled results for k_i.

	Data Collection Trip			
	1	2	3	4
CS1	0.0072	0.0031	0.0086	0.0004
CS2	0.0201	0.0139	0.0114	0.0148
CS3	0.0255	0.0170	0.0070	0.0177
CS4	0.0187	0.0186	0.0110	0.0169
CS5	0.0062	0.0230	0.0163	0.0200
CS6	0.0121	0.0251	0.0114	0.0213

Table 8.4   Results for k_i after scaling.

	Data Collection Trip			
	1	2	3	4
CS1	0.2578	0.3021	0.2747	0.2337
CS2	0.6770	0.5516	0.5982	0.6112
CS3	0.5427	0.5117	0.5391	0.5266
CS4	0.4397	0.4535	0.5340	0.5371
CS5	0.4365	0.4950	0.5560	0.5256
CS6	0.3843	0.4718	0.4790	0.4787

8.7   Damping Function, T

It can be seen in Figure 8.4 and Figure 8.5 that since Lee's equation is only applicable to the upper half of the profile, another equation must be used to define the lower half. In the case of Weeks Bay, which is a shallow estuary, the lower profile is best defined as linear as it approaches the deepest portion of the bay. Higher order polynomials were fit to the deeper portions but did not produce improved results for increased unknown parameters. Because the depth does not change significantly from the upper half of the profile to the deepest portion of the bay (<5 ft over 1000 ft), any curvature in the lower slope is so small that it cannot be accurately estimated. In order to transition from Equation 8.2 to a secondary equation used in the deeper portion, a damping function was generated.

The damping function utilized in this work is the exponential form of hyperbolic tangent (Equation 8.3). The parameter r is to be taken as some form of unitless horizontal change, while n is set as a constant.

$$T = \frac{e^{nr} - e^{-nr}}{e^{nr} + e^{-nr}}$$

Equation 8.3

The following equations for r were evaluated to determine the most appropriate for use in the damping function. The results were plotted in Figure 8.8; note the reversed axis to mirror the profile plots.

$$r = \frac{y}{y_0}$$

Equation 8.4 *a*

$$r = \frac{y_0 - y}{y_0}$$

Equation 8.4 *b*

$$r = \frac{y - y_0}{y_0}$$

Equation 8.4 *c*

79

$$r = \frac{y_0 - y}{y}$$

<div align="right">Equation 8.4 *d*</div>

$$r = \frac{y - y_0}{y}$$

<div align="right">Equation 8.4 *e*</div>

Restrictions placed on the damping equation included a unitless requirement and required increasing in value and range from 0 to 1. The increasing in value requirement eliminates Equation 8.4*b* and *c*. Slight alterations of these equations can be made to maintain these requirements. The remaining equations were tested as part of the new, modified equation.
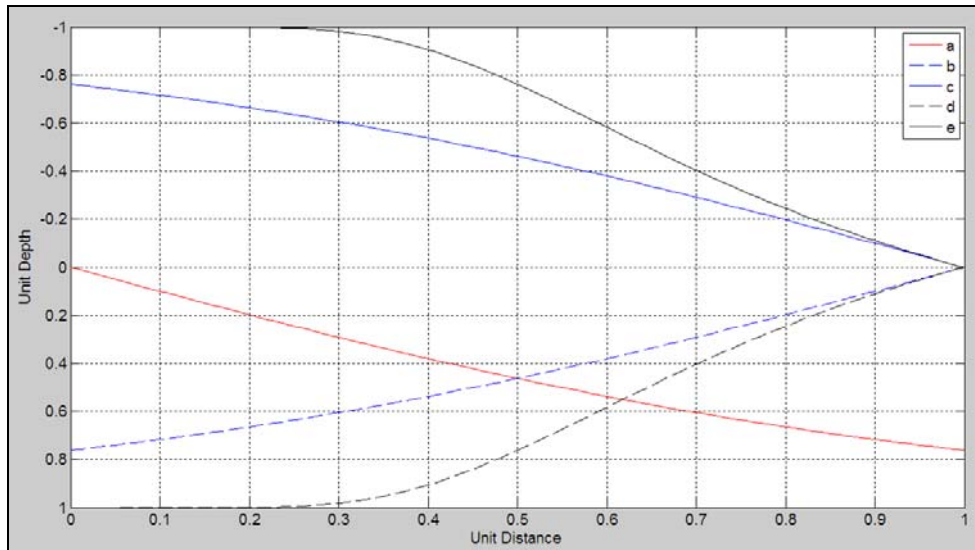
Figure 8.8   Comparison of T results using Equations 8.4 *a-e*.

As discussed previously, Weeks Bay is a small, shallow bay. As such, the interior bottom slope is essentially linear. A new equation was developed which combines with this new function, Equation 8.5, and Lee's original equation, Equation 8.1. These are described as

$$h = h_o e^{4k_i(y_o - y)}\left(\frac{y}{y_o}\right) \qquad \text{for } 0 \le y < y_o \qquad \text{Equation 8.1}$$

80

$$h = h_o + F_2\left(y - y_o\right) \qquad \text{for } y_o \le y < y_t \qquad \text{Equation 8.5}$$

$$F_2 = \frac{h_t - h_o}{y_t - y_o}$$

where (y_o, h_o) is the terminal depth, (y_t, h_t) is the termination of the profile, and F_2 is the lower slope.

The damping function, T, defined in Equation 8.3, is used to smoothly transition between the Equations 8.1 and 8.5. The final new equation is as follows:

$$h_{\text{mod}} = \left(T\right)\left[h_o e^{4k_i(y_o - y)}\left(\frac{y}{y_o}\right)\right] + \left(1 - T\right)\left[h_o + F_2\left(y - y_o\right)\right] \qquad \text{Equation 8.6}$$

where $T = \dfrac{e^{nr} - e^{nr}}{e^{nr} + e^{nr}}$ and $r = \dfrac{y_t - y}{y}$

The final equation which calculates profile depth, h_{mod}, is defined by the damping function, T, the wave attenuation parameter, k_i, and horizontal distance, y. The terminal depth, (y_o, h_o), is defined as the location at which a significant break in slope occurs. The constant, n, is used to define the shape of the damping function. The lower slope, F_2, and profile terminus, y_t are also utilized.

An iterative method was utilized to determine the optimal n for each profile. The results can be found in Table 8.5.

Table 8.5   Profile-specific n values.

Profile	Data Collection Trip			
	1	2	3	4
CS1	0.207	0.207	0.189	0.172
CS2	0.025	0.073	0.036	0.040
CS3	0.034	0.021	0.013	0.016
CS4	0.094	0.084	0.017	0.015
CS5	0.029	0.112	0.070	0.087
CS6	0.080	0.046	0.033	0.049

81

For most profiles, these values produce acceptable results. A typical profile showing a good fit is shown in Figure 8.9. Lee's original equation, Equation 8.1, produces exceptionally inaccurate results after the interior inflection point; however, the modified version, Equation 8.6, generates accurate results for the entire length of the profile.
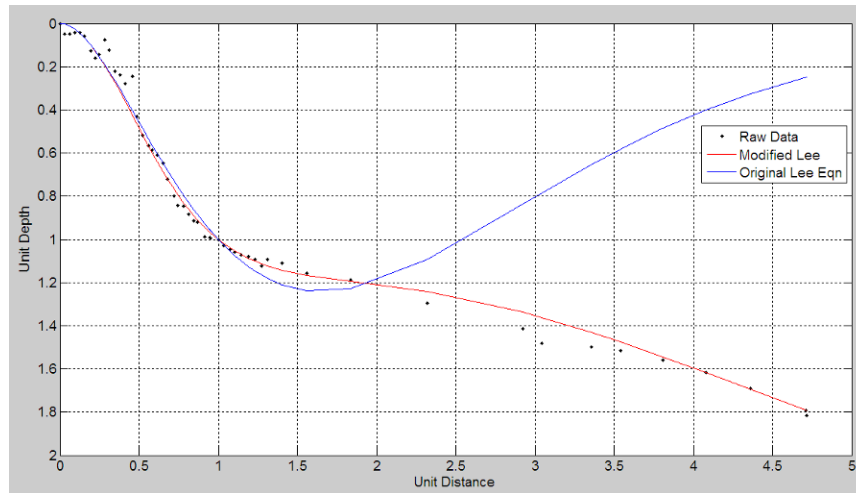
Figure 8.9   Comparison of Original Lee equation to Modified version.

However, in some cases, a slight degradation of accuracy was produced on the vertical shoreface. For these profiles, the remainder of the profile maintained more accurate results than Lee's original equation. Figure 8.10 shows a typical poor fit on the vertical shoreface. While the results in this region were slightly less precise, the remainder of the profile produced improved results.

82
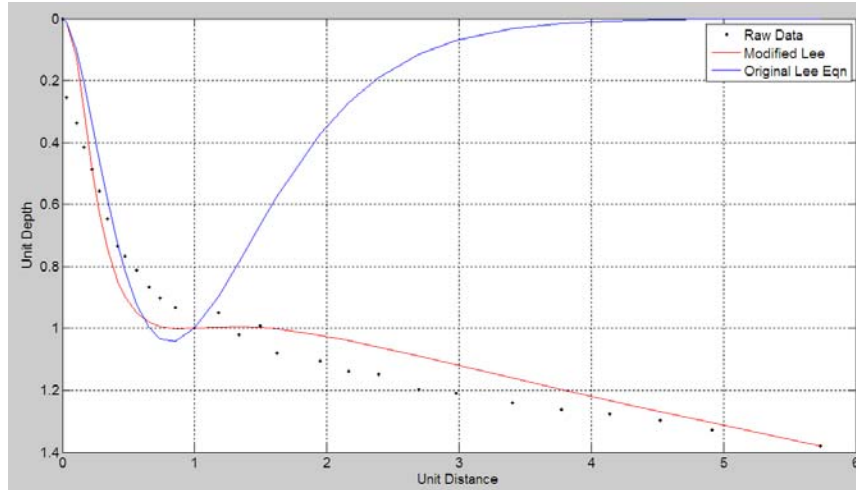
Figure 8.10   Comparison of original Lee equation and modified Lee

As a second approach, the average n value (0.073) was used as a constant and the k_i values were recalculated. The result for k_i and the associated E_{rms} values can be found in Table 8.6 and Table 8.7, respectively.

Table 8.6   Summary of k_i results using average n value.

Profile	Data Collection Trip				Average	Std Dev
	1	2	3	4	Average	Std Dev
CS1	0.1190	0.1296	0.2137	0.1760	0.1596	0.0438
CS2	0.7114	0.4996	0.5960	0.6150	0.6055	0.0868
CS3	0.4873	0.3410	0.3445	0.0566	0.3074	0.1805
CS4	0.2584	0.2016	0.0848	0.0469	0.1479	0.0988
CS5	0.0483	0.3767	0.4873	0.4293	0.3354	0.1967
CS6	0.0889	0.0585	0.0553	0.0581	0.0652	0.0159
Average	0.2856	0.2678	0.2969	0.2303		
Std Dev	0.2629	0.1663	0.2183	0.2383		

83

Table 8.7 E_{rms} values from k_i estimation.

	Data Collection Trip			
Profile	1	2	3	4
CS1	0.098	0.082	0.091	0.113
CS2	0.186	0.234	0.260	0.222
CS3	0.108	0.122	0.130	0.147
CS4	0.074	0.088	0.148	0.156
CS5	0.155	0.084	0.077	0.062
CS6	0.110	0.129	0.120	0.130

The use of the average n value with the values of k_i from Table 8.6 produced slightly improved results. Figure 8.11, a reproduction of the poor fit in Figure 8.10, demonstrates these enhanced results.
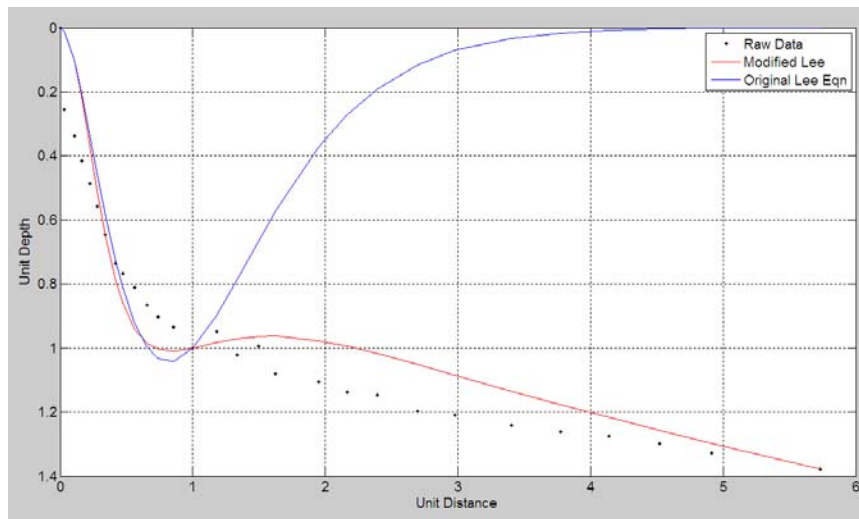
Figure 8.11   Reproduction of Figure 8.10 using average n.

The use of the average n of 0.073 and the k_i values found in Table 8.6 produced the most accurate results for the project data.

84

Several other equations were either tested or developed in an attempt to improve upon Equation 8.6. None of the equations discussed below produced improved results and all were less accurate than Equation 8.6 implemented with n=0.073.

8.8   Comparison to Physical Forcings

The k_i values were expected to have some correlation to physical forcings. It was not possible to comparatively analyze tidal influence and fresh water inflow parameters since all profiles experienced the same effects. Comparisons were made between grain size distributions (and ratios thereof), fetch, and the upper and lower slopes. It was hypothesized that changes in k_i would be linked directly to these parameters.

As can be seen in Table 8.6, the standard deviation of k_i for each profile varies significantly. The lower standard deviations, as in Profile CS6, are an indication of a stable profile during the data collection period whereas a higher standard deviation indicates variability. Graphical and statistical analysis of the correlation between the physical parameters and the k_i values was achieved using Microsoft Excel.

Figure 8.12 and Figure 8.13 show the relationship between fetch, dominant fetch, and k_i. Note the inverted axis of k_i in Figure 8.12. A significant inverse relationship between fetch and k_i can be seen in both plots. This relationship can also be seen in Table 8.8 with a correlation coefficient of -0.67 between fetch and k_i. Recalling Figure 8.7, increased k_i values indicate steeper profiles. Thus, the result is counterintuitive since a higher fetch would be expected to be associated with increased wave activity and a steeper, eroding bank.

85
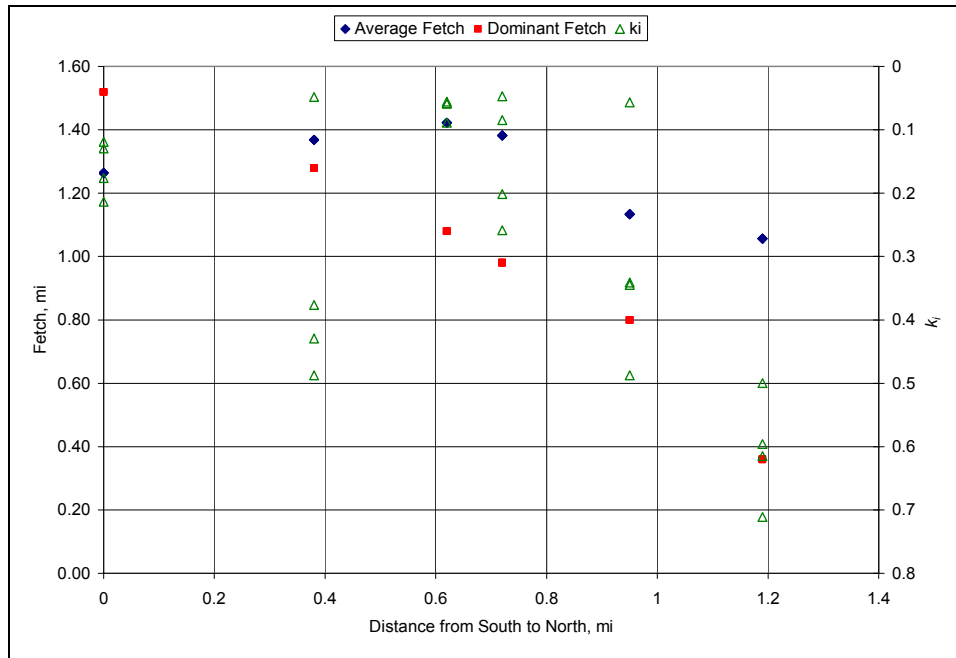
Figure 8.12   Comparison of fetch, dominant fetch, and k_i to distance.
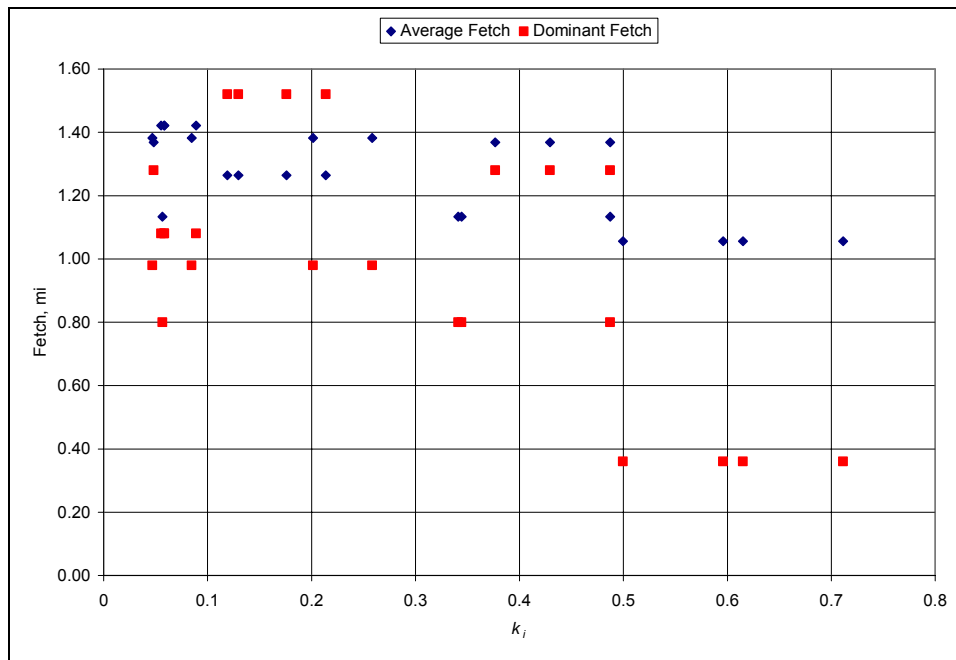
Figure 8.13   Variation of Fetch and Dominant Fetch with k_i.

86

Table 8.8   Correlation coefficients

Parameter	Correlation Coefficient
D20	-0.09
D50	-0.42
D80	-0.36
D80/D20	-0.06
D50/D20	-0.20
D80/D50	0.55
Fetch mi	-0.67

The relationships between k_i and the grain sizes D_{20}, D_{50}, and D_{80} have little to no correlation (Table 8.8). These relationships are shown graphically in Figure 8.14.
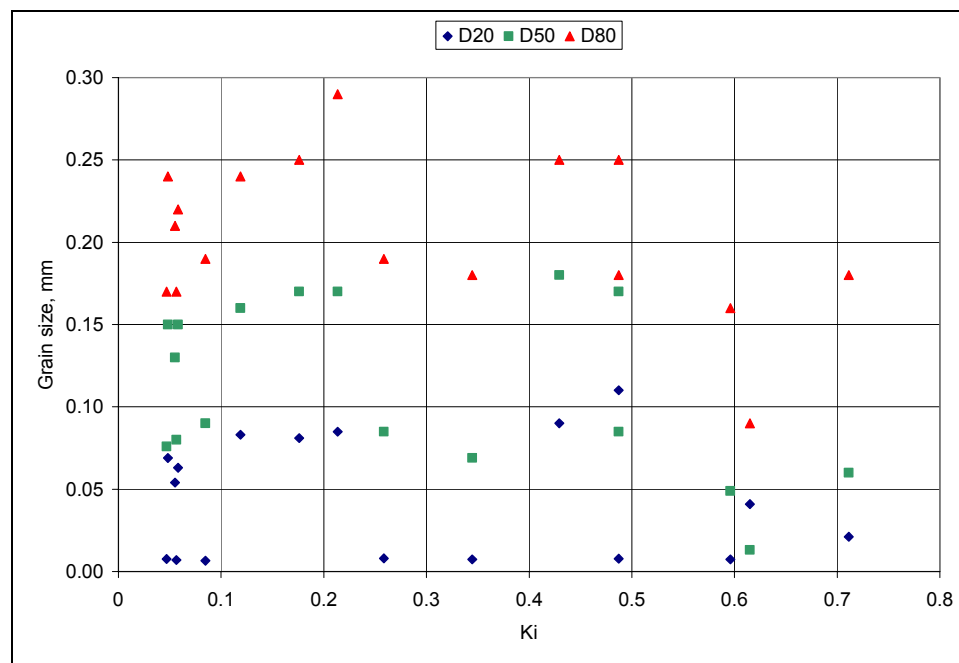
Figure 8.14   Comparison of grain size to k_i.

87

It was expected that these parameters be positively correlated since increased grain size may indicate erosion and thus a higher k_i value. The correlation value between D_{50} grain size and k_i of -0.42 may indicate that a relationship exists but that this analysis contained too few data points to accurately demonstrate the relationship.

The statistical analysis in Table 8.8 also shows the limited relationship between the grain size ratios D_{80} to D_{20} and D_{80} to D_{50} and k_i. Figure 8.15 also demonstrates this lack of relationship. The ratio of D_{80} to D_{50} has the only slightly positive correlation in the analysis. However, it can be seen in Figure 8.15 that there are essentially two series of D_{80}/D_{20} data points. The disjointed dataset is possibly the cause of the slight correlation.
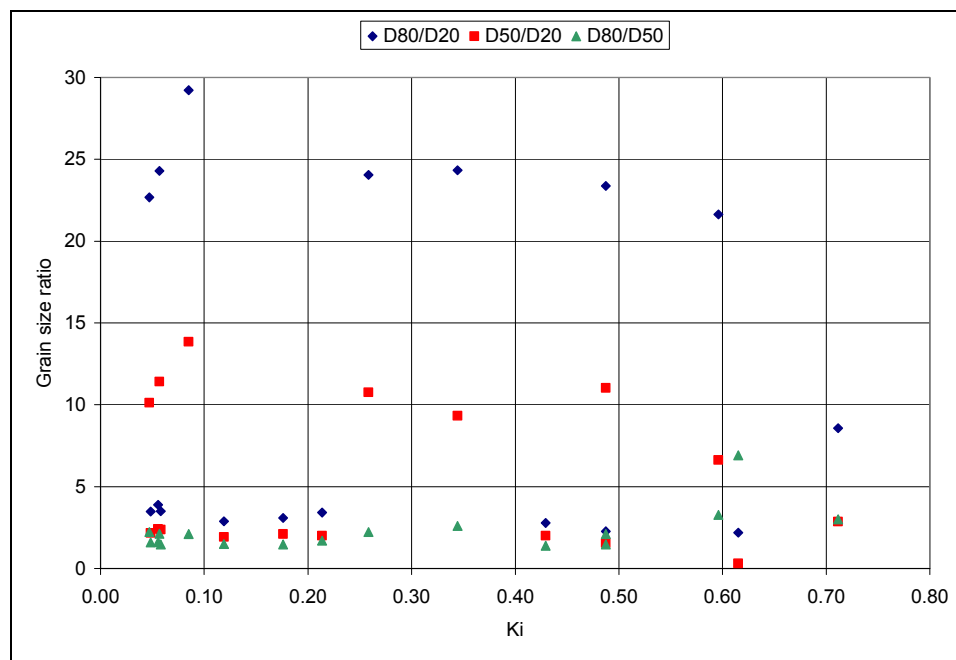
Figure 8.15   Comparison of grain size ratios to k_i.

A stronger relationship between grain size and k_i was anticipated. The lack of a significant relationship could be the result of analysis inaccuracies. The inherent error in

www.manaraa.com

the data collection, analysis, and other unaccounted for physical forcings could be responsible for slight changes.

8.9 Alternate Wave Equation

Lee's equation is based upon a widely accepted wave attenuation equation. An alternate wave equation,

$$H(y) = H_o \left(\frac{1}{1 + \alpha y} \right)$$
Equation 8.8

where H is the wave height, H_o is incident wave height, y is horizontal distance, and α is the wave attenuation parameter. Equation 8.8 was chosen to combine with energy flux and wave celerity to generate a new shoreline equation.

Equation 8.8 was combined with Equations 2.1 through 2.5 and integrated from (0,0) to (y,h). The resulting equation was required to pass through (y_o,h_o) leading to a new shoreline equation described as

$$h = h_o \left(\frac{y}{y_o} \right)^2 \left(\frac{1 + \alpha y}{1 + \alpha y_o} \right)^4$$
Equation 8.9

where h is water depth, y is horizontal distance, and α is the wave attenuation parameter.

Equation 8.9 varies monotonically and is consistently concave left (Figure 8.16). The effective range of α is [0.01 10]; values outside this range will not affect the results.

89
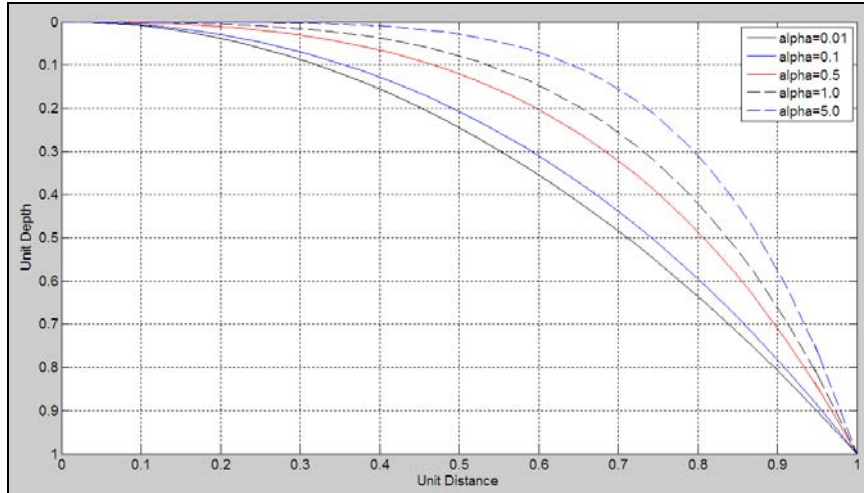
Figure 8.16   Profile, h, with variation of alpha.

Because the raw profile data all contain a second inflection point, this equation could not be used in this application. It may, however, be effective at modeling the on-shore berm.

8.10   Mehta Erosion Equation

A mudshore profile equation for erosion was also developed by Mehta et. al. and is described in Kirby (2002). While it has been specifically designed for straight eroding coasts, it was hypothesized that Weeks Bay may fall within the realm of 'applicable.' The Mehta equation is described as

$$\frac{h(x)}{h_0} = \left(1 - \frac{x}{L}\right)^{\frac{2}{3}}$$

Equation 8.10

where $h(x)$ is the depth of the profile, h_0 is the high water depth at x=0 and is equal to the tidal range, L is the distance from low to high water mark, and x is the horizontal distance.

90

Figure 8.17 shows the best fit among all the Weeks Bay profiles for Equation 8.10 and the complementary Equation 8.6. The resulting error is within acceptable limits. However, the majority of profiles were similar to the poor fit found in Figure 8.18. Equation 8.10 was not sufficient for use in this application.
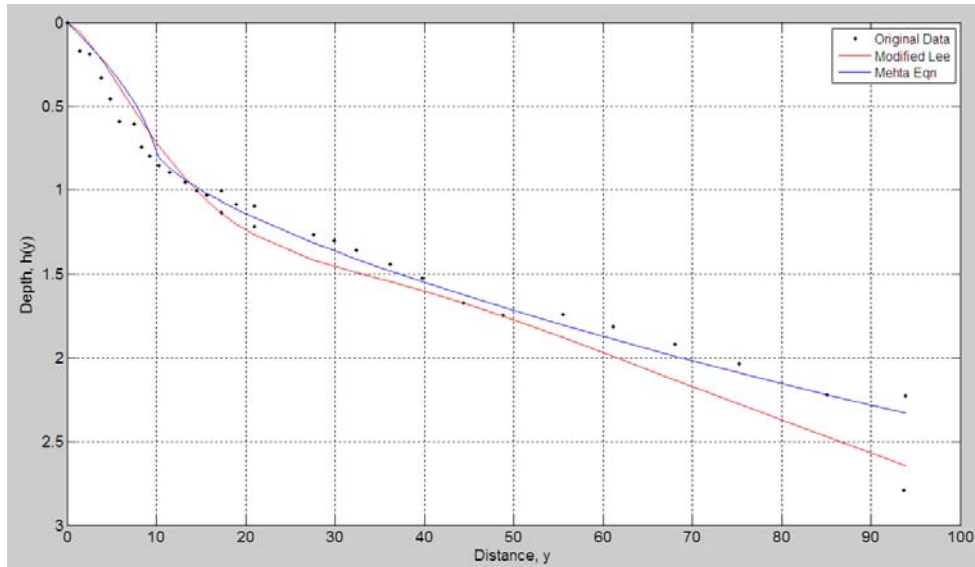
Figure 8.17   Analysis of correlation between Mehta and Modified Lee.
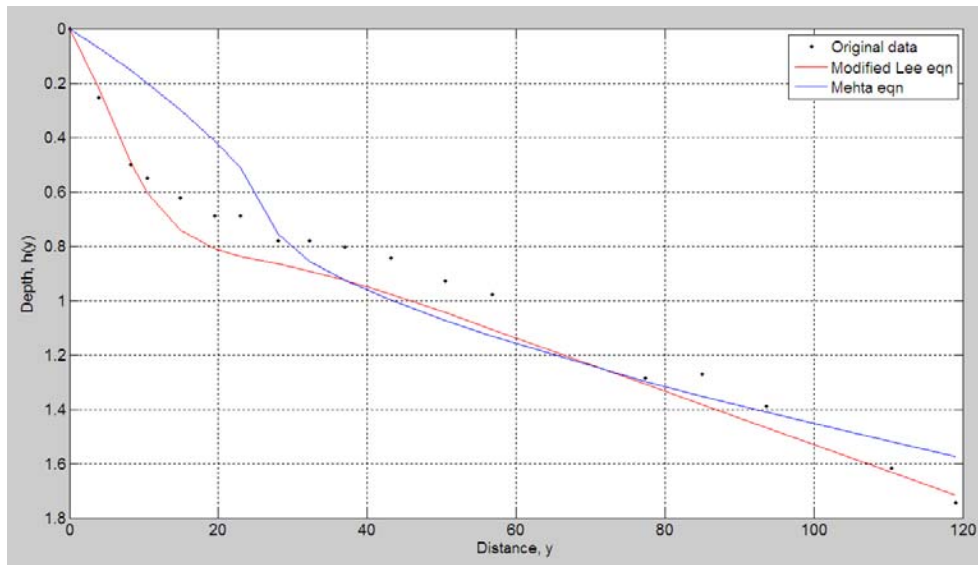
Figure 8.18   Analysis of correlation between Mehta and Modified Lee showing poor fit.

91

Note that Equation 8.10 passes through $(0, h_o)$ while Lee's equation passes through the origin, $(0,0)$. Therefore, Equation 8.10 was adjusted so the two could be plotted over the Weeks Bay data. Equation 8.10 had good correlation on some profiles (Figure 8.17) and poor on others (Figure 8.18). Additionally, note the concavity of Equation 8.10 in the upper region of the profile. The Weeks Bay data were consistently concave right while Equation 8.10 gives consistent concave left results. Since it was described as an equation for erosion, these results are suspect. For these reasons, Lee's equation was deemed the most appropriate in this application.

8.11 Conclusion

Of the many equations found in the literature, the one derived by S.C. Lee appears to be most applicable to the Weeks Bay dataset. The comparison analysis of the equation results to the raw data showed acceptable error and visual inspection of the results, including concavity, was satisfactory. The modified equation developed as a result of this work closely fits the Weeks Bay data.

The M-Files used as part of this work were generated such that the analysis could be completed using another dataset with relative ease. Most of the programming is automated with limited inputs required once the initial setup is complete.

While the location of the origin is still a reasonable question, placing it at either the peak of the on-shore berm or the land-water interface are both solutions which produce acceptable results.

Future work is recommended to collect adequate wave data to properly estimate wave attenuation and thus correlate with k_i. A data collection period sustained for at least a year is also recommended.

www.manaraa.com

Overall, the results generated using the modified version of Lee's equation were within error tolerances for the original dataset. However, while generalizations were possible, the comparison of the empirical parameters to the physical forcings proved to be inconclusive.

93

CHAPTER IX

NUMERICAL MODEL IMPLEMENTATION

One goal of this work is to provide an equation which can be implemented in a numerical model in order to model shoreline evolution. Most multiple-dimensional numerical models calculate morphologic change only in the bed, not the shoreline, and a shoreline adjustment computation is needed. Although there are numerous methods for implementation into a numerical model, two major cases are examined.

Case 1 is a coarse resolution model in which the entire shore profile is modeled as a single element. The remaining elements are modeled as standard interior elements. Case 2 is a fine resolution model. The modified shore profile equation is utilized from the shore to the end of the linear profile. The profile is separated into two or more elements for increased resolution.

9.1 Model Requirements

The developed equation will require several parameters from the numerical model.

- Original bathymetry for the shoreline

- The erosion/deposition $\left(\dfrac{\partial C}{\partial t} \right)$ rate at the nodal locations as determined by the water velocity, shear stress, and sediment loading

- Wind speed, direction, and fetch data, along with sediment composition will also be required

94

The initial bathymetry of the estuary must first be known. Calculation strings, along which the model will implement the new equation, are then defined (See discussion in Section 9.9). At each timestep, the areas between these boundary strings will be interpolated to determine elevations.

The model will output new bathymetry and a new boundary string. The location of the new boundary string is defined in (Figure 9.1). An eroding shore boundary is shifted outward along an imaginary line that extends the calculation string perpendicular to the boundary.
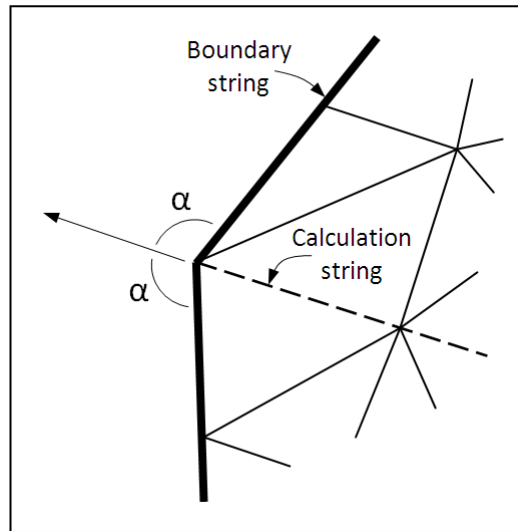
Figure 9.1   Evolution of boundary string.

9.2   Case 1 – Coarse Resolution Implementation

In Case 1, Lee's original equation, 8.1, is applied as a single cell. Changes in the bed elevation of the profile are driven by erosion or deposition volumes and changes in k_i. To demonstrate some basic principles in this approach, a simple schematic is shown in Figure 9.2 below. The initial timestep is shown in black while the following timestep is shown in blue. The remainder of this document follows this standard. Also note the

95

defined coordinate system required for the shoreline equations. Because the model uses a different coordinate system, relative distances were utilized. Integrations also required manipulation based on this coordinate system.
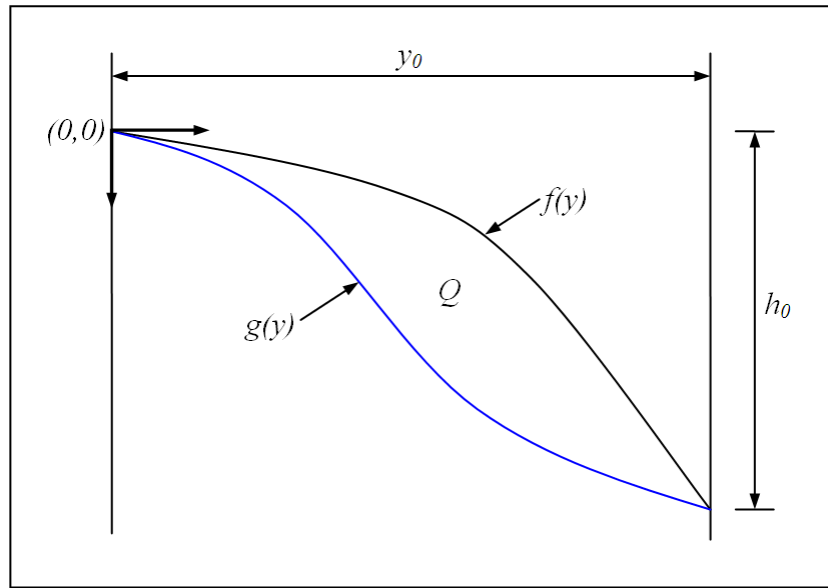
Figure 9.2   Basic schematic utilized in Case 1.

The general form of the integral defining the volume, Q is

$$Q = \int_0^{y_0} |f(y) - g(y)| dy$$ Equation 9.1

where $|f(y) - g(y)| = \begin{cases} f(y) - g(y) & \text{when } f(y) \geq g(y) \\ g(y) - f(y) & \text{when } g(y) \geq f(y) \end{cases}$.

The remainder of the calculations in this chapter are based on this concept.

It is important to note the integration limits of $f(y)$ (shown in Figure 9.3). This is critical since the coordinate system for $f(y)$ is different from the model system. The equations coordinate system does not need to be transformed if all inputs into f(y) are relative.
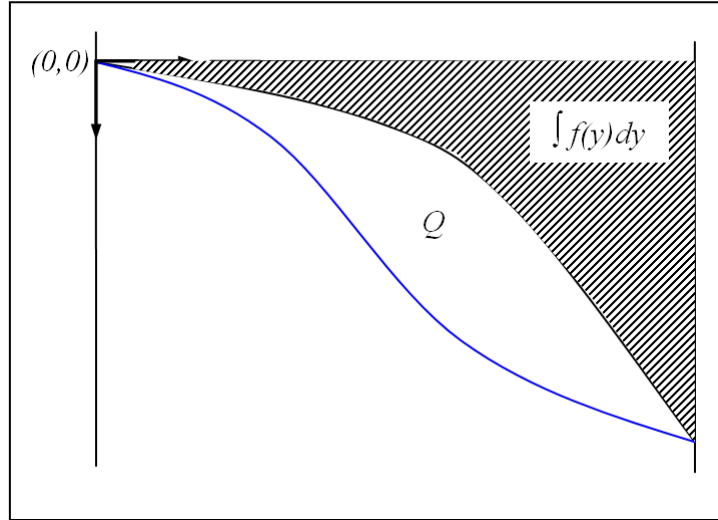
Figure 9.3   Integration limits of f(y).

Models which utilize a triangular mesh, such as ADH, or a Cartesian mesh cannot generate elements with curves. To accommodate this, the curve calculated by the shoreline equation must be converted into a volume-equivalent linear element. Figure 9.4 demonstrates how this is achieved. The new element is bounded on the interior by the adjacent cell height. The exterior height is calculated by using $Q_U = Q_L$.
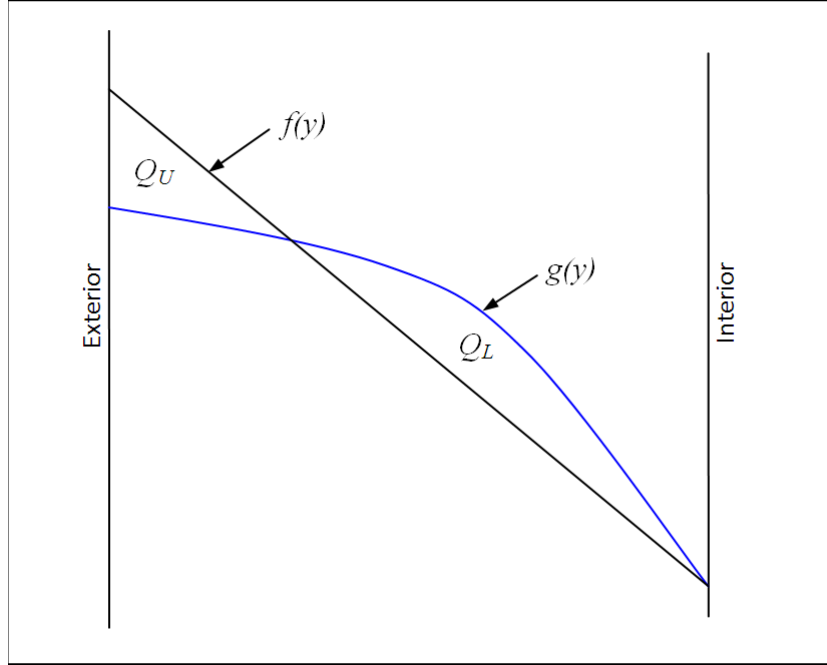
Figure 9.4   Conversion of curve to line.

Once this linear-equivalent is specified within the model as the element shape, the curve will be lost. For this reason, the linear element dimensions must be used in the volume calculations for the following time step.

For Case 1, Lee's original equation, 8.1, will be utilized. The integration of this equation is used to find the area under the curve which represents volume. The integration is summarized as the following:

$$w(y) = \int_0^{y_0} h_0 e^{4k_i(y-y_0)} \left(\frac{y}{y_0}\right)^2 dy \qquad \text{Equation 9.2}a$$

$$= \int_0^{y_0} \frac{h_0 \left(e^{4k_iy}\right) y^2}{\left(e^{4k_iy_0}\right) y_0^2} dy = \frac{h_0}{y_0^2}\left(e^{-4k_iy_0}\right) \int_0^{y_0} \left(e^{4k_iy}\right) y^2 dy \qquad \text{Equation 9.2}b$$

$$= \frac{h_0}{y_0^2}\left(e^{-4k_iy_0}\right) \left\{ \left| \frac{1}{k_i} y^2 e^{4k_iy} \right|_0^{y_0} - \frac{2}{k_i} \int_0^{y_0} y e^{4k_iy} dy \right\} \qquad \text{Equation 9.2}c$$

98

$$= \frac{h_0}{y_0^2}\left(e^{-4k_iy_0}\right)\left\{ \left|\frac{1}{k_i}\,y^2 e^{4k_iy}\right|_0^{y_0} - \frac{2}{k_i}\left|\frac{1}{16k_i^2}\left(4k_iy_0-1\right)e^{4k_iy}\right|_0^{y_0} \right\} \qquad \text{Equation } 9.2d$$

$$w(y) = \frac{h_0}{4k_i} - \frac{h_0}{32k_i^3 y_0}\left(4k_iy_0-1\right) - \frac{h_0}{32k_i^2 y_0}\left(e^{-4k_iy}\right) \qquad \text{Equation } 9.2e$$

9.3   Scenario development

A flow diagram has been generated to demonstrate three general scenarios encountered during model implementation (Figure 9.5). The diagram selects a scenario (and the associated series of equations) based on whether the cell is eroding or depositing and on the k_i value. A schematic of the three scenarios can be found in Figure 9.6.
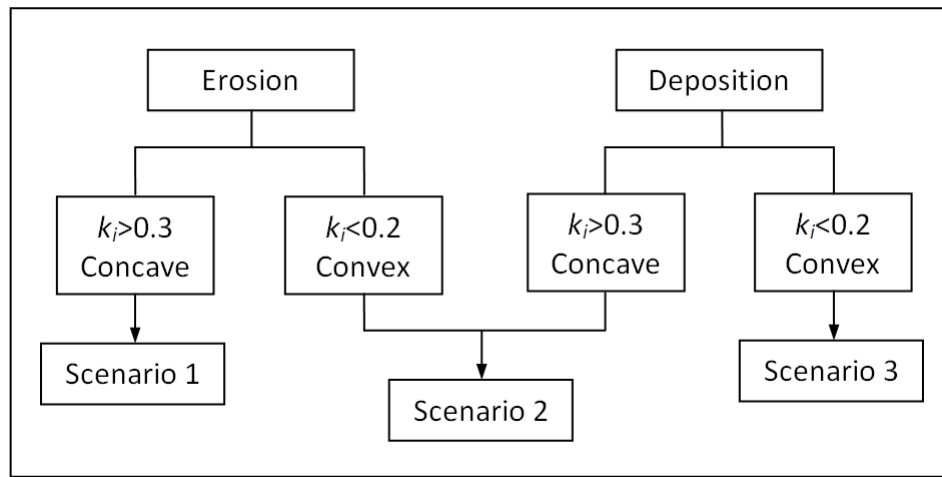
Figure 9.5   Flow diagram for implementation.

In Scenario 1, deposition is occurring along with a k_i value associated with a convex profile; this can only result in Figure 9.6a. Similarly, in Scenario 3, an eroding, concave profile can only be presented as is shown in Figure 9.6b. Scenario 2 includes all transitioning timesteps when the profile is changing from erosion to deposition or vice versa. In Scenario 2a, the profile is beginning to erode; however, the k_i value is still less than 0.2 (convex). The profile is still transitioning toward an eroding profile shape

99

(Figure 9.6c). Similarly, Figure 9.6d demonstrates a profile which was previously eroding and is now transitioning to deposition. Thus, the k_i value is still greater than 0.3. The equations used in each of these scenarios are discussed below.
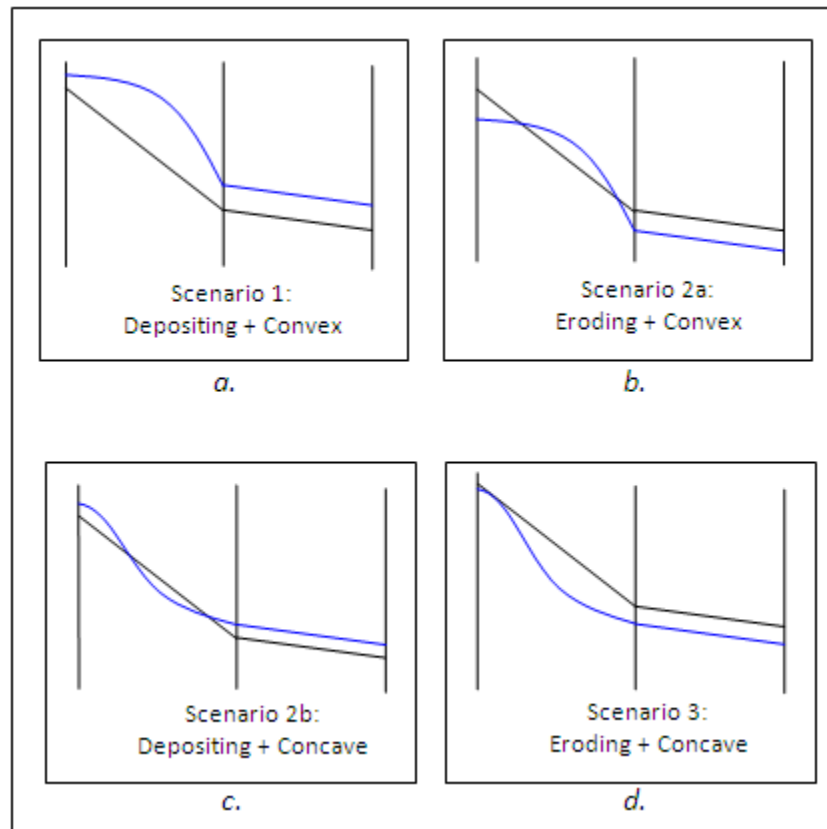
Figure 9.6   Schematics of four scenarios.

9.4   Scenario 1 Model Implementation

The first scenario occurs during deposition with k_i values less than 0.2. Figure 9.7 labels the variables used in this scenario. Element 1 is the 'shore' element and is bounded on the left by a solid vertical wall (not shown). Element 2 is the adjacent interior element. The black coloring denotes timestep i and the blue denotes timestep $i+1$. The unknowns,

Δy and Δh, are related to the remaining locations through a series of equations discussed below.

Figure 9.7   Definition sketch for Scenario 1.

For each time step, the movement of the shoreline, along with the new location of Element 1, is calculated. This is completed by a series of equations. First, the deposition for Element 2 is calculated along with the new bed location. The deposition for Element 1 is then calculated and utilized in the following equations. In order to determine the new location of Element 1, the deposition volume is set equal to the change in volume given by the movement of Element 1 boundaries. To define the areas required for computation, Figure 9.8 is given.

Figure 9.8   Definition of required points and calculation areas for Scenario 1.

The new location of Element 1 is found by calculated the following:

$$R_1 = \frac{(h_3 - h_6) + (h_3 - h_1)}{2}(y_3 - y_1)$$ Equation 9.3a

$$R_2 + R_3 + R_4 = (y_3 - y_4)(h_3 - h_4) - \int_0^{(y_4 - y_3)} g(y)dy$$ Equation 9.3b

$$R_3 = \tfrac{1}{2}(y_7 - y_6)(h_6 - h_7)$$ Equation 9.3c

$$R_4 = \tfrac{1}{2}(y_4 - y_5)(h_5 - h_4)$$ Equation 9.3d

$$R_5 = \tfrac{1}{2}(y_5 - y_7)(h_5 - h_2)$$ Equation 9.3e

$$E_D = R_1 + R_2 + R_5$$ Equation 9.4

$$m = \frac{(h_5 - h_4)}{(y_4 - y_5)}$$ Equation 9.5

Note that each location is labeled with a number, e.g. *6*, and the corresponding coordinate pair, e.g. (y_6, h_6). The area bounded by *2*, *5*, *4*, and *8* is deposition which occurred in the

original Element 2; this area was not included in the deposition of the new Element 1. The new Element 2, altered to accommodate the changing shore profile, is assumed to be bounded by the bed shape produced by deposition. In other words, the intersection of the new Element 1 and Element 2 was assumed to fall on the line *5-9*. Thus, the slope equation, m, is used in conjunction with the equation for deposition, E_D. These are combined and solved for the values Δy and Δh, from which the remaining locations can be calculated.

9.5   Scenario 2 Model Implementation

Mathematically, this is the most complex scenario. There are many potential interactions between the linear bed from the previous timestep and the new profile curve. The curves may indicate erosion in a portion of the element and deposition in another. Handling these differences in an entirely mathematic environment is complex.

The location(s) at which the two equations intersect must be calculated. Due to the potential shape of the profile curve, the two curves may intersect at more than one location. Solving for these locations requires a series of equations and coding knowledge that is outside the scope of this document.

9.6   Scenario 3 Model Implementation

Scenario 3 involves an eroding element with k_i greater than 0.3. Figure 9.9 defines the areas and locations utilized in this scenario. Similar to Scenario 1, the black coloring symbolizes the initial timestep while the blue coloring symbolizes the following timestep.
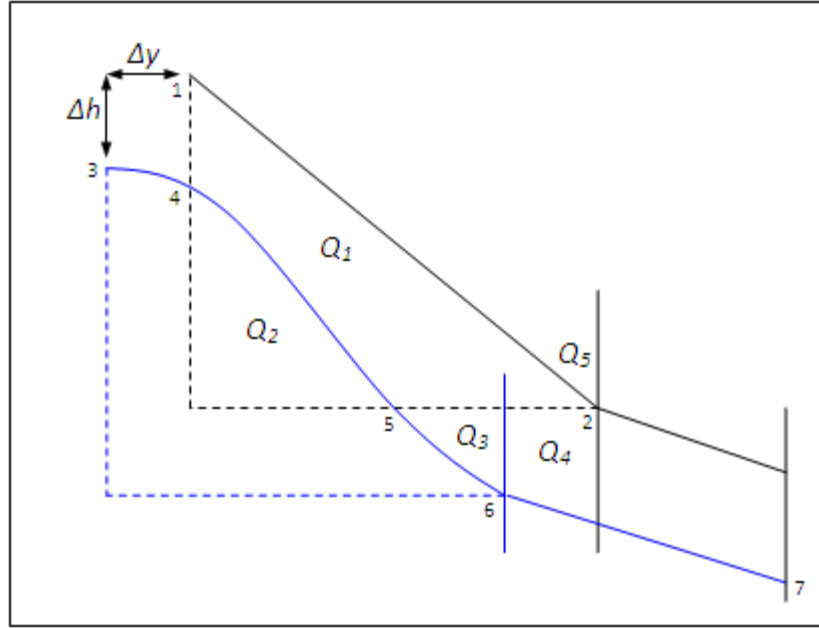
Figure 9.9   Definition sketch for Scenario 3.

Equations 9.6 a-e are used to calculate the areas found in Figure 9.9. These are subsequently combined with Equation 9.7 and Equation 9.8 to solve for the unknowns, Δy and Δh.

$$Q_1 + Q_2 = \tfrac{1}{2}(y_2 - y_1)(h_1 - h_2) \qquad\qquad \text{Equation } 9.6a$$

$$Q_2 = (y_5 - y_4)(h_4 - h_5) - \left[\int_{(y_4-y_3)}^{(y_5-y_3)} g(y)dy - (y_5 - y_4)(h_3 - h_4) \right] \text{Equation } 9.6b$$

$$Q_3 = \int_{(y_5-y_3)}^{(y_6-y_3)} g(y)dy - (y_6 - y_5)(h_3 - h_5) \qquad\qquad \text{Equation } 9.6c$$

$$Q_4 = \frac{(h_2 - h_7) + (h_2 - h_6)}{2}(y_2 - y_6) \qquad\qquad \text{Equation } 9.6d$$

$$E_D = Q_1 + Q_3 + Q_4 \qquad\qquad \text{Equation } 9.7$$

$$m = \frac{(h_6 - h_7)}{(y_7 - y_6)} \qquad\qquad \text{Equation } 9.8$$

104

Note that in Figure 9.9, the new element is shifted down and to the left. The effects of generating mass in the new element needs to be considered. An accommodation may be required to resolve conservation of mass within the model.

9.7   Case 2 – Fine Resolution Implementation

The second case considered in this analysis is the application of the modified shore profile equation, 8.6. In Case 2, a fine resolution mesh is utilized to define elements from the shore boundary to the end of the linear profile. Each profile may span from 2 to n elements. The k_i value in this scenario would be determined by physical forcings and sediment supply. A definition sketch showing possible element locations is included in Figure 9.10. The elements are defined as vertical lines with labels at the top. A second flow diagram (Figure 9.11) demonstrates three generalized scenarios for Case 2. The flow diagram is then used to direct the model in the proper calculation method.
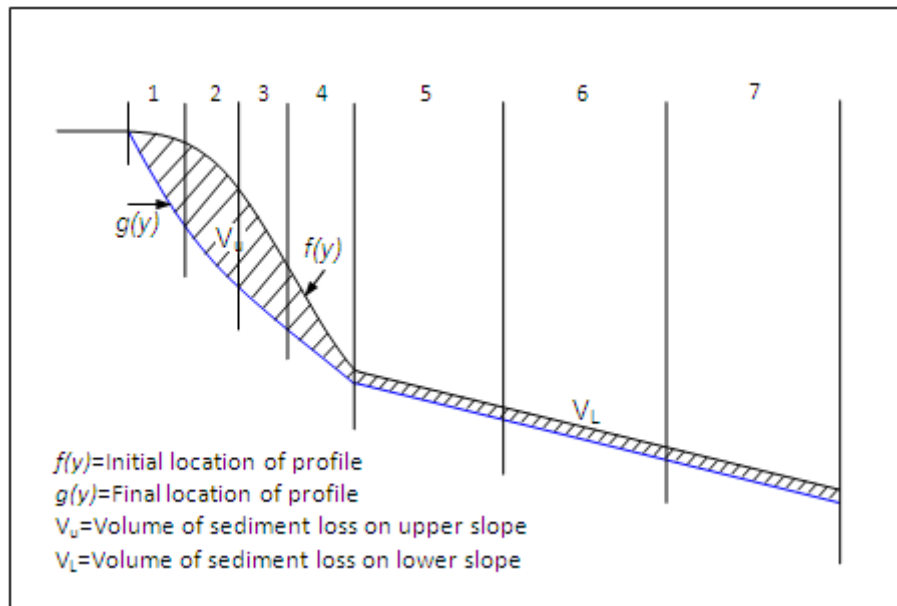
Figure 9.10   Definition sketch for Case 2.
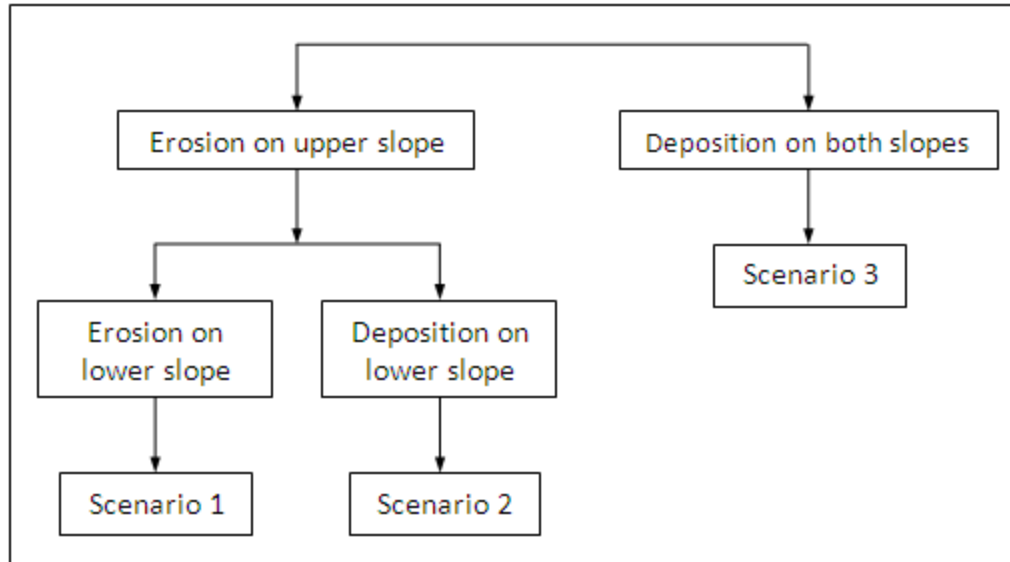
Figure 9.11   Flow diagram for Case 2.

For bays and estuaries, the shoreline evolution equation can be applied from the shoreline to the end of the linear profile or the centerline of the water body (See Section A-A in Figure 9.12). Similarly, a mirror equation can be used on the opposite shore. For coastlines, the interior end point would be located at the depth in which sedimentation is no longer modeled or no significant change can be monitored. This distance will vary with each application and will be left to the discretion of the modeler.
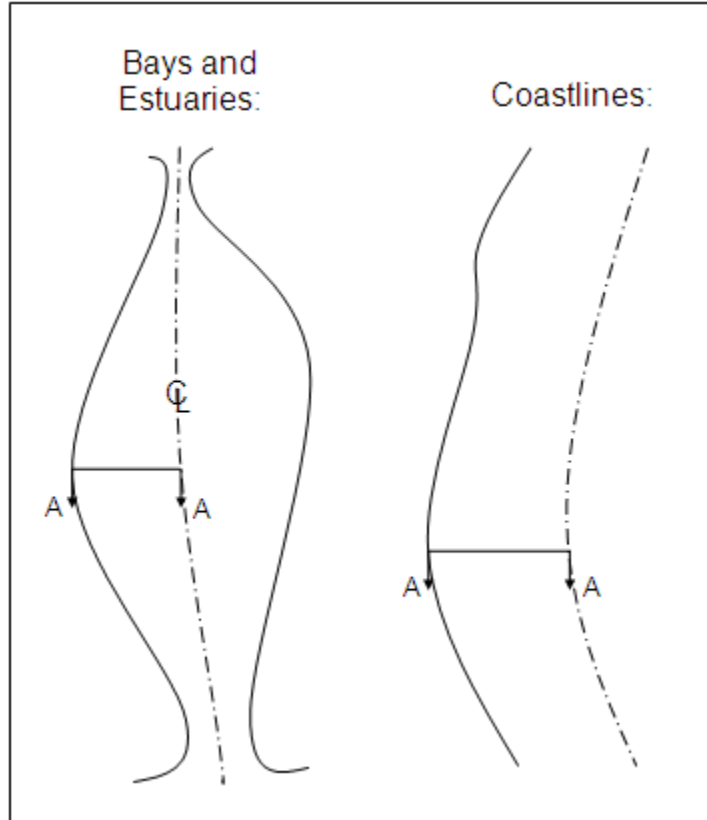
Figure 9.12   Schematic profile in plan view.

In Scenario 1, erosion occurs on both the upper and lower slopes (Figure 9.13). Eroded sediment then either travels in suspension or as bed load away from the profile. In Scenario 2, erosion occurs on the upper slope, while deposition occurs on the lower slope (Figure 9.14). This scenario could be caused by wave action increasing erosion in the surf zone, from mass erosion of the bank, or from mud fluidizing and moving downhill. Scenario 3 demonstrates deposition occurring across the entire profile length (Figure 9.15). This coincides with an accreting shoreline.

107
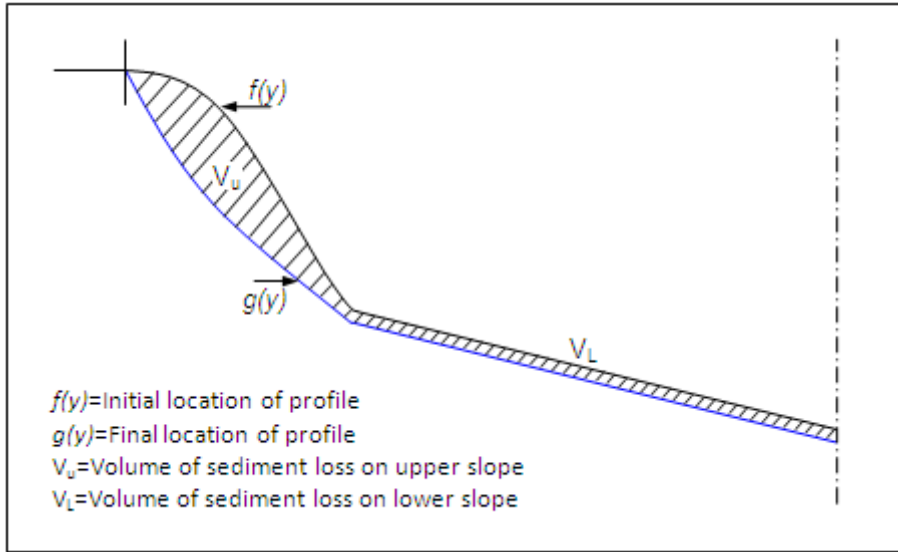
Figure 9.13   Definition sketch for Scenario 1 in Case 2.
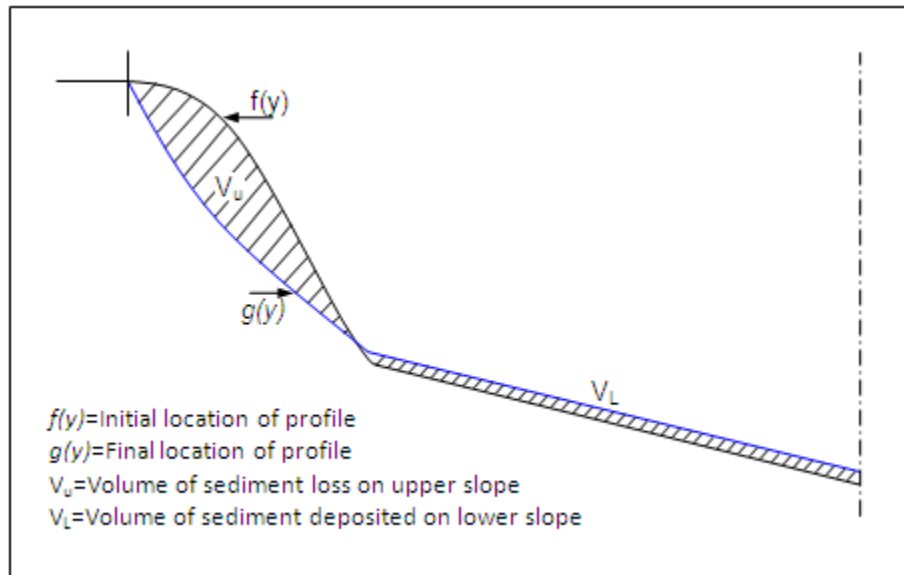
Figure 9.14   Definition sketch for Scenario 2 in Case 2.
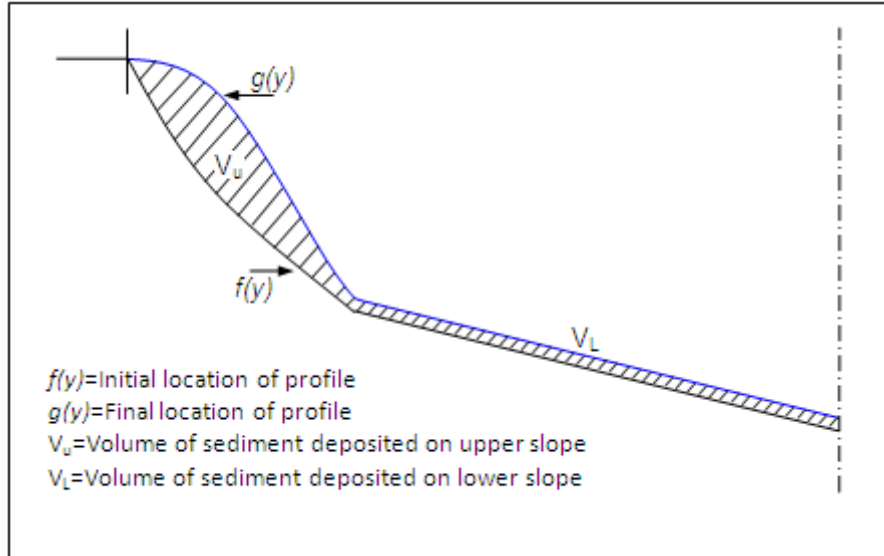
Figure 9.15   Definition sketch for Scenario 3 in Case 2.

The above figures were generated to show the general trend; the upper slope may or may not change in concavity. The lower slope is assumed to maintain the same slope but shift upwards or downwards depending on the occurrence of either erosion or deposition.

9.8   Scenario 1 and Scenario 3 for Case 2

In Scenario 1 as well as in Scenario 3, the area beneath the curve is required. Similar to Case 1, the integration of the curve must be calculated; however, Equation 8.6 cannot be integrated without advanced computer software. These scenarios were therefore considered outside the scope of this document.

9.9   Scenario 2 in Case 2

In Scenario 2, the upper slope is eroding while the lower slope is depositing. As mentioned, Equation 8.6 was unable to be integrated; however, for demonstration purposes, the integration of Equation 8.1 was utilized. The following is the derivation of

109

the equations using a slightly different approach than those used in Case 1. A definition sketch for the derivation can be found in Figure 9.16. Some repetition of previously discussed equations are included for clarity.
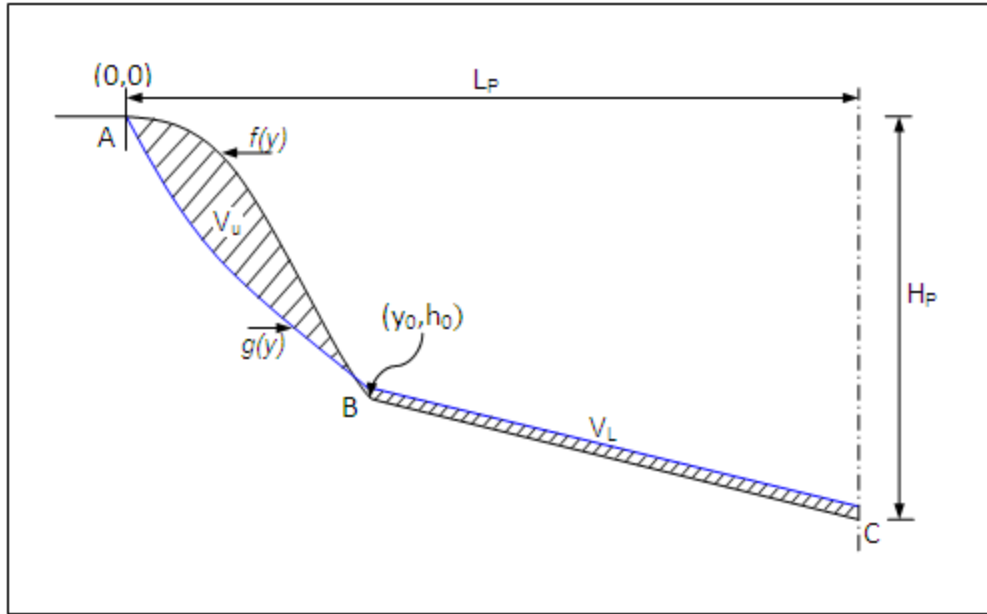
Figure 9.16 Definition sketch for derivation of Scenario 2 equations.

The volume of sediment removed from the upper slope, V_u, is then transported to the lower slope. It is assumed that this entire volume is retained as bed material without any loss to suspension.

For the upper portion of the profile, the area under the curve, A_u, is found by integrating Equation 8.1 for the initial, $f(y)$, and final, $g(y)$, profile curves from 0 to y_0. The area A_U is related to volume by Equation 9.9 where L is the distance between profiles.

$$V_u = A_u \cdot L$$
<div align="right">Equation 9.9</div>

$$A_u = \int_0^{y_0} g(y) - \int_0^{y_0} f(y)$$
<div align="right">Equation 9.10</div>

<div align="center">110</div>

$$f(y) = h_0 e^{4k_i(y-y_0)} \left(\frac{y}{y_0} \right)^2 dy \qquad \text{Equation 9.11}$$

Equations 9.10 and 9.11 were combined and evaluated to determine the change in volume from the initial to the final curve. Since the only distinction between *f(y)* and *g(y)* is the constant k_i, a single *f(y)* equation was integrated then added back into Equation 9.10. The integration and simplification can be found in Equations 9.12a-e.

$$w(y) = \int_0^{y_0} h_0 e^{4k_i(y-y_0)} \left(\frac{y}{y_0} \right)^2 dy \qquad \text{Equation 9.12}a$$

$$= \int_0^{y_0} \frac{h_0 \left(e^{4k_i y} \right) y^2}{\left(e^{4k_i y_0} \right) y_0^2} dy = \frac{h_0}{y_0^2} \left(e^{-4k_i y_0} \right) \int_0^{y_0} \left(e^{4k_i y} \right) y^2 dy \qquad \text{Equation 9.12}b$$

$$= \frac{h_0}{y_0^2} \left(e^{-4k_i y_0} \right) \left\{ \left| \frac{1}{k_i} y^2 e^{4k_i y} \right|_0^{y_0} - \frac{2}{k_i} \int_0^{y_0} y e^{4k_i y} dy \right\} \qquad \text{Equation 9.12}c$$

$$= \frac{h_0}{y_0^2} \left(e^{-4k_i y_0} \right) \left\{ \left| \frac{1}{k_i} y^2 e^{4k_i y} \right|_0^{y_0} - \frac{2}{k_i} \left| \frac{1}{16k_i^2} (4k_i y_0 - 1) e^{4k_i y} \right|_0^{y_0} \right\} \qquad \text{Equation 9.12}d$$

$$w(y) = \frac{h_0}{4k_i} - \frac{h_0}{32k_i^3 y_0} (4k_i y_0 - 1) - \frac{h_0}{32k_i^2 y_0} \left(e^{-4k_i y} \right) \qquad \text{Equation 9.12}e$$

The lower portion of Figure 9.16 is enlarged to create Figure 9.17. The variables found in Figure 9.17 are then used to evaluate the volume of sediment deposited on the lower slope, V_L.

111
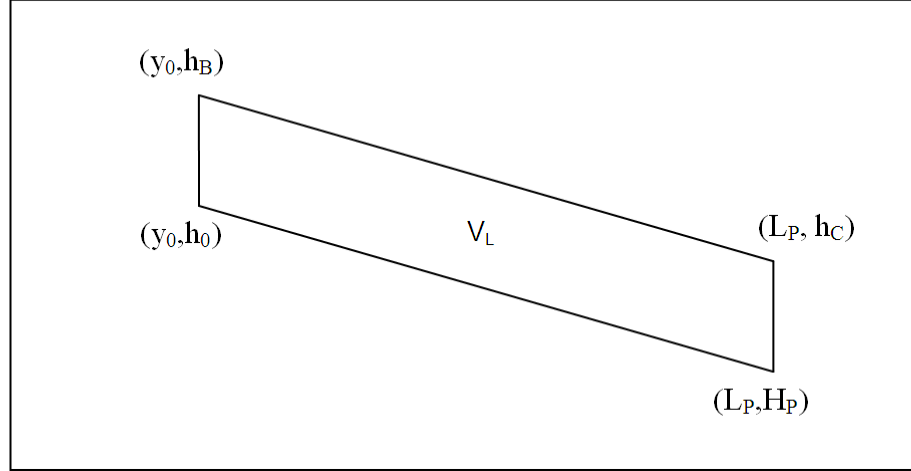
Figure 9.17   Definition sketch for lower portion of profile.

Equation 9.13 shows the relationship between the volume V_L and the area A_L. Equation 9.14, and its counterpart, Equation 9.15, show the results of the calculation of the area, A_L. The variables in these equations are defined in Figure 9.17.

$$V_L = A_L \cdot L \qquad \text{Equation 9.13}$$

$$A_L = (L_P - y_0)(h_0 - h_B) \qquad \text{Equation 9.14}$$

$$h_C = h_B - h_o + H_P \qquad \text{Equation 9.15}$$

The results from Equations 9.9 and 9.13 are then set equal since the entire sediment volume is considered to have moved downslope (Equation 9.16). This is further simplified into the final equation, 9.17. Note that k_i, V_U, and V_L are known or estimated parameters. Unknowns are the new elevations, h_B and h_C. These will then be solved for to redefine the mesh.

$$\left\{ \left[\frac{h_0}{4k_i} - \frac{h_0}{32k_i^3 y_0}(4k_i y_0 - 1) - \frac{h_0}{32k_i^2 y_0}\left(e^{-4k_i y}\right) \right]_2 - \left[\frac{h_0}{4k_i} - \frac{h_0}{32k_i^3 y_0}(4k_i y_0 - 1) - \frac{h_0}{32k_i^2 y_0}\left(e^{-4k_i y}\right) \right]_1 \right\} \cdot L = (L_P - y_0)(h_0 - h_B) \cdot L$$

Equation 9.16

112

$$\left\{ \begin{matrix} \left[\dfrac{h_0}{4k_i} - \dfrac{h_0}{32k_i^3 y_0}\left(4k_i y_0 - 1\right) - \dfrac{h_0}{32k_i^2 y_0}\left(e^{-4k_i y}\right) \right]_2 \\[4mm] -\left[\dfrac{h_0}{4k_i} - \dfrac{h_0}{32k_i^3 y_0}\left(4k_i y_0 - 1\right) - \dfrac{h_0}{32k_i^2 y_0}\left(e^{-4k_i y}\right) \right]_1 \end{matrix} \right\} = \left(L_P - y_0\right)\left(h_0 - h_B\right)$$

<div align="right">Equation 9.17</div>

9.10   Additional Considerations for Case 2.

In order to implement Case 2 in a numerical model, definition strings in which the equation would be applied would need to be defined perpendicular to the shoreline upon initial mesh construction. The model would then interpolate the mesh between the strings. (Figure 9.18).
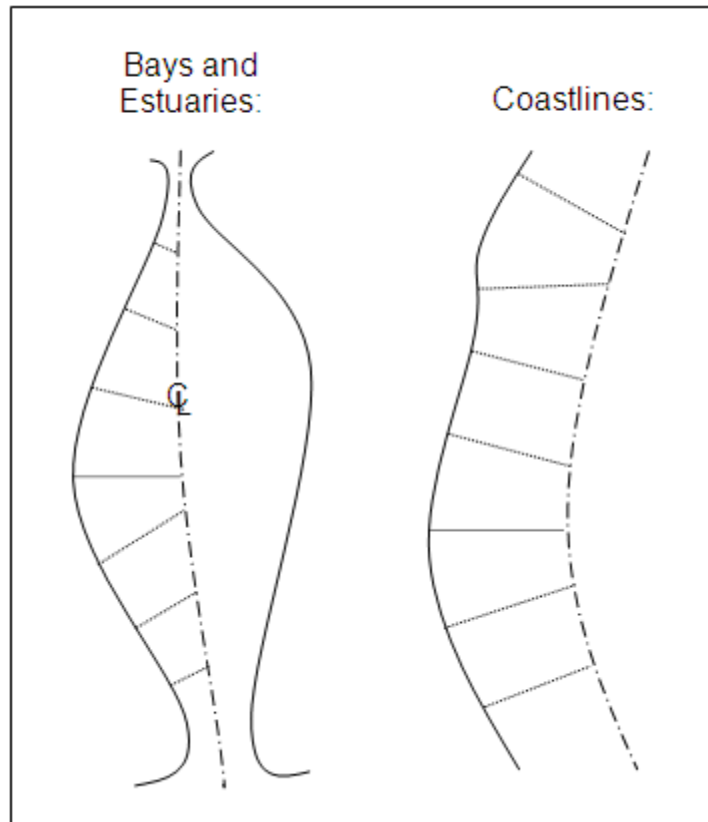
Figure 9.18   Possible locations of profile strings.

113

Additionally, shifting of the shoreline must also be calculated. In the previous steps, the profile origin and location of y_0 remain constant for $0.01 < k_i < 0.5$ (the typical range of k_i). Once k_i drops below this range, erosion will continue to occur at the same rate; however, the shape of the profile will remain constant and erosion will be achieved mathematically by shifting the origin landward. The length of the upper half of the profile, y_0, would remain constant, but the terminal depth, h_0, would shift in accordance with erosion. Similarly, when k_i is higher than 0.5, deposition will occur in the opposite manner.

Movement of the shoreline based solely on wave impact would proceed at a much higher rate than movement based only on a forcing such as tidal flux. Also, vegetated shores would provide protection against movement of the origin, but not necessarily changes to the profile shape. Further investigation into the dynamics of k_i along with extensive data collection is recommended to better understand the relationship between k_i and shoreline composition.

CHAPTER X

CONCLUSIONS

The goal of this research was to obtain a physics-based algorithm for shoreline erosion and deposition of fine sediments in a tidal environment. A tiered approach was utilized to analyze the problem at various levels, using Weeks Bay, Alabama, as a test site. The Tier 1 Approach of Slope Analysis provided rough guidelines and information about the geometry of each profile. The Tier 2 Approach, while not successful, aimed to define the profile geometry through Wavelet transforms and produce new parameters to link to the physical forcings. The Tier 3 Approach of enhancing widely accepted equations for shoreline geometry produced satisfactory results.

The new algorithm, Equation 8.6, modified an equation developed by S.C. Lee to include the entire shore profile. A mathematical representation of the shore profile from the land-water interface to the termination of the linear profile can be modeled using the developed equation.

Additionally, implementation of the new algorithm as well as Lee's original equation was analyzed. Fine and coarse resolution models were considered as well as several scenarios for deposition and erosion.

10.1 Slope Analysis

The results of the slope analysis provided information regarding the general geometry of each profile. The analysis showed that the rate of shoreline change was minimal during the data collection period. According to the concept of concavity

115

developed by Kirby, all Weeks Bay profiles are concave and thus appear to be erosional. However, analyzing the change in slope presented no distinguishable change, either erosional or depositional, during the monitoring period.

Additionally, the slope analysis did not show a significant relationship between the upper and lower slopes of the profiles. The lower slopes in Weeks Bay tended to be equal and constant across all profiles while the upper slopes increased from south to north.

It was expected that a longer fetch would increase wave activity, thereby causing erosion of the shore and a steepening of the upper slope. However, an inverse relationship was found between fetch and upper slope. As the fetch increased, the slope became less steep. It is important to note that the differences in slope are minimal, 3.5° to 10°. The inverse relationship is possibly caused by a limited data collection period and thus too few data points.

As another step in the slope analysis, a first approach to determining a shore profile equation was analyzed. Curve-fitting was utilized to evaluate the general shape of the profiles and to determine if a single curve could be used to define the entire profile. A second order polynomial provided a good fit for the upper portion of the profile; however, no simple curve was found that could accurately define the entire profile. The lower portion was best described as linear.

10.2 Wavelets

The Tier 2 Approach of using wavelets to analyze the data was a unique and innovative method. The approach required significant data manipulation since wavelets are generally used for signal processing. The data were required to be equally spaced

along the length of the profile. The spacing was varied during data collection in order to fully capture the steep portions of the shoreline. In order to efficiently collect data in the lower slope region as well, the spacing was increased beyond the interior inflection point. Cubic spline interpolation was used to transform the data into equally spaced segments. Two levels of wavelet analysis were utilized, Level 1 and Level 5. It was expected that the Level 5 analysis be more accurate than the Level 1 analysis. Both levels produced an Approximation array, A, and a Detail array, D. The Approximation captures the general trend of the signal while the Detail captures the minute changes. As the level is increased, the Approximation defines the general signal more accurately and the Detail begins to contain only the noise.

For this application, it was anticipated that the Approximation characterize the general shape of the profile and would be consistent across all profiles. The Detail was expected to contain minor changes which could be attributed to variations in the physical forcings. The correlation between the two was also analyzed to identify any relationship. Neither of these analyses demonstrated any significant correlation.

Utilizing wavelets with this technique proved ineffective for several reasons. The wavelet reconstruction of the profile 'signal' was inaccurate by as much as 60%. Poor reconstruction suggests the technique is not appropriate for this application. Rather than taking the form of the profile shape as anticipated, the Approximation tends to be shaped similar to the waveform. For this reason, any potential relationship between the Detail and physical forcings was insignificant.

10.3 Shoreline Erosion Equations

Several shoreline erosion equations were examined for this work. The most effective at modeling the Weeks Bay shoreline was the original equation by S.C. Lee (Equation 8.1) (1995). The equation, along with the second equation Lee generated, Equation 8.2, was analyzed for potential improvements. Since Equation 8.2 did not improve results without requiring additional empirical parameters, Equation 8.1 remained the focus of this work.

Defining the location of the origin and the terminal depth was a topic of great interest. The locations used by Lee were ineffective for use in Weeks Bay. The locations of the origin which provided the most improved results were the land-water interface at MTL and the peak of the on-shore berm. Minimal wave heights required the terminal depth location defined by Lee to be too near the land-water interface to be effective. The terminal depth was instead taken as the location of the interior inflection point rather than the point at which the waves no longer affect bottom sediments. This produced excellent results for the upper region of the profile. The remainder of the profile, however, required a different equation.

Since Weeks Bay is shallow, the interior bottom slope is nearly horizontal and does not change significantly enough to differentiate. Therefore, a new equation was developed taking the bottom slope as linear. Equation 8.6 modified Equation 8.1 by implementing a damping function which smoothly transitioned between Lee's original equation and the linear bottom slope. The new, modified equation produced excellent results across the entire profile.

The wave attenuation parameter, k_i, varied only slightly from profile to profile. Implementation into a numerical model will be possible using minimal field data.

Changes over time to the profile can be modeled with this equation using k_i as the primary evolutionary parameter.

10.4 Numerical Model Implementation

Implementation into a numerical model can be achieved in several ways. The approach was separated into two general cases for which three scenarios were considered. In Case 1, a coarse resolution model, the entire shore profile was assumed to be contained in a single element. In Case 2, a fine resolution model, the profile was separated into two or more elements to increase accuracy. The three scenarios for each case included a deposition model, an erosion model, and a transition model.

10.5 Recommendations for Future Research

A more extensive data collection effort as well as a longer collection period is recommended in following this work. Further data collection is to include analysis of waves at several locations simultaneously to better understand wave attenuation in the region. Wave attenuation, and thus k_i, can then be linked directly to recorded meteorological parameters, allowing for accurate long-term analysis. A more in-depth knowledge of the effect of marsh grasses on shoreline change would also support future research. Simultaneous collection of velocity and suspended sediment concentrations is recommended at each of the inlets and outlet of Weeks Bay. These data will allow for a more accurate sediment model of the bay.

Additionally, numerical model implementation should be investigated further. Initially, this will include additional numerical integration of the scenarios described in Chapter 9. Subsequently, the coding of a subroutine defining shore profile evolution,

www.manaraa.com

along with testing and evaluation of the new equation, can then be completed in a numerical model.

10.6 Project Outcome

The final equation developed, Equation 8.6, produced improved results for all profiles examined. The equation was accurate and nearly within the error tolerance of the data collection method. It allows for the use of a single equation to define an entire profile and also generates more accurately shaped profiles in numerical models while still allowing for changes due to a dynamic wave environment. Implementation into a numerical model is possible using the final equation developed by this work.

BIBLIOGRAPHY

Bearman, J.A., Friedrichs, C.T., Jaffe, B.E., Foxgrover, A.C. 2010. "Spatial trends in tidal flat shape and associated environmental parameters in South San Francisco Bay." *Journal of Coastal Research* 26, no. 2: 342-349.

Dean, R.G. and R.A. Dalrymple. 2002. *Coastal Processes with Engineering Applications*. New York: Cambridge University Press.

Diaz-Ramirez, J.N., W.H. McAnally, and J.L. Martin. 2010. "Weeks Bay Watershed Hydrology Simulation." Northern Gulf Institute, Mississippi State University, MS.

Google Earth. 30° 23' 52" N and 87° 49' 52" W. 1 Feb 2008. 10 Sept 2010.

Hardaway, C.S. and R.J. Byrne. 1999. *Shoreline Management in Chesapeake Bay*. Virginia Sea Grant Publication VSG-99-11. Virginia Institute of Marine Science, College of William and Mary.

Kirby, R. 2002. "Distinguishing accretion from erosion-dominated muddy coasts." *Muddy Coasts of the World: Processes, Deposits and Function*. Ed. T. Healy, et. al. Amsterdam: Elsevier Science B.V. 61-81.

Lee, S.C. 1995. "Response of mud shore profiles to waves." PhD Diss., University of Florida.

Lee, S.C., A. J. Mehta. 1997. "Problems in characterizing dynamics of mud shore profiles." *Journal of Hydraulic Engineering*. 123, no. 4: 351-361.

Mathworks, The, Inc. 2011. Matlab online software documentation. http://www.mathworks.com/products/matlab/. (accessed 10 Dec 2010).

McAnally, W. H., et. al. 2007. "Management of Fluid Mud in Estuaries, Bays, and Lakes. I: Present State of Understanding on Character and Behavior." *Journal of Hydraulic Engineering*. 133, No. 1: Jan 2007.

Mehta, A.J. and McAnally, W.H. 2008. "Chapter 4: Fine-grained sediment transport." *ASCE Manual 110: Sedimentation Engineering: processes, measurements, modeling, and practice*.

121

National Estuarine Research Reserve System (NERRS). 2010. "Centralized Data Management Office." Online Data Export System. http://cdmo.baruch.sc.edu/. (accessed 1 Sept 2010).

National Oceanic and Atmospheric Administration GEODAS (NOAA) 2010. "GEODAS Grid Translator Design-a-Grid". http://www.ngdc.noaa.gov/mgg/gdas/gd_designagrid.html. (accessed 28 Dec 2010).

National Oceanic and Atmospheric Administration (NOAA) 2010. "Tides and Currents Online Data Retrieval". Weeks Bay, AL Station ID No. 8732828. Accessed 31 May 2010.

Operational Science Advisory Team (OSAT). 2010. "Summary report for sub-sea and sub-surface oil and dispersant detection: Sampling and monitoring." Prepared for Paul F. Zukunft, US Coast Guard, Federal On-Scene Coordinator, Deepwater Horizon MC252.

Roberts, W. and R.J.S. Whitehouse. 2001. "Predicting the profile of intertidal mudflats formed by cross-shore tidal currents." *Coastal and Estuarine Fine Sediment Processes*. Ed. W.H. McAnally and A.J. Mehta. Amsterdam: Elsevier Science B.V. 263-285.

Rodriguez, H.N. and A.J. Mehta. 2000. "Longshore transport of fine-grained sediment." *Continental Shelf Research*. 20: 1419-1432.

Sharp, J.A. 2009. "Adaptive hydraulics model for Weeks Bay, Alabama." NGI/MSU TN 2.

United States Geological Survey (USGS). Louisiana Coastal wetlands: a resource at risk. Online Fact Sheet. Marine and coastal geology program. http://marine.usgs.gov/fact-sheets/LAwetlands/lawetlands.html. (accessed 4 Oct 2010).

United States Geological Survey (USGS). "National Water Information System: Web Interface". *Fish River near Silver Hill, AL*. Station No. 02378500. (accessed 1 Sept 2010).

United States Geological Survey (USGS). "National Water Information System: Web Interface". *Magnolia River at US 98 Near Foley, Alabama*. Station No. 02378500. (accessed 1 Sept 2010).

Weeks Bay Foundation Website. http://www.weeksbay.org/. (accessed 1 Sept 2010).

APPENDIX A

MATLAB SCRIPT FILES

LEVEL DATA PROCESSING

```
% +++++++++++++++++++++++++++++++++++++++++++++++
%% Data Loader
%   INSERT DATE OF MEASUREMENT
%   PHYSICALLY COPY CROSS SECTION DATA INTO MIDCS# VARS

clear all
load 'level.txt'
header=char('meas no','distance ft','height ft','error','date');
date=05202010;          %insert date of measurement
[m,n]=size(level);

for i=1:m
    mid(i,1)=level(i,2);
    mid(i,2)=level(i,5)/1000;
    mid(i,3)=level(i,7)/1000;
    mid(i,4)=level(i,11);
    mid(i,5)=date;
    mid(i,6)=0;
end

midCS1=[];
midCS2=[];
midCS3=[];
midCS4=[];
midCS5=[];
midCS6=[];

load cs      %cs.mat contains all previously processed profiles


%% +++++++++++++++++++++++++++++++++++++++++++++++
%% Benchmark Removal Proccessing
%   COMMENT OUT ANY CS YOU DO NOT NEED
%   ENSURE BM ARE LOCATED PROPERLY IN THE FILE

bm1=(midCS1(1,3)+midCS1(2,3))/2;
bm2=(midCS2(3,3)+midCS2(4,3))/2;
bm3=(midCS3(1,3)+midCS3(1,3))/2;
bm4=(midCS4(1,3)+midCS4(2,3))/2;
bm5=(midCS5(1,3)+midCS5(2,3))/2;
bm6=(midCS6(1,3)+midCS6(2,3))/2;


hbm1=(midCS1(5,2)+midCS1(6,2))/2;
hbm2=(midCS2(5,2)+midCS2(6,2))/2;
hbm3=(midCS3(3,2)+midCS3(4,2))/2;
hbm4=(midCS4(9,2)+midCS4(9,2))/2;
hbm5=(midCS5(5,2)+midCS5(6,2))/2;
hbm6=(midCS6(5,2)+midCS6(6,2))/2;
```

124

```
for i=1:size(midCS1,1)
    midCS1(i,3)=midCS1(i,3)-bm1;
    midCS1(i,2)=midCS1(i,2)+(20-hbm1);
end
for i=1:size(midCS2,1)
    midCS2(i,3)=midCS2(i,3)-bm2;
    midCS2(i,2)=midCS2(i,2)+(20-hbm2);
end
for i=1:size(midCS3,1)
    midCS3(i,3)=midCS3(i,3)-bm3;
    midCS3(i,2)=midCS3(i,2)+(20-hbm3);
end
for i=1:size(midCS4,1)
    midCS4(i,3)=midCS4(i,3)-bm4;
    midCS4(i,2)=midCS4(i,2)+(20-hbm4);
end
for i=1:size(midCS5,1)
    midCS5(i,3)=midCS5(i,3)-bm5;
    midCS5(i,2)=midCS5(i,2)+(20-hbm5);
end
for i=1:size(midCS6,1)
    midCS6(i,3)=midCS6(i,3)-bm6;
    midCS6(i,2)=midCS6(i,2)+(20-hbm6);
end

%Physically delete the benchmarks from the midCS
%then run the following cell


%% +++++++++++++++++++++++++++++++++++++++++++++++
%% Concatenation of Profile data
%  CAUTION: ONLY RUN ONE TIME, MAKE SURE YOU ARE READY
%  AFTER RUNNING, DELETE ALL VARIABLES EXCEPT CS# AND HEADER AND SAVE
AS cs.mat

CS1=cat(1,CS1,midCS1);
CS2=cat(1,CS2,midCS2);
CS3=cat(1,CS3,midCS3);
CS4=cat(1,CS4,midCS4);
CS5=cat(1,CS5,midCS5);
CS6=cat(1,CS6,midCS6);


%% +++++++++++++++++++++++++++++++++++++++++++++++
%% Plotter for Profiles
% Plots all 6 profiles on one screen

subplot(2,3,1),plot(CS1(1:40,2),CS1(1:40,3),'.k',CS1(41:97,2),CS1(41:97
,3),'.b',CS1(98:143,2),CS1(98:143,3),'.r',CS1(144:198,2),CS1(144:198,3)
,'.m')
legend('03262010','04152010','05062010','05202010')
title('CS1')
```

125

```
set(gca,'YDir','reverse')
grid on
subplot(2,3,2),plot(CS2(1:71,2),CS2(1:71,3),'.k',CS2(72:130,2),CS2(72:1
30,3),'.b',CS2(131:172,2),CS2(131:172,3),'.r',CS2(173:230,2),CS2(173:23
0,3),'.m')
legend('03262010','04152010','05062010','05202010')
title('CS2')
set(gca,'YDir','reverse')
grid on
subplot(2,3,3),plot(CS3(1:45,2),CS3(1:45,3),'.k',CS3(46:84,2),CS3(46:84
,3),'.b',CS3(85:116,2),CS3(85:116,3),'.r',CS3(117:159,2),CS3(117:159,3)
,'.m')
legend('03042010','04152010','05062010','05202010')
title('CS3')
set(gca,'YDir','reverse')
grid on
subplot(2,3,4),plot(CS4(1:51,2),CS4(1:51,3),'.k',CS4(52:94,2),CS4(52:94
,3),'.b',CS4(95:133,2),CS4(95:133,3),'.r',CS4(134:183,2),CS4(134:183,3)
,'.m')
legend('03042010','04152010','05062010','05202010')
title('CS4')
set(gca,'YDir','reverse')
grid on
subplot(2,3,5),plot(CS5(1:22,2),CS5(1:22,3),'.k',CS5(23:60,2),CS5(23:60
,3),'.b',CS5(61:97,2),CS5(61:97,3),'.r',CS5(98:142,2),CS5(98:142,3),'.m
')
legend('03042010','04152010','05062010','05202010')
title('CS5')
set(gca,'YDir','reverse')
grid on
subplot(2,3,6),plot(CS6(1:38,2),CS6(1:38,3),'.k',CS6(39:83,2),CS6(39:83
,3),'.b',CS6(84:114,2),CS6(84:114,3),'.r',CS6(115:157,2),CS6(115:157,3)
,'.m')
legend('03262010','04152010','05062010','05202010')
title('CS6')
set(gca,'YDir','reverse')
grid on


%% ++++++++++++++++++++++++++++++++++++++++++++++
%% Plotter for Profile including Marsh Edge
% Plots all 6 profiles on one screen

subplot(2,3,1),plot(CS1(1:40,2),CS1(1:40,3),'.k',32.1,4.2220,'ob')
legend('03262010','Marsh Edge')
title('CS1')
set(gca,'YDir','reverse')
subplot(2,3,2),plot(CS2(1:71,2),CS2(1:71,3),'.k',48.04,2.778,'ob')
legend('03262010','Marsh Edge')
title('CS2')
set(gca,'YDir','reverse')
subplot(2,3,3),plot(CS3(1:45,2),CS3(1:45,3),'.k',27.77,4.120,'ob')
legend('03042010','Marsh Edge')
title('CS3')
set(gca,'YDir','reverse')
```

126

```
subplot(2,3,4),plot(CS4(1:51,2),CS4(1:51,3),'.k',32.31,3.342,'ob')
legend('03042010','Marsh Edge')
title('CS4')
set(gca,'YDir','reverse')
subplot(2,3,5),plot(CS5(1:22,2),CS5(1:22,3),'.k',26.26,3.7460,'ob')
legend('03042010','Marsh Edge')
title('CS5')
set(gca,'YDir','reverse')
subplot(2,3,6),plot(CS6(1:38,2),CS6(1:38,3),'.k',19.34,4.494,'ob')
legend('03262010','Marsh Edge')
title('CS6')
set(gca,'YDir','reverse')


%% ++++++++++++++++++++++++++++++++++++++++++++++++
%% Plot One Profile at a Time
% Uncomment appropriate profile

% plot(CS1(41:97,2),CS1(41:97,3),'-b',CS1(98:143,2),CS1(98:143,3),'--
r',CS1(144:198,2),CS1(144:198,3),'-.m')
% legend('04152010','05062010','05202010')
% title('CS1')
% set(gca,'YDir','reverse')
% grid on

% plot(CS2(72:130,2),CS2(72:130,3),'-
b',CS2(131:172,2),CS2(131:172,3),'--r',CS2(173:230,2),CS2(173:230,3),'-
.m')
% legend('04152010','05062010','05202010')
% title('CS2')
% set(gca,'YDir','reverse')
% grid on

% plot(CS3(46:84,2),CS3(46:84,3),'-b',CS3(85:116,2),CS3(85:116,3),'--
r',CS3(117:159,2),CS3(117:159,3),'-.m')
% legend('04152010','05062010','05202010')
% title('CS3')
% set(gca,'YDir','reverse')
% grid on

% plot(CS4(52:94,2),CS4(52:94,3),'-b',CS4(95:133,2),CS4(95:133,3),'--
r',CS4(134:183,2),CS4(134:183,3),'-.m')
% legend('04152010','05062010','05202010')
% title('CS4')
% set(gca,'YDir','reverse')
% grid on

% plot(CS5(23:60,2),CS5(23:60,3),'-b',CS5(61:97,2),CS5(61:97,3),'--
r',CS5(98:142,2),CS5(98:142,3),'-.m')
% legend('04152010','05062010','05202010')
% title('CS5')
% set(gca,'YDir','reverse')
% grid on
```

127

```
plot(CS6(39:83,2),CS6(39:83,3),'-b',CS6(84:114,2),CS6(84:114,3),'--
r',CS6(115:157,2),CS6(115:157,3),'-.m')
legend('04152010','05062010','05202010')
title('CS6')
set(gca,'YDir','reverse')
grid on
```

```
%%++++++++++++++++++++++++++++++++++++++++++++++++
%% Data Loader
% clear
% Data is in variables labeled CS*, where * represents the profile
number.
%      Columns:
%      1-Measurement no.
%      2-Distance
%      3-Depth
%      Rows are measurements and all data collected are compiled into
one
%      variable for each profile.
%      'code' - defines the row number which begins individual survey
days.
%SLOPECHANGE - visual estimate of inflection point
%CHANGE - indicates that value must be changed with each run.

load insert .mat filename

code=[1 37 90 131 179;1 34 58 81 110;1 40 65 90 125;1 42 69 96 131;1 22
57 91 132;1 30 67 95 133];

SLOPECHANGE=[
23    32    20    25;
16    14    12    14;
19    13    9     12;
16    18    10    12;
7     22    17    19;
15    16    10    15];

%%
%%++++++++++++++++++++++++++++++++++++++++++++++++++
%% Scaling Based on Slopechange = Terminal Depth:(h0,y0)
% h= depth, Col 1 ; y=distance along profile, Col 2
clear Erms h Mod part Orig ModSC

% INPUTS =======================================
Orig=CS6;    %CHANGE
CSno=6;      %CHANGE
date=4;      %CHANGE
%===============================================

start=code(CSno,date);
terminus=code(CSno,(date+1))-1;
slopechange=SLOPECHANGE(CSno,date);
if date==1
    m=0;
else
    m=start-1;
end
```

129

```
for i=start:terminus
    Mod(i-m,1)=(Orig(i,3)-Orig(start,3));
    Mod(i-m,2)=(Orig(i,2)-Orig(start,2));
end
l=length(Mod);
h0=Mod(slopechange,1);
y0=Mod(slopechange,2);

for i=1:l
    ModSC(i,1)=Mod(i,1)/h0;
    ModSC(i,2)=Mod(i,2)/y0;
end
CS_SC=ModSC;

clear Mod Orig h h0 i j ki l m part start terminus tol y y0 slopechange
CSno

%% Concatenate scaled survey days:
CS6_SC=vertcat(CS_SC1,CS_SC2,CS_SC3,CS_SC4);




%%++++++++++++++++++++++++++++++++++++++++++++++++++
%% Solver for Initial ki
% Can rerun for different equations by changing h(i,1) below
% h= depth Col 1 ; y=distance along profile Col 2
clear Erms h Mod part Orig

% INPUTS =======================================
for CSno=[1 2 3 4 5 6]
    if CSno==1
        Orig=CS1_SC;
    elseif CSno==2
        Orig=CS2_SC;
    elseif CSno==3
        Orig=CS3_SC;
    elseif CSno==4
        Orig=CS4_SC;
    elseif CSno==5
        Orig=CS5_SC;
    elseif CSno==6
        Orig=CS6_SC;
    end
    for date=[1 2 3 4]

%=================================================
start=code(CSno,date);
terminus=code(CSno,(date+1))-1;
slopechange=SLOPECHANGE(CSno,date);
if date==1
    m=0;
else
    m=start-1;
end
```

130

```matlab
    for i=start:terminus
        Mod(i-m,1)=Orig(i,1);
        Mod(i-m,2)=Orig(i,2);
    end
    l=length(Mod);
    h0=Mod(slopechange,1);
    y0=Mod(slopechange,2);
    Erms=5;
    ki=0;
    tol=.8;

    for j=1:10000
        ki=ki+.0001;
        for i=1:slopechange    %slopechange or l depending on eqn used
            y=Mod(i,2);
            h(i,1)=h0*exp(4*ki*(y0-y))*(y/y0)^2;
            part(i,1)=(h(i,1)-Mod(i,1))^2;
        end
        Erms(j+1,1)=sqrt((sum(part))/l);                    %Chooses k based
on
        if ((Erms(j+1)>Erms(j)) && (Erms(j+1)<tol))
            display('***Minimized Erms***')                 %Minimum RMS
            break
        elseif j==10000
            display('***Reached maximum iterations***')
        end
    end

    KI(CSno,date)=ki;
    KI_ERMS(CSno,date)=Erms(j);
        end
    end
    KI
    KI_ERMS
    clear Mod Orig h h0 i j ki l m part start terminus tol y y0 slopechange
    date CSno



    %%+++++++++++++++++++++++++++++++++++++++++++++++++
    %% Solver for Beta
    % h= depth Col 1 ; y=distance along profile Col 2
    clear Erms h Mod part Orig

    % INPUTS ========================================
    for CSno=[1 2 3 4 5 6]
        if CSno==1
            Orig=CS1_SC;
        elseif CSno==2
            Orig=CS2_SC;
        elseif CSno==3
            Orig=CS3_SC;
        elseif CSno==4
            Orig=CS4_SC;
```

131

```
        elseif CSno==5
            Orig=CS5_SC;
        elseif CSno==6
            Orig=CS6_SC;
        end
        for date=[1 2 3 4]

%=============================================
start=code(CSno,date);
terminus=code(CSno,(date+1))-1;
slopechange=SLOPECHANGE(CSno,date);
ki=KI(CSno,date);
F=-US(CSno,date);
if date==1
    m=0;
else
    m=start-1;
end

for i=start:terminus
    Mod(i-m,1)=Orig(i,1);
    Mod(i-m,2)=Orig(i,2);
end
l=length(Mod);
h0=Mod(slopechange,1);
y0=Mod(slopechange,2);
Erms=5;
b=1;
tol=.8;

for j=1:100000
    b=b+.001;
    for i=1:slopechange    %slopechange or l????

        y=Mod(i,2);
        h(i,1)=h0*exp(4*ki*(y0-y))*(y/y0)^2;
        leenew(i,1)=F*y*exp(-b*y)+(h0-F*y*exp(-b*y))*exp(4*ki*(y0-
y))*(y/y0)^2;
        part(i,1)=(leenew(i,1)-Mod(i,1))^2;
    end
    Erms(j+1,1)=sqrt((sum(part))/l);          %Chooses b based on
    if ((Erms(j+1)>Erms(j)) && (Erms(j+1)<tol))
%         display('***Minimized Erms***')                    %Minimum
RMS
        break
    elseif j==10000
%         display('***Reached maximum iterations***')
        Erms(j)=.9999;
    end
end

BETA(CSno,date)=b;
BETA_ERMS(CSno,date)=Erms(j);
    end
end
```

132

```
BETA
BETA_ERMS
clear Mod Orig h h0 i j ki l m part start terminus tol y y0 slopechange
date CSno

%%+++++++++++++++++++++++++++++++++++++++++++++++
%% **Plotter**
load final_results
clear Mod leeOrig figure leenew corrector
% INPUTS =======================================
Orig=CS5_SC;        %CHANGE
CSno=5;             %CHANGE
date=2;             %CHANGE
% =============================================
start=code(CSno,date);
terminus=code(CSno,(date+1))-1;
ki=KI(CSno,date);
us=US(CSno,date);
ls=LS(CSno,date);
slopechange=SLOPECHANGE(CSno,date);
b=BETA(CSno,date);
F=-us;
if date==1
    m=0;
else
    m=start-1;
end

for i=start:terminus
    Mod(i-m,1)=Orig(i,1);
    Mod(i-m,2)=Orig(i,2);
end
l=length(Mod);
h0=Mod(slopechange,1);
y0=Mod(slopechange,2);

for i=1:l %% l or slopechange
    y=Mod(i,2);
    leeOrig(i,1)=h0*exp(4*ki*(y0-y))*(y/y0)^2;
    leenew(i,1)=F*y*exp(-b*y)+(h0-F*y*exp(-b*y))*exp(4*ki*(y0-
y))*(y/y0)^2;
    corrector(i,1)=F*y*exp(-b*y);
end


plot(Mod(:,2),Mod(:,1),'.k',Mod(1:slopechange,2),leenew(1:slopechange,1
),'r',Mod(1:slopechange,2),leeOrig(1:slopechange,1),'b')
set(gca,'YDir','reverse')
% ylim([0 .1])
xlim([0 1])
grid on
legend('Raw Data','Lee Eqn w/corrector','Original Lee Eqn')
clear start terminus ki us ls slopechange l h0 y0 y
```

133

```
%%++++++++++++++++++++++++++++++++++++++++++++++++
%% Data Loader
%% Load data from Lee Equation with scaling
% clear
% Data is in variables labeled CS*, where * represents the profile
number.
%     Columns:
%     1-Measurement no.
%     2-Distance
%     3-Depth
%     Rows are measurements and all data collected are compiled into
one
%     variable for each profile.
%     'code' - defines the row number which begins individual survey
days.
%SLOPECHANGE - visual estimate of inflection point
%CHANGE - indicates that value must be changed with each run.

load insert .mat filename

code=[1 37 90 131 179;1 34 58 81 110;1 40 65 90 125;1 42 69 96 131;1 22
57 91 132;1 30 67 95 133];

SLOPECHANGE=[
23    32    20    25;
16    14    12    14;
19    13    9     12;
16    18    10    12;
7     22    17    19;
15    16    10    15];


%% ++++++++++++++++++++++++++++++++++++++++++++++++
%%  Iteration for N
% h= depth Col 1 ; y=distance along profile Col 2
clear Erms h Mod part Orig T KCP lee

% INPUTS =======================================
for CSno=[1 2 3 4 5 6]
    if CSno==1
        Orig=CS1_SC;
    elseif CSno==2
        Orig=CS2_SC;
    elseif CSno==3
        Orig=CS3_SC;
    elseif CSno==4
        Orig=CS4_SC;
    elseif CSno==5
        Orig=CS5_SC;
```

134

```matlab
    elseif CSno==6
        Orig=CS6_SC;
    end
    for date=[1 2 3 4]

%================================================
start=code(CSno,date);
terminus=code(CSno,(date+1))-1;
slopechange=SLOPECHANGE(CSno,date);
ki=KI(CSno,date);
if date==1
    m=0;
else
    m=start-1;
end

for i=start:terminus
    Mod(i-m,1)=Orig(i,1);
    Mod(i-m,2)=Orig(i,2);
end
l=length(Mod);
h0=Mod(slopechange,1); %This is just 1
y0=Mod(slopechange,2); %This is just 1
Erms=5;
tol=5;
n=.001;
ht=Mod(l,1);
yt=Mod(l,2);
F2=(ht-h0)/(yt-y0);

for j=1:10000
    n=n+.001;
    for i=1:l    %slopechange or l depends on eqn used
        y=Mod(i,2);
        if y==0
             y=0.01;
        end
        r=n*(yt-y)/y;
        T(i,1)=(exp(r)-exp(-r))/(exp(r)+exp(-r));

        lee=h0*exp(4*ki*(y0-y))*(y/y0)^2;
%        Z(i,1)=lee*(1-T(i))-T(i)*(a+LS*y);
        KCP(i,1)=lee*(T(i))+(1-T(i))*(h0+F2*(y-y0));
        part(i,1)=(KCP(i,1)-Mod(i,1))^2;
    end
    Erms(j+1,1)=sqrt((sum(part))/l);               %Chooses param based on
    if ((Erms(j+1)>Erms(j)) && (Erms(j+1)<tol)) %Minimum RMS
%        display('***Minimized Erms***')  %Can turn on for display
        break
    elseif j==10000
%        display('***Reached maximum iterations***')
    end
end
```

135

```
N(CSno,date)=n;
N_ERMS(CSno,date)=Erms(j);
    end
end
N
N_ERMS
clear Mod Orig h h0 i  ki  m  start terminus tol y y0 slopechange date
CSno


%% ++++++++++++++++++++++++++++++++++++++++++++++++
%% Second Iteration for ki Using Average n=0.073
% h= depth Col 1 ; y=distance along profile Col 2
clear Erms h Mod part Orig T KCP Lee

% INPUTS =======================================
for CSno=[1 2 3 4 5 6]
    if CSno==1
        Orig=CS1_SC;
    elseif CSno==2
        Orig=CS2_SC;
    elseif CSno==3
        Orig=CS3_SC;
    elseif CSno==4
        Orig=CS4_SC;
    elseif CSno==5
        Orig=CS5_SC;
    elseif CSno==6
        Orig=CS6_SC;
    end
    for date=[1 2 3 4]

%================================================
start=code(CSno,date);
terminus=code(CSno,(date+1))-1;
slopechange=SLOPECHANGE(CSno,date);
n=0.073;
if date==1
    m=0;
else
    m=start-1;
end

for i=start:terminus
    Mod(i-m,1)=Orig(i,1);
    Mod(i-m,2)=Orig(i,2);
end
l=length(Mod);
h0=Mod(slopechange,1);
y0=Mod(slopechange,2);
Erms=5;
ki=0;
tol=.8;
ht=Mod(l,1);
yt=Mod(l,2);
F2=(ht-h0)/(yt-y0);
```

136

```
for j=1:10000
    ki=ki+.0001;
    for i=1:l            %slopechange or l depends on eqn used
        y=Mod(i,2);
        if y==0
            y=0.01;
        end
        r=n*(yt-y)/y;
        T(i,1)=(exp(r)-exp(-r))/(exp(r)+exp(-r));

        lee=h0*exp(4*ki*(y0-y))*(y/y0)^2;
%       Z(i,1)=lee*(1-T(i))-T(i)*(a+LS*y);
        KCP(i,1)=lee*(T(i))+(1-T(i))*(h0+F2*(y-y0));

        part(i,1)=(KCP(i,1)-Mod(i,1))^2;
    end
    Erms(j+1,1)=sqrt((sum(part))/l);         %Chooses k based on
    if ((Erms(j+1)>Erms(j)) && (Erms(j+1)<tol))
%       display('***Minimized Erms***')      %Minimum RMS
        break
    elseif j==10000
%       display('***Reached maximum iterations***')
    end
end

KI(CSno,date)=ki;
KI_ERMS(CSno,date)=Erms(j);
    end
end
KI
KI_ERMS
clear Mod Orig h h0 i j ki l m part start terminus tol y y0 slopechange
date CSno




%%++++++++++++++++++++++++++++++++++++++++++++++
%% Plotter
load final_results
clear Mod figure T KCP lee
Orig=CS2_SC;      %CHANGE
CSno=2;           %CHANGE
date=4;           %CHANGE

start=code(CSno,date);
terminus=code(CSno,(date+1))-1;
ki=KI(CSno,date);               %ki from previous
us=US(CSno,date);               %Upper slope
ls=LS(CSno,date);               %Lower slope
slopechange=SLOPECHANGE(CSno,date);
b=BETA(CSno,date);
F=-us;
n=0.073;    %CHANGE
if date==1
```

137

```
        m=0;
else
        m=start-1;
end

for i=start:terminus
        Mod(i-m,1)=Orig(i,1);
        Mod(i-m,2)=Orig(i,2);
end
l=length(Mod);
h0=Mod(slopechange,1);
y0=Mod(slopechange,2);


ht=Mod(l,1);
yt=Mod(l,2);
F2=(ht-h0)/(yt-y0);

for i=1:l %% l or slopechange depending on eqn used
        y=Mod(i,2);
        if y==0
            y=0.01;
        end
        r=n*(yt-y)/y;
        T(i,1)=(exp(r)-exp(-r))/(exp(r)+exp(-r));
        lee(i,1)=h0*exp(4*ki*(y0-y))*(y/y0)^2;
%          Z(i,1)=lee*(1-T(i))-T(i)*(a+LS*y);
        KCP(i,1)=lee(i,1)*(T(i))+(1-T(i))*(h0+F2*(y-y0));
end

plot(Mod(:,2),Mod(:,1),'.k',Mod(:,2),KCP(:,1),'r',Mod(:,2),lee(:,1),'b'
)
set(gca,'YDir','reverse')
% ylim([0 .1])
% xlim([0 1])
grid on
legend('Raw Data','Modified Lee','Original Lee Eqn')
clear start terminus ki us ls slopechange l h0 y0 y
```

APPENDIX B

IRB LETTERS

109 A Woodstone Place
Clinton, MS 39056

March 31, 2011

Dear Dr. Charles Finkl:

I am completing a doctoral dissertation at Mississippi State University entitled "Development of a Shore Profile Algorithm for Tidal Estuaries Dominated by Fine Sediments." I would like your permission to reprint in my dissertation excerpts from the following publication:

Bearman, J.A., Friedrichs, C.T., Jaffe, B.E., Foxgrover, A.C. 2010. "Spatial trends in tidal flat shape and associated environmental parameters in South San Francisco Bay." *Journal of Coastal Research* 26, no. 2: 342-349.

The figure to be reproduced is Figure 9 in the above article and can be found at the end of this document.
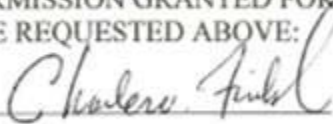
The requested permission extends to any future revisions and editions of my dissertation, including non-exclusive world rights in all languages, and to the prospective publication of my dissertation by ProQuest through its UMI® Dissertation Publishing business. ProQuest may produce and sell copies of my dissertation on demand and may make my dissertation available for free internet download at my request. These rights will in no way restrict republication of the material in any other form by you or by others authorized by you. Your signing of this letter will also confirm that you own (or your company owns) the copyright to the above-described material.

If these arrangements meet with your approval, please sign this letter where indicated below and return it to me. Thank you very much.

Sincerely,

Kimberly C. Pevey
kcpevey@gmail.com

PERMISSION GRANTED FOR THE
USE REQUESTED ABOVE:

Charles Finkl

Date: _1 April 2011_

140

109 A Woodstone Place
Clinton, MS 39056

March 31, 2011

Dear Mr. Sharp:

I am completing a doctoral dissertation at Mississippi State University entitled "Development of a Shore Profile Algorithm for Tidal Estuaries Dominated by Fine Sediments." I would like your permission to reprint in my dissertation excerpts from the following publication:

Sharp, J.A. 2009. "Adaptive hydraulics model for Weeks Bay, Alabama." NGI/MSU TN 2.

The figure to be reproduced is Figure 2 in the above technical note and can be found at the end of this document.
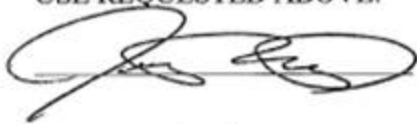
The requested permission extends to any future revisions and editions of my dissertation, including non-exclusive world rights in all languages, and to the prospective publication of my dissertation by ProQuest through its UMI® Dissertation Publishing business. ProQuest may produce and sell copies of my dissertation on demand and may make my dissertation available for free internet download at my request. These rights will in no way restrict republication of the material in any other form by you or by others authorized by you. Your signing of this letter will also confirm that you own (or your company owns) the copyright to the above-described material.

If these arrangements meet with your approval, please sign this letter where indicated below and return it to me. Thank you very much.

Sincerely,

Kimberly C. Pevey
kcpevey@gmail.com

PERMISSION GRANTED FOR THE
USE REQUESTED ABOVE:

Date: __4/1/2011__

109 A Woodstone Place
Clinton, MS 39056

March 31, 2011

Dear Dr. Diaz-Ramirez:

I am completing a doctoral dissertation at Mississippi State University entitled "Development of a Shore Profile Algorithm for Tidal Estuaries Dominated by Fine Sediments." I would like your permission to reprint in my dissertation an excerpt from the following publication:

Diaz-Ramirez, J.N., W.H. McAnally, and J.L. Martin. 2010. "Weeks Bay Watershed Hydrology Simulation." Northern Gulf Institute, Mississippi State University, MS.

The figure to be reproduced is Figure 1 in the above article and can be found at the end of this document.
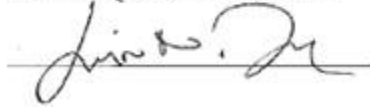
The requested permission extends to any future revisions and editions of my dissertation, including non-exclusive world rights in all languages, and to the prospective publication of my dissertation by ProQuest through its UMI® Dissertation Publishing business. ProQuest may produce and sell copies of my dissertation on demand and may make my dissertation available for free internet download at my request. These rights will in no way restrict republication of the material in any other form by you or by others authorized by you. Your signing of this letter will also confirm that you own (or your company owns) the copyright to the above-described material.

If these arrangements meet with your approval, please sign this letter where indicated below and return it to me. Thank you very much.

Sincerely,

Kimberly C. Pevey
kcpevey@gmail.com

PERMISSION GRANTED FOR THE
USE REQUESTED ABOVE:

Date: April 4/2011

Tom Byron <Tom.Byron@mathworks.com>   **Fri, Apr 8, 2011 at 3:32 PM**
To: "kcpevey@gmail.com" <kcpevey@gmail.com>
Cc: Elaine Mull <Elaine.Mull@mathworks.com>

Ms. Pevey,

I'm writing you because I was forwarded your request to use certain MathWorks' images from the Wavelet Toolbox documentation in your dissertation. We're happy to grant you the requested permission, but we will do so through this e-mail, rather than through the requested letter.

In view of that, MathWorks hereby grants you a royalty-free, non-exclusive, non-transferrable, worldwide license to publish as part of your dissertation, in unmodified form, the MathWorks images appended below, provided that you individually attribute the images as follows: © 2011 The MathWorks, Inc., image used by express permission.

We appreciate your taking the time to make this request. Please let me know if you have any further questions or concerns.

Sincerely,

Tom Byron

Thomas Byron, Esq.

The MathWorks, Inc.
3 Apple Hill Drive
Natick, MA 01760-2098
(508) 647-2095

143